UNIVERSIDADE ESTADUAL DE CAMPINAS
Faculdade de Engenharia Química

LEONARDO VILAR MOURA

PRODUCTION OF FURFURAL FROM XYLOSE: DETERMINATION OF KINETIC PARAMETERS AND SIMULATION OF A REACTIVE STRIPPING PROCESS

PRODUÇÃO DE FURFURAL A PARTIR DE XILOSE: OBTENÇÃO DE PARÂMETROS CINÉTICOS E SIMULAÇÃO DO PROCESSO DE STRIPPING REATIVO

CAMPINAS
2019

LEONARDO VILAR MOURA

PRODUCTION OF FURFURAL FROM XYLOSE: DETERMINATION OF KINETIC PARAMETERS AND SIMULATION OF A REACTIVE STRIPPING PROCESS

PRODUÇÃO DE FURFURAL A PARTIR DE XILOSE: OBTENÇÃO DE PARÂMETROS CINÉTICOS E SIMULAÇÃO DO PROCESSO DE STRIPPING REATIVO

Dissertação apresentada à Faculdade de Engenharia Química da Universidade Estadual de Campinas como parte dos requisitos para a obtenção do título de Mestre em Engenharia Química.

Dissertation presented to the School of Chemical Engineering of the University of Campinas in partial fulfillment of the requirements for the degree of Master in Chemical Engineering.

Supervisor/Orientador: Prof. Dr. Raphael Soeiro Suppino

ESTE TRABALHO CORRESPONDE À VERSÃO FINAL DA DISSERTAÇÃO DEFENDIDA PELO ALUNO LEONARDO VILAR MOURA E ORIENTADA PELO PROF. DR. RAPHAEL SOEIRO SUPPINO.

CAMPINAS
2019

Ficha catalográfica
Universidade Estadual de Campinas
Biblioteca da Área de Engenharia e Arquitetura
Rose Meire da Silva - CRB 8/5974

M865p

Moura, Leonardo Vilar, 1993-
Production of furfural from xylose: determination of kinetic parameters and simulation of a reactive stripping process / Leonardo Vilar Moura. – Campinas, SP : [s.n.], 2019.

Orientador: Raphael Soeiro Suppino.
Dissertação (mestrado) – Universidade Estadual de Campinas, Faculdade de Engenharia Química.

1. Furaldeido. 2. Xilose. 3. Catálise heterogênea. 4. Processos químicos - Simulação por computador. I. Suppino, Raphael Soeiro, 1984-. II. Universidade Estadual de Campinas. Faculdade de Engenharia Química. III. Título.

Informações para Biblioteca Digital

Título em outro idioma: Produção de furfural a partir de xilose: obtenção de parâmetros cinéticos e simulação do processo de stripping reativo
Palavras-chave em inglês:
Furfural
Xylose
Heterogeneous catalysis
Chemical Processes - Computer simulation
Área de concentração: Engenharia Química
Titulação: Mestre em Engenharia Química
Banca examinadora:
Raphael Soeiro Suppino [Orientador]
João Batista Oliveira dos Santos
Roger Josef Zemp
Data de defesa: 14-10-2019
Programa de Pós-Graduação: Engenharia Química

Identificação e informações acadêmicas do(a) aluno(a)
- ORCID do autor: https://orcid.org/0000-0001-6720-6407
- Currículo Lattes do autor: http://lattes.cnpq.br/9984052318918184

Folha de Aprovação da Defesa de Dissertação de Mestrado defendida por Leonardo Vilar Moura aprovada em 14 de outubro de 2019 pela banca examinadora constituída pelos seguintes doutores:

Prof. Dr. Raphael Soeiro Suppino (Orientador)
FEQ/UNICAMP

Prof. Dr. Roger Josef Zemp
FEQ/UNICAMP

Dr. João Batista Oliveira dos Santos
DEQ/UFSCAR

ATA da Defesa com as respectivas assinaturas dos membros encontra-se no SIGA/Sistema de Fluxo de Dissertação/Tese e na Secretaria do Programa da Unidade.

Acknowledgment

I would like to thank my parents, Osvaldo and Silvia, for all the love and support throughout my upbringing and education.

My beloved sister, Fernanda, for her kindness, friendship and her presence in my life despite the geographic distance between us for the past few years.

My girlfriend, Mariela, for her support and the countless joyful moments we shared along the way.

My supervisor, Prof. Dr. Raphael Soeiro Suppino, for his guidance, teaching, and comprehension through the execution of this work.

The members of LEPCatBior, Diogo, Letícia, Luiz and Mayra for the delightful routine we created together and all the lessons they taught me. Their support for the conduction of this work was crucial.

Mara and Éder from LDPC for the support and friendship.

Kathlen for supporting me throughout the conduction of TPD analysis.

FEQ and all its members/staff for the infrastructure and assistance provided during all these years as an undergraduate and graduate student.

This study was financed in part by the Coordenação de Aperfeiçoamento de Pessoal de Nível Superior - Brasil (CAPES) - Finance Code 001.

Resumo

O furfural é uma molécula plataforma oriunda da biomassa, produzida a partir da reação de desidratação da xilose e promissora alternativa aos derivados do petróleo como base para produção de insumos e combustíveis de origem renovável. Neste projeto, catalisadores à base de Nb_2O_5 suportados em Al_2O_3 foram preparados pelo método de impregnação úmida e submetidos a tratamentos com H_3PO_4 e HNO_3, com o objetivo de aumentar sua acidez, essencial para a desidratação da xilose ao furfural. Os sólidos foram caracterizados por fisissorção de N_2, XRF, difração a laser, TPD-NH_3 e FTIR visando relacionar seus desempenhos catalíticos às propriedades físico-químicas. Todos os catalisadores foram calcinados a 300 °C previamente aos testes catalíticos. Estes foram conduzidos em um reator batelada, sob atmosfera de N_2 (4 MPa) e com água compondo o meio reacional. A partir dos resultados dos testes catalíticos (quantificação feita por HPLC) a diferentes temperaturas (150, 160 e 170 °C), uma equação para taxa de reação foi obtida, bem como energias de ativação aparentes para a rede de reações escolhida para representar o desempenho de cada catalisador. Observou-se que o catalisador tratado com H_3PO_4 apresentou seletividade ao furfural significativamente maior que os demais catalisadores, embora a uma menor taxa de reação aparente. Os parâmetros cinéticos da reação com este catalisador foram empregados no simulador Aspen Plus® com vistas à análise de um sistema em que a reação de desidratação da xilose e a separação do furfural formado sejam conduzidas em uma etapa de *stripping* reativo. A otimização do processo por meio de planejamento experimental encontrou o máximo rendimento e recuperação de furfural no topo da coluna com valores de 85.2% e 74.0%, respectivamente. Por fim, observou-se que o emprego adequado de catalisadores heterogêneos para o processo de produção de furfural pode levar a significativos ganhos em termos de consumo de energia e de vapor no processo.

Palavras-chave: furfural, xilose, catálise heterogênea, simulação de processos.

Abstract

Furfural is a building-block molecule derived from biomass, produced from the xylose dehydration reaction and a promising alternative to petroleum-derived products as a starting point for the production of chemicals and fuels from renewable sources. In this project, Nb_2O_5 catalysts supported on Al_2O_3 were prepared by wet impregnation method and treated with H_3PO_4 and HNO_3, aiming for an increase in acidity, which is essential for dehydration of xylose to furfural. The solids were characterised by N_2 physisorption, XRF, laser diffraction, TPD-NH_3, and FTIR in order to relate their catalytic performances to physico-chemical properties. All catalysts were calcined at 300 °C prior to catalytic testing. These tests were conducted in a batch reactor under N_2 atmosphere (4 MPa) with water as a solvent. From catalytic tests results (quantification by HPLC) at different temperatures (150, 160 and 170°C), a reaction rate was obtained, as well as apparent activation energies for each catalyst and its proposed reaction network. The catalyst treated with H_3PO_4 showed higher selectivity to furfural than the other catalysts, although at a lower apparent reaction rate. The kinetic parameters from this catalyst were used in the Aspen Plus® software to analyse a process in which xylose dehydration reaction and furfural separation were conducted in a reactive stripping column. The process optimisation using design of experiments achieved a maximum yield and furfural recovery at the top of the column of 85.2% and 74.0%, respectively. It was observed that the appropriate use of heterogeneous catalysts for the furfural production process can lead to significant gains in energy and steam consumption in the process.

Keywords: furfural, xylose, heterogeneous catalysis, process simulation.

List of Figures

List of Tables

List of Abbreviations

2-MF	2-methylfuran
2-MTHF	2-methyltetrahydrofuran
2PT	2-pentanone
BAS	Brønsted acid sites
BET	Brunauer-Emmett-Teller
BJH	Barret-Joyner-Halenda
CCRD	Central Composite Rotatable Design
CPME	Cyclopentyl methyl ether
DHA	Dihydroxyacetone
DOE	Design of Experiments
FA	Furfuryl alcohol
FAC	Formic acid
FTIR	Fourier-Transform Infrared Spectroscopy
FUR	Furfural
GLU	Glucoaldehyde
GLY	Glyceraldehyde
GVL	Gamma-valerolactone
HA	Hydroxyacetone
HD	Hydrogen deuteride
HDO	Hydrogen-deuterium oxide
HMF	Hydroxymethylfurfural
HPLC	High Performance Liquid Chromatography
I	Intermediates
IUPAC	International Union of Pure and Applied Chemistry
LA	Levulinic acid

LAC	Lactic acid
LAS	Lewis acid sites
LHHW	Langmuir–Hinshelwood–Hougen–Watson
LYX	Lyxose
MIBK	Methyl isobutyl ketone
PB	Plackett-Burman
PHL	Pre-hydrolysate liquor
RTD	Residence time distribution
T-T-DF	Two- and tridimensional furilic oligomers
TBR	Trickle-bed reactor
TPD	Temperature-Programmed Desorption
XRF	X-ray Fluorescence
XYL	Xylose

List of Symbols

a_{ij}	UNIQUAC binary parameters
b_{ij}	UNIQUAC binary parameters
α_i	Reaction order with respect to i
C_{WP}	Weisz-Prater number
D_{eff}	Effective diffusion coefficient
D_{pore}	Pore diameter
ΔG_R	Change in Gibbs free energy
ΔS_R	Change in entropy
ΔH_R	Change in enthalpy
E_a	Apparent activation energy
F_i	Mole flow of compound i
$\phi([i])$	Concentration function
k_i	Apparent rate constant
m_{cat}	Catalyst mass
N	Number of stages
N_r	Number of reactive stages
n_i	Moles of component i
N_A	Avogadro's number
P	Pressure
r_i	Reaction rate with respect to i
r_{obs}	Observed reaction rate
R_p	Particle size
R_A	Solute molecule radius
R	Gas constant
S	Selectivity

S_{BET}	Specific surface area (BET)
S_m	Cross-sectional area of the adsorbate molecule
t	Time
T	Temperature
V	Volume
V_m	Monolayer specific volume
V_{ads}	Adsorbed specific volume
X, x	Factor in design of experiments
χ	Conversion
Y	Yield
ξ	Objective function (least squares)
ψ	Carbon balance
μ_B	Solvent viscosity
$[i]$	Concentration of i

Contents

Chapter 1

Introduction

The development of renewable energy sources and sustainable feedstocks in a variety of industries have been growing for the past years. Their minimal environmental impact and low cost make them an alternative to a future greener society. The increasing competitiveness of renewable energies at a global level and the engagement of public and private scientific sectors should enable and accelerate a transition to a more sustainable scenario, and in particular increase energy security and mitigate the risks of climate change (CHU; MAJUMDAR, 2012).

In this context, biomass is of prime importance as an alternative to fossil fuels, given its vast abundance and applicability - ranging from the production of renewable fuels to the supply of building-block molecules for the production of high added-value compounds in different chemical industries (CHU; MAJUMDAR, 2012). The versatility of biomass enables it to be transformed into solid, liquid or gaseous fuels and has strongly contributed to the increase in its use in several sectors: heating of homes, electricity generation and transportation. According to a recent report by the World Energy Resources Bioenergy (2016), about 10% of the global energy supply comes from biofuels, with increasing trends in the coming decades. At the European Union (EU) level, bioeconomy is already responsible for about 18.5 million employments and has an annual turnover of 2.3 trillion euro (HASSAN; WILLIAMS; JAISWAL, 2019).

The large abundance of biomass at a low cost, originating mainly from agricultural residues, livestock and organic waste, places it in a prominent role for a future with significant participation of renewable fuels and raw materials (IPCC *Fourth Assessment Report: Climate Change* , 2007).

Lignocellulosic biomass is an important renewable source of carbon and considered to be the most abundant form of biomass. It is estimated that approximately 476 million tons of lignocellulosic will be needed by 2030, and bio-based products are expected to be worth 50 billion euro by the same year (HASSAN; WILLIAMS; JAISWAL, 2019).

Among the components of the hemicellulosic fraction of lignocellulosic biomass, xylose can be subjected to a dehydration reaction to produce a compound of interest: furfural. Furfural has gained prominence in recent years given its ability to generate several four or five-carbon molecules (C_4 or C_5). One of them is furfuryl alcohol (FA), produced by the hydrogenation of furfural; and liquid alkanes used as fuels, as reported by Li, Jia and Wang (2016).

The concept of biorefinery, a sustainable and cost-effective way of producing bioproducts (food, chemicals, materials) and bioenergy (fuel, power, heat) from biomass processing, has gained attention aiming to unlock the potential value of lignocellulosic biomass. In terms of biofuel production, there are to this date about 67 lignocellulosic biorefineries operating worldwide and global market of bioproducts is expected to reach $1128 billion dollars in 2022. Besides, Brazil and the United States are major players, particularly in the biofuel sector (HASSAN; WILLIAMS; JAISWAL, 2019). However, a biorefinery design faces several challenges due to the specific conditions that it must operate in order to reach a minimum of economic feasibility. The choice of suitable feedstocks and the scaling-up of small scales biorefineries design are an important and preliminary step to be tackled by industries and academia (SERNA-LOAIZA; GARCÍA-VELÁSQUEZ; CARDONA, 2019). In light of these challenges, the use of heterogeneous catalysts offers a promising scenario to convert renewable feedstocks into fuels and chemicals, particularly due to the possibility of catalyst regeneration and gains in terms of energy consumption in separation steps. However, the challenges for future biorefineries still rely on the development of active, stable and selective heterogeneous catalysts that should be achieved by combining fundamental with applied research (LIN; HUBER, 2009; S. KIM et al., 2019).

In this scenario of growing biomass prominence, Brazil is in a favourable position for its use due to country's vast biodiversity and its wide availability. Thus, the present project is interested in studying the process of furfural production from xylose

dehydration, integrating the reaction system along with the separation of the product formed, aiming the process intensification.

Chapter 2

Literature Review

Biomass refers to all the degradable and transformable organic materials that can be converted into chemicals and energy. There are different sources of biomass and they can be placed in different categories. One example of category divides biomass into plant resources, microbial sources and municipal solid waste. Plant resources include forest woody feedstocks (soft wood and hard wood) and agricultural residues (SINDHU et al., 2019). The municipal solid waste is a heterogeneous biomass composed of plant and animal products as well as non-biomass combustible materials. They can be utilised for producing a variety of fuels and chemicals (SINDHU et al., 2019). The main approaches for first and second generation biomass conversion are depicted in Figure 2.1.

Figure 2.1: Opportunities for first and second generation biomass conversion.

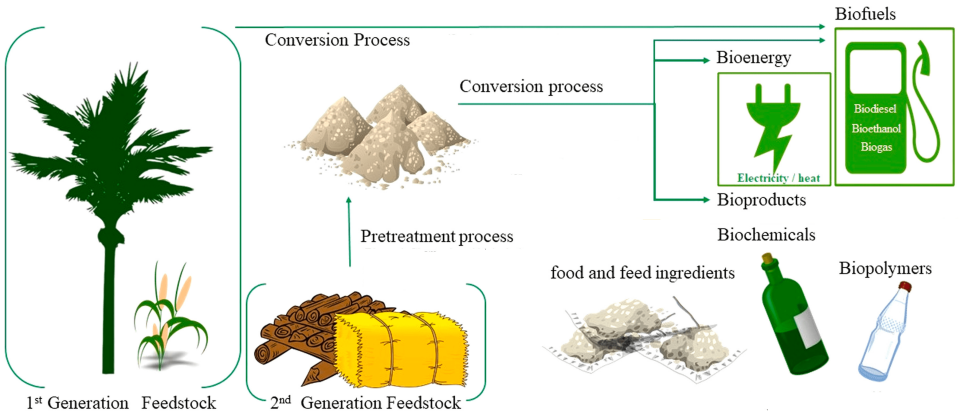

Source: Adapted from Hassan, Williams and Jaiswal (2019).

The use of food crops, in particular, their edible fractions, has caused several controversies due to the "food versus fuel" debate and competitive use of land. Consequently, the first generation of lignocellulosic feedstocks (food crops) has been

continuously replaced by the second generation. The latter includes non-food crops, such as agricultural residues and agro-industrial waste (HASSAN; WILLIAMS; JAISWAL, 2019).

Third generation (marine biomass, especially algae) has also been studied as an alternative non-food feedstock. Bioethanol and biodiesel can be produced by microalgae mostly due to their high lipid content, and rapid growth capacity (SINDHU et al., 2019). However, technical challenges still need to be overcome to achieve feasible conversion technologies along with mastery of cultivation scale-up (HASSAN; WILLIAMS; JAISWAL, 2019).

2.1 Lignocellulosic Biomass

The abundance of lignocellulosic in agricultural residues and waste overcomes "fuel versus food" debate and paves the path for a green and sustainable production of fuels, chemicals and consequently for a reduction in CO_2 emissions (LI; JIA; WANG, 2016). The different routes for converting lignocellulosic biomass are shown in Figure 2.2.

Figure 2.2: Main approaches for lignocellulosic biomass conversion.

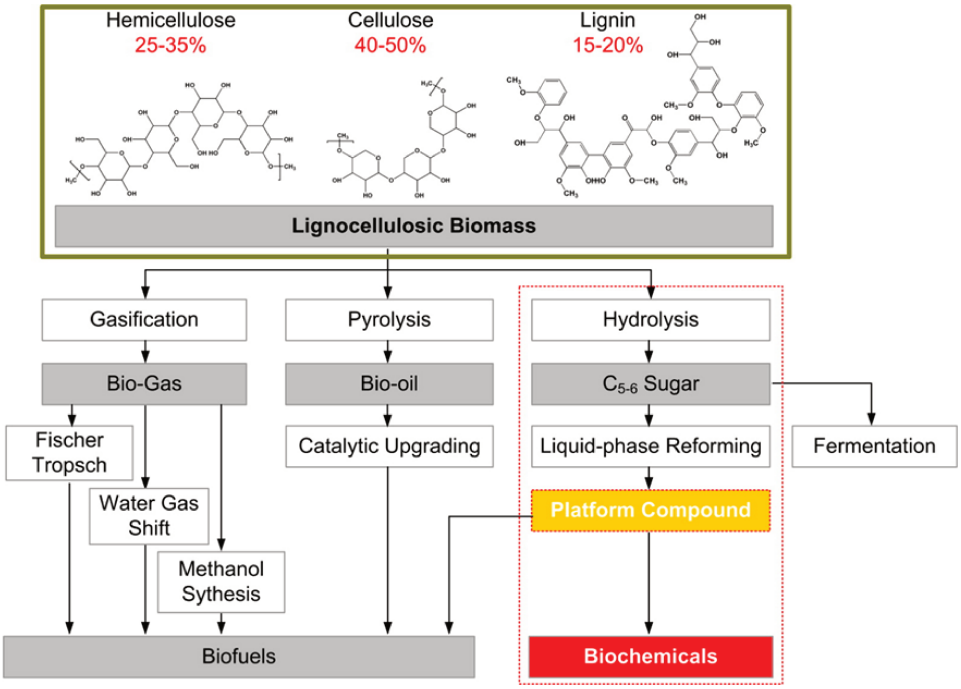

Source: Li, Jia and Wang (2016).

Lignocellulosic biomass is a complex structure containing three different fractions: hemicellulose, cellulose, and lignin. Its composition ranges from about 20-30%

hemicellulose, 40-50% cellulose and 15-20% lignin (LI; JIA; WANG, 2016). In general, physical and chemical steps are involved to separate these biomass fractions, such as milling and acidic hydrolysis. Subsequently, such fractions are commonly submitted to gasification, pyrolysis and hydrolysis processes (ALONSO; BOND; DUMESIC, 2010; LI; JIA; WANG, 2016). Although its vast abundance and possibilities, full lignocellulosic valorisation still remains a challenge mostly due to the releasing of fermentable sugars during lignocellulosic pretreatment and conversion steps (HASSAN; WILLIAMS; JAISWAL, 2019).

Cellulose is the largest fraction of lignocellulosic biomass and the most abundant source of biomass. It is a long-chain polymer composed of D-glucose monomers found in wood, plant leaves and stalks among the other fractions of lignocellulosic biomass. Although it is generally considered a plant material, some bacteria are also found to produce cellulose (SUSHEEL et al., 2011). Even though large quantities of cellulose are available, pretreatment is often required to separate from the complex structure of lignocellulosic biomass. In general, cellulose separation in the pulp and paper industries is performed by steam explosion, mild oxidation, and treatment with dilute alkali (L. DHEPE P.; FUKUOKA, 2008). Steam explosion is an important step of biomass valorisation as it changes its structure by breaking lignin seal and allowing disruption of the crystalline structure of cellulose (Figure 2.3).

Figure 2.3: Scheme of lignocellulosic pretreatment.

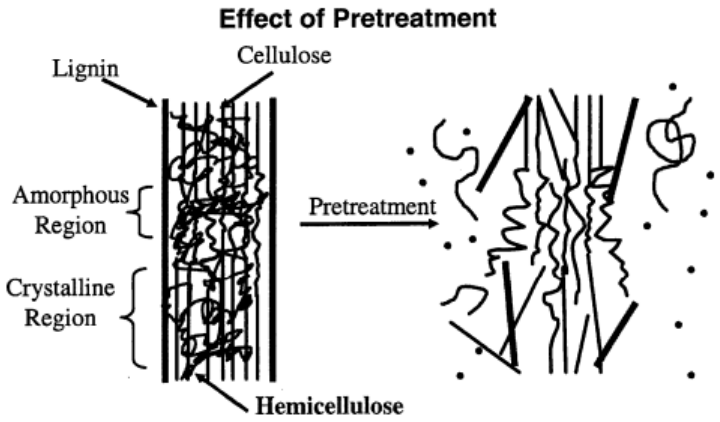

Source: Mosier et al. (2005).

Consequently, this step is responsible for making cellulose more accessible to the enzymes that convert the carbohydrate polymers into fermentable sugars (MOSIER et al., 2005). Along with steam explosion, several pretreatment possibilities have been

investigated, including chemical, biological, and physicochemical methods. However, commonly used pretreatment techniques result in high energy consumption and the formation of undesirable products (HASSAN; WILLIAMS; JAISWAL, 2019).

In this scenario, the development of more efficient pretreatment processes and scalable technologies are essential to economically sustainable biomass valorisation.

Similarly to the other fractions of lignocellulosic biomass, lignin utilisation relies on cost-effective processes for its extraction, conversion and thus valorisation into value-added chemicals or fuels. Extraction is often hampered by the high reactivity of lignin and its fractions, which can undergo repolimerisation (condensation) and form new C-C bonds, generating a wide range of intermediates of different properties (SCHUTYSER et al., 2018). The main processes for lignin extraction include Kraft pulping, sulfite pulping, soda pulping, or hydrolysis by hot water, dilute acid, alkaline, or enzymes (HONGLIANG et al., 2019). Lignin conversion technologies include similar processes to the ones used in petroleum refinery, such as gasification, pyrolysis, hydrocracking, acid, alkali hydrolysis, and oxidative/reductive conversion (HONGLIANG et al., 2019). The Figure 2.4 depicts general strategies for lignin conversion.

The hemicellulose fraction (25-35%) present in lignocellulosic biomass is a complex branched polymer of carbohydrate species such as glucose or xylose, substituted with other sugars: arabinose, xylose, galactose, fucose, mannose, glucose, or glucuronic acid (MOSIER et al., 2005). Pretreatments of hemicellulose include hemicellulases and acids in order to hydrolyze carbohydrate polymer in smaller fractions.

Figure 2.4: Strategies for lignin conversion.

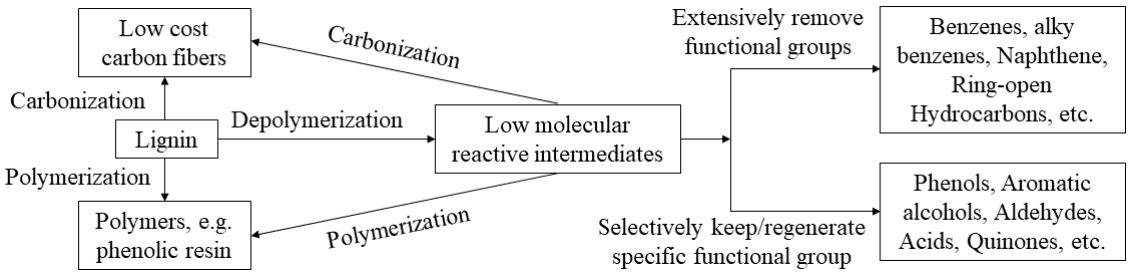

Source: Adapted from Hongliang et al. (2019).

The five or six-carbon sugars resulted from pretreatment steps, such as steam explosion or hot water treatment, are highly promising in terms of producing platform compounds or directly ethanol by fermentation. Xylose (five-carbon) monomers in

particular, which are obtained from hydrolyzed polymeric xylans under mild conditions, can undergo dehydration reactions to form platform molecules, such as furfural, 5-hydroxymethylfurfural (HMF), levulinic acid (LA) (ALONSO; BOND; DUMESIC, 2010; LI; JIA; WANG, 2016; MOSIER et al., 2005; C. WANG et al., 2018).

2.2 Furfural

Furfural ($C_5H_4O_2$, furan-2-carbaldehyde, 2-furaldehyde) is a heteroaromatic furan ring with an aldehyde functional group possessing high solvent selectivity towards aromatics and unsaturated compounds in general. Furfural intermediate polarity, being soluble in both highly polar and non-polar substances, also justifies its direct application as a selective solvent (MARISCAL et al., 2016). The general physical properties of furfural are given in Table 2.1, whereas furfural molecular structure is presented in Figure 2.5.

Figure 2.5: Furfural molecular structure.

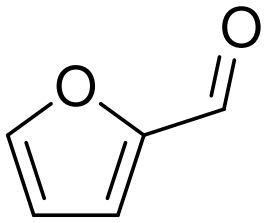

Table 2.1: Physical properties of furfural.

Molecular weight	96.08
Boiling point (°C)	161.7
Freezing point (°C)	-36.5
Density at 25 °C	1.16
Critical pressure, P_c (MPa)	5.502
Critical temperature, T_c (°C)	397
Solubility in water, wt% (25 °C)	8.3
Heat of vaporisation (liquid) (kJ/mol)	42.8
Viscosity, mPa.s (25 °C)	1.49
Heat of combustion at 25 °C (kJ/mol)	234.4
Enthalphy of formation (kJ/mol)	-151
Autoignition temperature (°C)	315

Source: Yan et al. (2014).

Although furfural can be produced from fossil-based raw materials by catalytic oxidation of 1,3-dienes, the production of furfural by biomass-based routes in lignocellulosic biorefineries is way more competitive in economic terms for its use in

polymer, fuel, agricultural and pharmaceutical industries (CHHEDA; ROMÁN-LESHKOV; DUMESIC, 2007; MARISCAL et al., 2016). The market of furfural is estimated to be 300,000 ton globally, however, three different countries account for approximately 90% of its production: China (70% of total production capacity), Dominican Republic and South Africa (MARISCAL et al., 2016).

Furfural is also a promising platform molecule (or building-block) that can be subjected to various catalytic processes, such as decarboxylation, selective hydrogenation, oxidation, and hydrogenolysis, in order to obtain fuels and compounds of interest (Figure 2.7). In terms of fuels, two of the potential compounds produced from the hydrogenation reaction of furfural are 2-methylfuran (2-MF) and 2-methyltetrahydrofuran (2-MTHF), which after being subjected to further treatments are converted into conventional fuels. The value-added compounds, such as valerolactone, 1,5-pentanediol, cyclopentanone, dicarboxylic acids, butanediol, and butyrolactone, are essentially obtained by selective hydrogenation and/or hydrogenolysis sequences in the case of C_5 compounds, whereas the C_4 undergo a first step of selective oxidation of furfural (LI; JIA; WANG, 2016). The interest in the use of furfural has also been demonstrated by the increasing number of publications containing the word furfural in their titles year after year (Figure 2.6).

Figure 2.6: Number of published articles containing "furfural" in title.

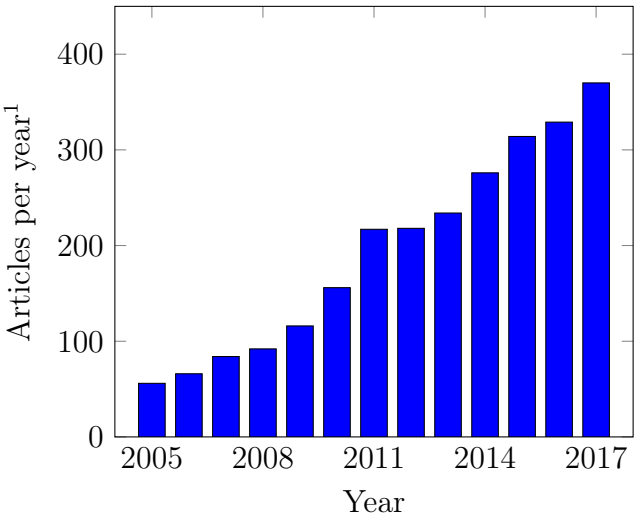

The main product obtained from furfural is furfuryl alcohol (FA). Its production corresponds to approximately 65% of all furfural use where the latter is

[1]Data obtained from *Google Scholar*, accessed on 26th of April 2018.

hydrogenated in liquid or gas phase reactions using mainly Cu, Co, Ni, Pd, Pt based catalysts (LI; JIA; WANG, 2016; MARISCAL et al., 2016).

Figure 2.7: Furfural-derived chemicals and biofuels.

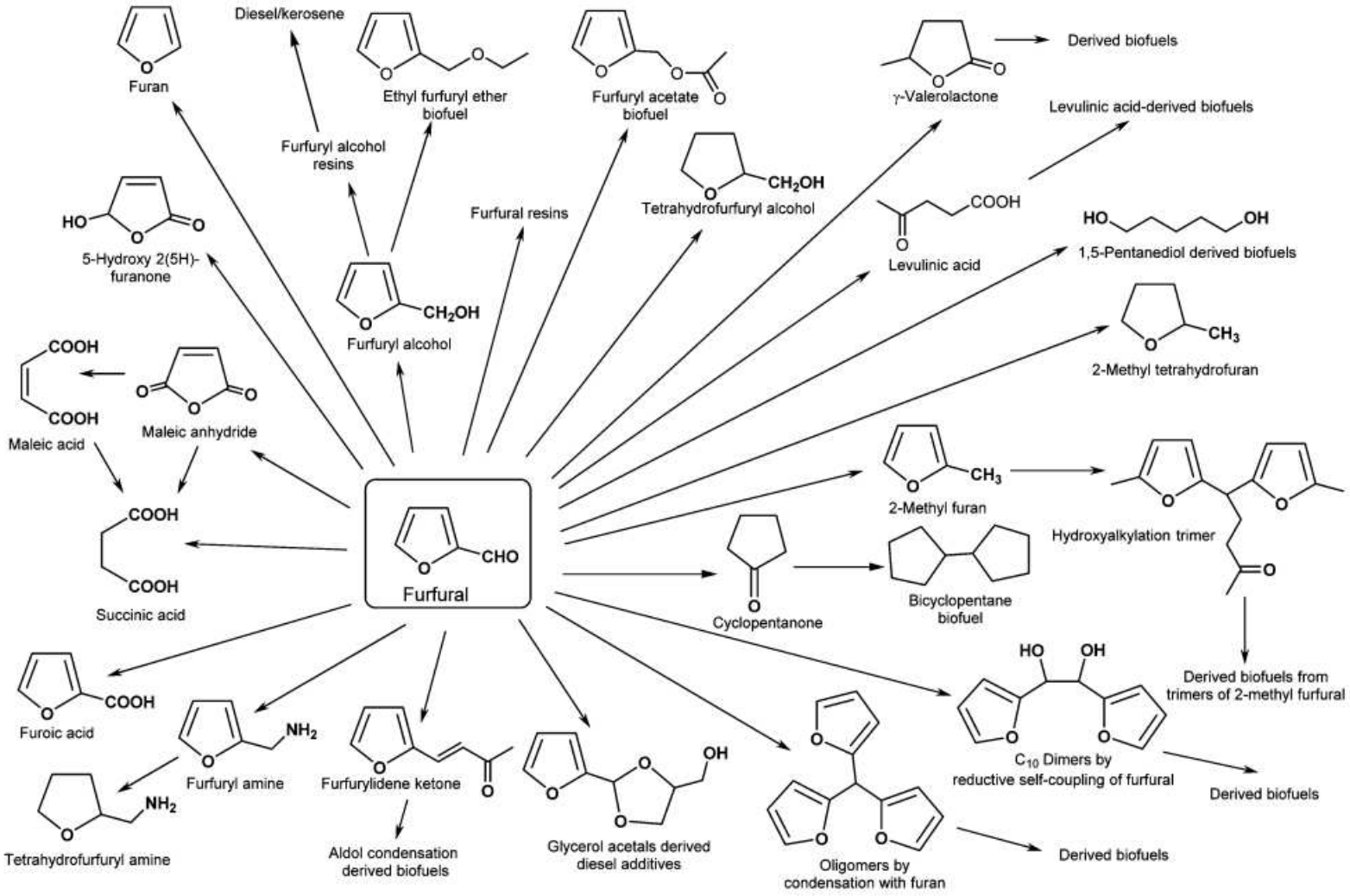

Source: Mariscal et al. (2016).

2.2.1 Furfural Production Processes

Quaker Oats Batch Process

The first industrial process of producing furfural known as "Quaker Oats" came out in 1921, and it is until now industrially used. It was first employed using xylan (polysaccharide composed essentially of xylose units) present in the hemicellulosic fraction of lignocellulosic biomass. However, this process faces both environmental and cost obstacles. Notably the use of acidic and corrosive homogeneous catalysts, especially sulphuric acid, and a low yield of furfural, hamper post-processing during the separation step (LI; JIA; WANG, 2016).

The Quaker Oats process was a batch-type process where sulphuric acid, water, and raw material are added to a mixer and then fed to the reactors. The downstream step includes an azeotropic distillation column; a decanter due to the limited solubility of furfural in water and; two columns for low boilers recovery and furfural dehydration, respectively (ZEITSCH, 2000a). The Quaker Oats batch process is presented in Figure 2.8.

Figure 2.8: The Quaker Oats batch process. 1-Mixer, 2-Reactor, 3-Screw Press, 4-Secondary Steam Generator, 5-Azeotropic distillation column, 6-Decanter, 7-Condenser, 8-Recovery column for low boilers, 9-Furfural dehydration column, HPS-High pressure steam, LPS-Low pressure steam.

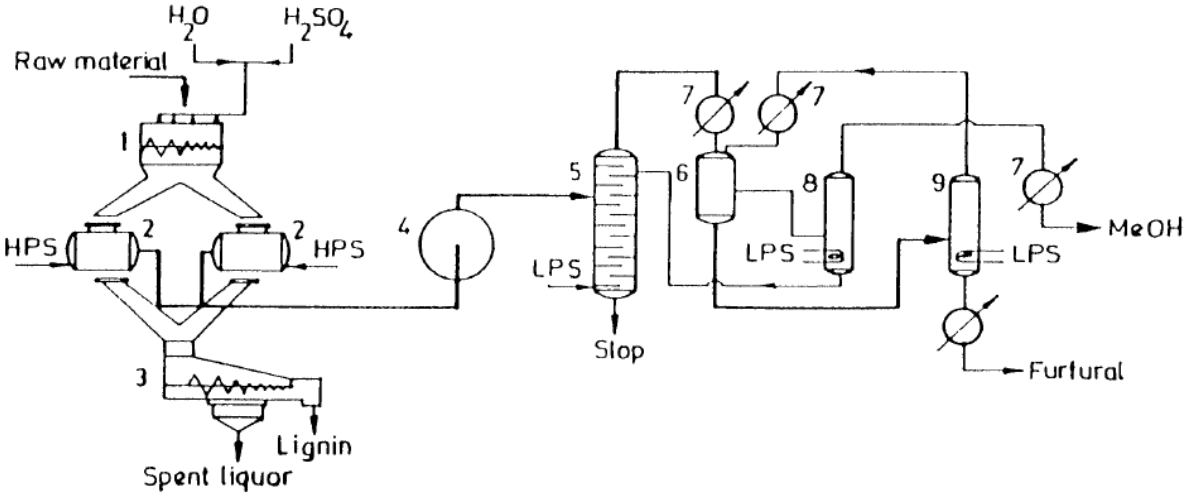

Source: Zeitsch (2000a).

Although it is still used to this date, the Quaker Oats batch process faces various disadvantages, such as long residence time because of the low temperature required to avoid degradation, high requirement of sulphuric acid, special measures

against corrosion, an extremely acid residue, high consumption of water vapour (ZEITSCH, 2000a).

Agrifurane Batch Process

The Agrifurane process, also named Petrole Chimie, is a batch process that uses several reactors in series. The initial feed slurry is formed from a mixture of raw material and the filtrate of a belt filter press and possess a solid-liquid ratio of 1:6 by weight. The latest Agrifurane process has reduced sulphuric acid consumption and uses about 1% of this catalyst, which is attained by its recovery in the filtrate after belt filter press step. Thus, the feed slurry is composed of raw material and recycled filtrate. Primary and secondary steam are fed into the first reactor to attain 177 °C (9.35 bar), while the second reactor is fed with steam from the first one, and so forth. Eventually, some primary steam is added to the second reactor in order to make up for the pressure loss. In the last reactor the temperature is around 161 °C (6.34 bar) (ZEITSCH, 2000a).

Although its reduced consumption of homogeneous catalyst, a large quantity of steam is also necessary for this process. Along with these disadvantages, it is also worth mentioning the high cost of investment, including the valve control system for the purpose of giving each charge the same treatment, the belt filter press for dewatering the residue and a drier to make the belt filter cake burnable. Because of that, this process is considered obsolete these days (ZEITSCH, 2000a).

Quaker Oats Continuous Process

A few decades after designing Quaker Oats batch process, a continuous process was developed. The furfural yield in this process was about 55% and a residence time of one hour. Although the continuous process enhanced significantly compared to the batch one, the use of sulphuric acid was still a drawback, as no-acid attempts led reactor jamming because of insufficient softening of the raw material (bagasse). In addition to some technical drawbacks, the declining interest of the parent company Great Lakes in the furfural market and unfortunate relationships between Quaker Oats and bagasse supplier led the plant to cease operation in 1997 (ZEITSCH, 2000a).

Escher Wyss Continuous Process

In the Escher Wyss process, the raw material is fed on the top of a fluid bed system and descends inside a central pipe, as depicted in Figure 2.9. Sulphuric acid is sprayed inside the central pipe, forming a 3% catalyst moist. The steam is injected on the bottom of the system, maintaining the feed in a fluid bed state as it reaches the central pipe, where hydrolysis and dehydration reactions take place (ZEITSCH, 2000a).

Figure 2.9: The Escher Wyss continuous process.

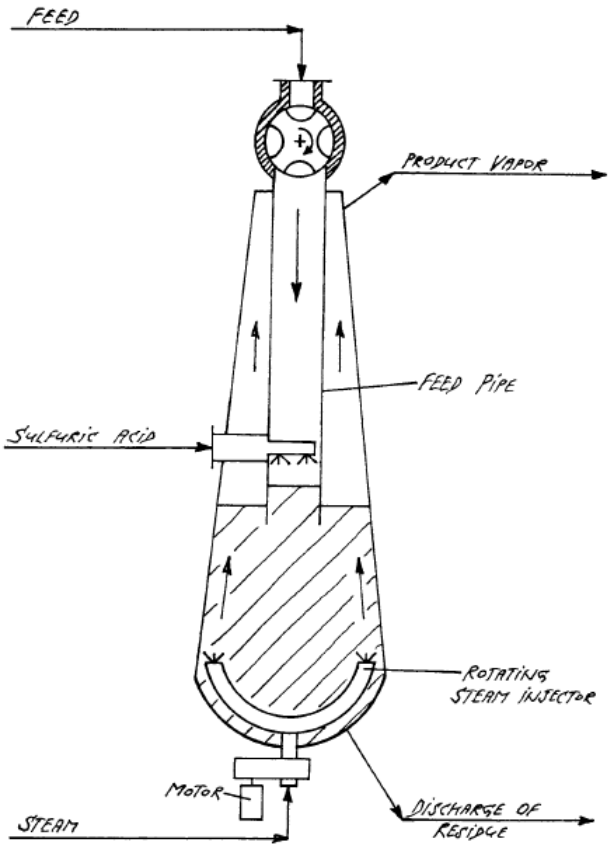

Source: Zeitsch (2000a).

The Escher Wyss process is no longer used and presented some various disadvantages, such as intense corrosion caused by acid spray at the operating temperature; sensitivity of steam flow, causing the fluid bed either to collapse or to be carried out upward (ZEITSCH, 2000a).

Rosenlew Continuous Process

The Rosenlew continuous process can be viewed as a stripping column energised by hot steam injection (10 bar) on the bottom and raw material (bagasse)

injection on the top. The higher carboxylic acids formed during the reaction and other acids (acetic acid and formic acid) contribute to the autocatalytic aspect of Rosenlew process (ZEITSCH, 2000a). The furfural along with volatile products are carried by steam flowing in counter-current mode and leave the top of the column for downstream processing (Figure 2.10).

Figure 2.10: The Rosenlew continuous process.

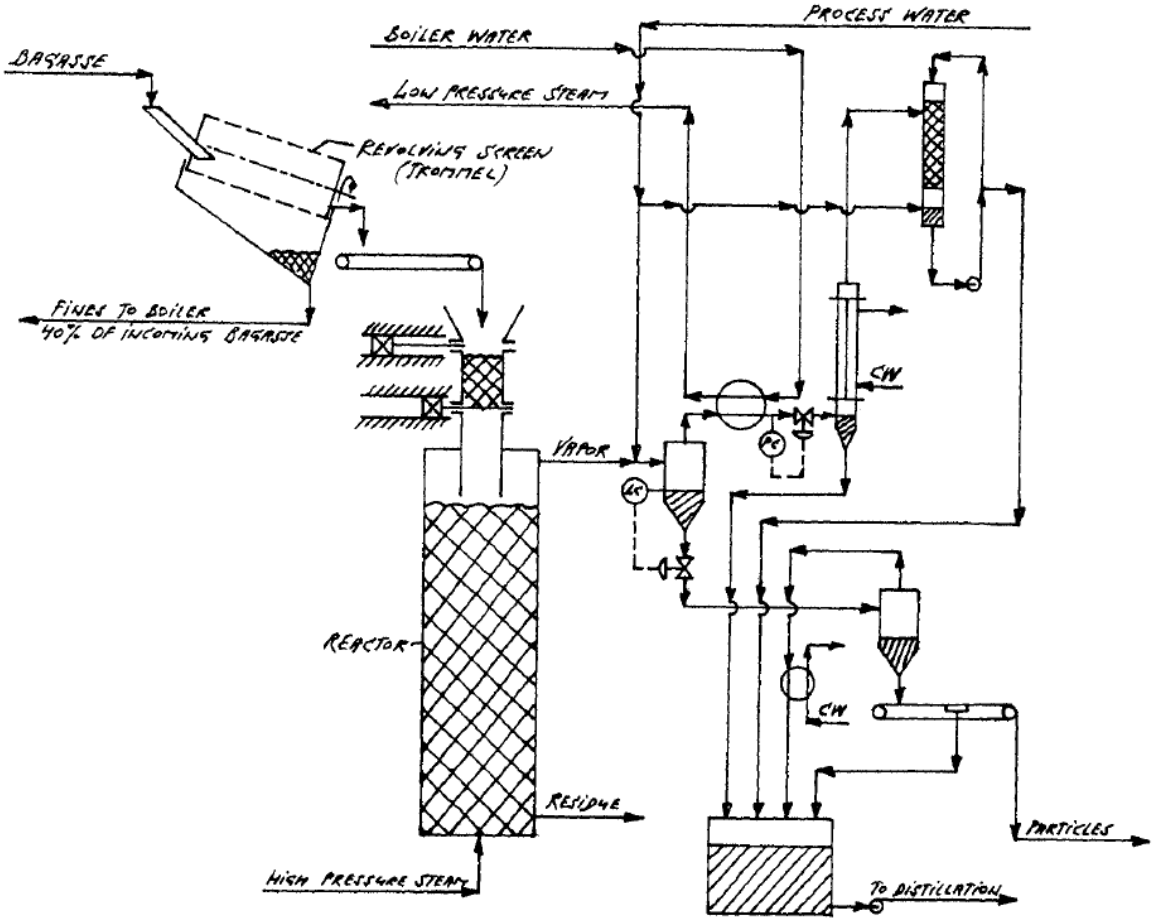

Source: Zeitsch (2000a).

In addition to chemical complications during Rosenlew process, mass transfer resistance also hampers the overall performance of the column for the following reasons:

- Non uniform acid concentration throughout the reactor and formation of a vertical profile. The acids formed during the reaction are carried to the top by steam flow, which leads to acid condensation over incoming particles and increases acid concentration. Consequently, the acid concentration is approximately zero at the bottom and increases upward.

- Furfural has also a vertical concentration profile. As furfural is formed mostly downward the column inside the particles and is stripped upward by steam, the opposite behaviour occurs upward, where acid concentration is lower. At the top, furfural is condensed on cold incoming raw material and enters the particles by diffusion, thus decreasing its concentration in vapor phase.

- Rosenlew process has no injection of acid in the feed stream. In this scenario, the startup process can take a long time (days) before "triggering" the autocatalytic process. Eventually, external acid addition can be made to accelerate startup operation and to reach steady-state.

- The process is sensitive to steam input. If steam input is relatively low, secondary reactions can take place as furfural is not efficiently stripped and thus furfural yield is reduced. On the other hand, high steam input results in acid stripping along with furfural, affecting the rate of reaction throughout the column.

Supratherm Process

Supratherm is a continuous process operating at temperatures between 200 and 240 °C. Bagasse is initially mixed with sulphuric acid solution recycled from the belt filter press in order to form a flowable slurry. The latter is pumped into the reactor where hot steam (230 °C) is also injected to rapidly cause temperature increase and hydrolysis. The reacted pulp is fed into a cyclone where vapor product is rich in furfural, water, and organic acids whilst the bottom product is recovered for further recycling. The vapor product containing furfural is fed to the first distillation column which operates at reduced pressure (ZEITSCH, 2000a).

The Supratherm process is an effective continuous process due to its advantages compared to other processes, such as a continuous operation mode guaranteed by small quantities of water and sulphuric acid required in the make-up current; short residence time and high temperatures avoiding condensation and resinification reactions and; high quality of the vapor fraction, meaning high furfural concentration and absolutely free of particles. However, the most significant disadvantage is the high cost for the investment and maintenance of the belt filter press and drier (ZEITSCH, 2000a).

SupraYield Process

In the SupraYield process, a thermally insulated reactor (1) is charged with raw material acidified or not (the reaction can take place without the addition of external acids, that is, the reaction is autocatalysed by organic acids) and heated by hot steam injection through valve (2) while valves (3) and (4) remain closed. In order to maximise mass transfer rate of furfural from liquid to vapour phase immediately after its formation, SupraYield process approach is to maintain reaction medium in a constant state of boiling. Thus, furfural loss is reduced as its concentration in liquid phase remains small enough to avoid side/degradation reactions (ZEITSCH, 2000a).

Figure 2.11: The SupraYield process.

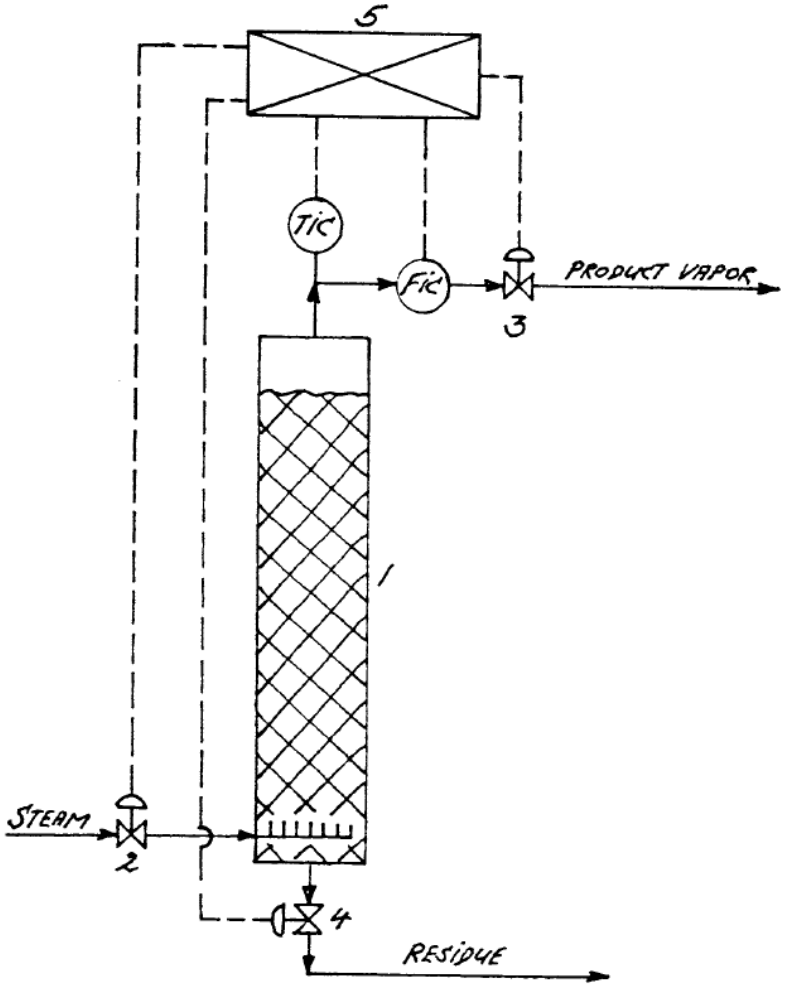

Source: Zeitsch (2000a).

When charge moisture is increased by direct contact with steam, valve (3) is partially opened (gradual decompression) in order to produce a steady flow of vapour product on the top and cause a slow drop in temperature. During the very short heating

process, the steam condenses, thus increasing the moisture content of the charge. Then, valve 2 is closed and a leaking valve 3 is opened so as to produce a steady small flow of product vapour by gradual decompression. This causes a slow drop in temperature. When the desired temperature is reached, valve (3) is closed to end first "delayed decompression". This procedure is continuously repeated while furfural is still being produced, otherwise, digestion is complete by opening valve (4) to discharge residue. Moreover, the valve operations are controlled by automatic control (5) (ZEITSCH, 2000a).

Scenario and Conclusion

The process intensification of both furfural production and separation has become a promising approach. Most industrial processes for furfural production described in the literature use homogeneous catalysts (notably sulphuric acid) and deal with costly separation steps and corrosion issues. With the interest of overcoming such difficulties, the use of heterogeneous catalysts for lignocellulosic biomass conversion has become an interesting choice (LIN; HUBER, 2009), which can be applied to the xylose dehydration to increase furfural yield and reduce separation costs (LI; JIA; WANG, 2016). In addition to the advantage in terms of separation by the use of heterogeneous catalysts, several studies have been investigating the issue concerning the separation step after the dehydration reaction of xylose, either by using different solvents in reaction medium (HU et al., 2014) or by furfural stripping from liquid phase immediately after its formation.

Most important industrial processes for furfural production are presented in Table 2.2 along with their main parameters. The review of the most relevant furfural process is an important step of process research and design towards a sustainable and economically feasible process for the near future. Accordingly, the following Sections of this literature review will focus on catalysts, solvents and integrated processes for furfural production.

Table 2.2: Processes for furfural production.

Process name	**Process type**	**Temperature (°C)**	**Catalyst**	**Substrate**	**Furfural yield (%)**
Quaker Oats	Batch	153	H_2SO_4	Oat hulls	≤ 50
Quaker Oats	Continuous	184	H_2SO_4	Bagasse	55
Agrifurane	Batch	161-177	H_2SO_4	N/A	N/A
Escher Wyss	Continuous	170	H_2SO_4	Corncob	N/A
Rosenlew	Continuous	N/A	Carboxylic acids	Bagasse	N/A
Zeitsch/SupraYield	Continuous	240	H_2SO_4	N/A	50-70
Supratherm	Continuous	200-240	H_2SO_4	Bagasse	N/A

Source: Zeitsch (2000a). (N/A: Not available)

2.3 Reactive Separation Processes

According to Stankiewicz and Moulijn (2000), one important trend in today's industry is process intensification. Process intensification consists in the development of innovative equipment and techniques that result in significant improvements in chemical manufacturing and processing, leading to lower energy consumption, decrease in the waste formation and more sustainable processes and technologies.

Multi-functional reactors can be seen as a reactive unit, usually, a reactor, integrated with one or multiple unit operations. In the case of a reactive separation, several possibilities are available: reactive distillation or stripping, reactive extraction, reactive crystallisation, chromatographic reactors, reverse-flow reactors, periodic separating reactors (STANKIEWICZ; MOULIJN, 2000).

Reactive or catalytic distillation has gained increasing attention over the past years because of its demonstrated potential to enhance overall process performance, notably capital productivity and selectivity, reduced energy cost and reduction of solvent use. In general, reactive separation is employed to overcome either separation or reacting limitations. Some of the advantages include using reaction to improve separation, which is the case for azeotropes or reacting away undesired contaminants; or using separation to tackle reaction limitations, such as equilibrium limitations, improving selectivity, or removing catalyst poisons (MALONE; DOHERTY, 2000). In the case of processes where one or more reactants or products are degraded by operating close to their boiling temperature, it is suggested to operate similarly to a stripping column, which gives more freedom in the choice of operating temperature and pressure, and in the concentrations and feeding points of the liquid reactants (SCHILDHAUER et al., 2005).

Stripping is defined as a process in which the contact between a liquid mixture and a vapour phase results in selective removal of components from the liquid phase to the vapour phase through mass transfer effects. In general, stripping columns are employed along with absorption columns as a way to regenerate and recycle the absorbent. Both stripping and absorption process have techniques and design procedures widely known and industrially applied, mainly because of concerns regarding the control of pollutants emissions. In these processes, the phenomena involved may be both physical and chemical, since there may be a chemical reaction between the solute and the absorbent (SEADER; HENLEY; ROPER, 2010).

The reactive stripping process can also be conducted and applied industrially. Yu, Zhou and Tan (1997) simulated a multi-stage catalytic stripping system for the production of bisphenol-A from acetone and phenol. In this process, N_2 is employed as the carrier gas and an ion exchange resin as a solid catalyst forming a gas-liquid-solid system. In addition, the non-equilibrium model proposed by Yu, Zhou and Tan (1997) showed good agreement with experimental values and was more rigorous than the quasi-homogeneous liquid-solid model.

Kumar et al. (2013) investigated reactive stripping for catalytic exchange of hydrogen isotopes in a tickle-bed reactor (TBR), as depicted in Figure 2.12. Aiming the conversion of HDO to HD, the process was subdivided into two steps occurring within the same equipment: (*i*) hydrogen-deuterium oxide (HDO) change from liquid to gas phase and; (*ii*) reaction of HDO with H_2 to form hydrogen deuteride (HD) and H_2O in the presence of a Pt-C-PTFE catalyst. The proposed TBR reactor has an advantage over the conventional isotopic exchange method because it uses only one unit to perform the catalytic reaction and to perform mass transfer between the gas and liquid phases. Furthermore, it was found that, among the reactor operating parameters, the temperature is the one with the greatest influence on the system performance and its optimal values are between 80 and 90 °C; the optimum gas to liquid flow rate ratio values are between 1.2 and 1.5 of the minimum ratio.

Figure 2.12: Experimental setup used by Kumar, Mohan and Mahajani (2013).

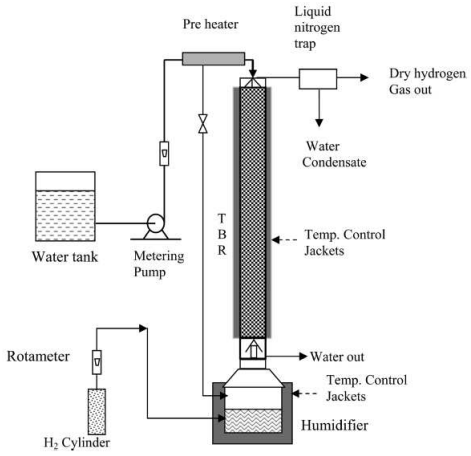

Source: Kumar, Mohan and Mahajani (2013).

In order to increase the efficiency of the furfural production process, the integration of reaction with the separation steps would result in significant progress compared to the current production processes employed industrially. However, studies

regarding continuous reactive separation processes for furfural production are scarce in the literature (METKAR et al., 2015).

In this scenario, Yang et al. (2013) investigated the reactive extraction process of furfural produced from xylose dehydration in a batch reactor, using formic acid as homogeneous catalyst and ortho-nitrotoluene as co-solvent. Formic acid concentration, temperature, volumetric percentage of co-solvent and residence time were the parameters investigated and, in the optimal condition, furfural yield achieved 71% and selectivity greater than 90%. Furthermore, it was found that the addition of halides, regardless of concentration, increased furfural yield and selectivity.

Agirrezabal-Telleria, Gandarias and Arias (2013) investigated the production of furfural from pentosan-rich biomass and xylose. In their study, a furfural production simulation was built in Aspen Plus using N_2 as the stripping agent in order to economically evaluate the process and compare to current steam-stripping process. In their simulation, two blocks were utilised to simulate this process: a reactor based on reactant conversion was followed by a flash separator to strip nitrogen from liquid phase. In summary, a cost reduction of approximately 60% can be reached by using N_2 as the stripping agent.

Metkar et al. (2015) studied the furfural production by means of a reactive distillation process using a solid acid catalyst. In the experiment, the mixture of water, xylose, and sulfolane (co-solvent) was fed in liquid phase at the top of the column, where it descends towards the catalytic bed for xylose dehydration and furfural formation, as shown in Figure 2.13. The produced furfural is carried to the top of the column by the carrier gas (N_2 and steam). At the base of the column, N_2 and steam are fed and the remaining unreacted xylose is collected in a container, together with sulfolane and secondary products. This study represents the first work demonstrating the concept of continuous reactive distillation for furfural production, using sulfolane and acid catalysts. The highest furfural yield (75%) was obtained with a xylose feed and a H-mordenite type zeolite ($Si/Al = 10$) catalyst bed under 175 °C. It was also remarked that steam increased furfural recovery on the top of the column, although its use could difficult further separation steps.

Figure 2.13: Scheme of experimental setup used by Metkar et al. (2015).

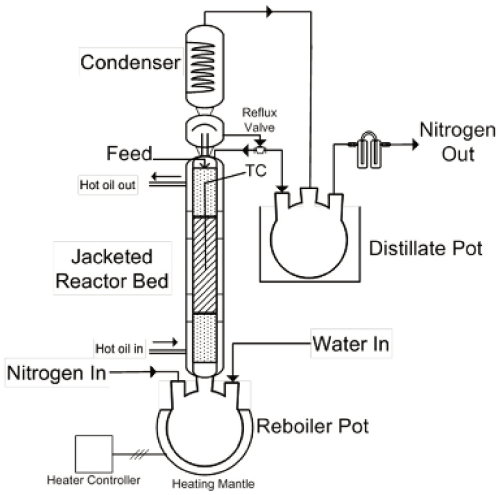

Source: Metkar et al. (2015).

Krzelj et al. (2019) investigated by experiments and modelling the use of hydrogen as non-condensable stripping agent for the production of furfural using sulphuric acid as catalyst. In addition to considerable energy savings obtained, further energy integration could also be performed by furfural hydrogenation to produce value-added chemicals. Based of thermodynamic and kinetics information, a first-principle reactor model was successfully developed to describe experimental results, which was also used to optimise a continuous process of furfural production. In the case of batch experiments with continuous nitrogen stripping, a maximum furfural yield of about 72% was achieved.

2.4 Furfural Production

The dehydration of xylose carried out in most industrial processes for furfural production uses mineral acids such as sulphuric acid, phosphoric acids in aqueous medium as homogeneous catalysts. However, furfural production has been investigated over the past years by several different routes, including in the absence of catalysts or in the presence of homogeneous or heterogeneous catalysts (DELBECQ et al., 2018). The general mechanism of xylose conversion to furfural can be expressed in a simplified way, as depicted in Figure 2.14.

The following review will tackle these three main routes (absence of catalysts, homogeneous and heterogeneous catalysts), especially by heterogeneous catalysis which is the focus of this work.

Figure 2.14: Simplified reaction network for D-xylose.

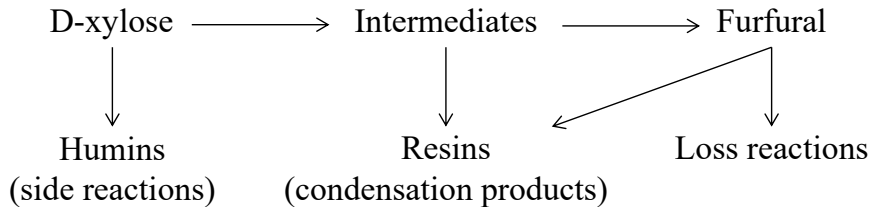

Source: Adapted from Marcotullio and De Jong (2010).

2.4.1 Production of Furfural Without Catalysts

Xylose dehydration to furfural takes place in acidic conditions, which is the reason why most authors have been investigating homogeneous and heterogeneous acid catalysts. However, by-products formed during xylose dehydration, such as carboxylic acids, can also autocatalyse the reaction. Thus, hot water pretreatment under catalyst-free conditions can generate acids to enhance xylose dehydration to furfural (MARISCAL et al., 2016; DELBECQ et al., 2018).

Production of furfural from sugars or native biomass, such as wheat straw, in critical solvents has been investigated by Gairola and Smirnova (2012). Under catalyst-free conditions, furfural was simultaneously obtained from 4% D-xylose and extracted by supercritical CO_2 yielding about 68% at 230 °C, pressure of 12 MPa, and CO_2 flow rate of 3.6 g/min.

Although xylose dehydration can be conducted in the absence of catalysts, the latter is a more promising path towards selective and economically feasible furfural production.

2.4.2 Production of Furfural Using Homogeneous Catalysts

Homogeneous catalysts are dissolved in reaction medium, which facilitates the interaction with the substrate. Consequently, one of the most relevant drawbacks of using homogeneous catalysts is catalyst recovery and product separation from reaction media. Dehydration of xylose using homogeneous catalysts have been investigated in the presence

of mineral acids (H_2SO_4, HCl, H_3PO_4), organic acids, and metal salts (DELBECQ et al., 2018).

Mineral acids are seldom used alone in aqueous reaction media. Several studies have been investigating the use of inorganic salts as reaction promoters; the use of appropriate co-solvents to decrease side reactions and facilitate furfural extraction, and the heating by microwave technology.

Choudhary, Sandler and Vlachos (2012) investigated xylose dehydration in a biphasic and a monophasic system containing HCl, $CrCl_3$ and both HCl/$CrCl_3$. It was found that under appropriate proportions of both Brønsted (HCl) and Lewis ($CrCl_3$) acids furfural yield can reach about 76% in a biphasic system composed of water and toluene. On the other hand, isolated HCl or $CrCl_3$ in the same system yielded 26.7% and 34.5%, respectively. In the presence of HCl and $CrCl_3$, both acids play an important role: (*i*) Lewis acid ($CrCl_3$) is responsible for the isomerisation of xylose to xylulose and (*ii*) Brønsted acid (HCl) dehydrates xylulose to furfural (Figure 2.15). Although Brønsted acid isolated could lead to furfural formation, the energy barrier is higher in this reaction path.

Figure 2.15: Schematic pathway to produce furfural from D-xylose in the presence of single Brønsted acid catalysts or both Lewis and Brønsted acid catalysts.

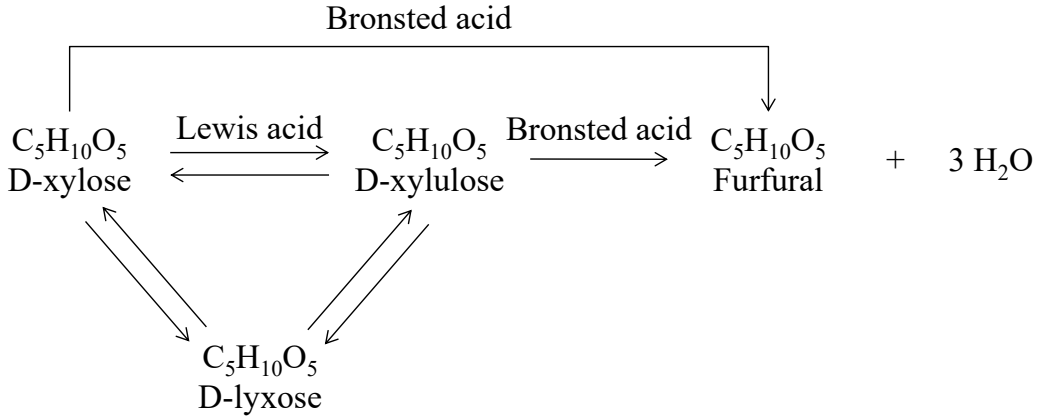

Source: Adapted from Choudhary, Sandler and Vlachos (2012).

The effect of chloride salts addition to H_2SO_4 and HCl was studied by Marcotullio and De Jong (2010). It was found that Cl^- could enhance xylose dehydration to furfural in acidic solutions under $170 - 200\,^{\circ}C$. Kinetics experiments at $200\,^{\circ}C$ showed that the addition of 2.5 wt.% KCl to HCl enhanced furfural yield from 68.7 to 74.1%, whilst 3.5 wt.% NaCl addition to H_2SO_4 had an even higher increase in

yield, from 61.4 to 75.3%. According to the authors, this result indicates that a particular step of xylose dehydration is catalysed by both H^+ and Cl^- to form a 1,2-enediol intermediate, which is represented by species (2) in Figure 2.16. The 1,2-enediol intermediate (2) can either react in presence of H^+ to form furfural or equilibrate with both aldo (1) and keto (3) form of the sugar.

Figure 2.16: Mechanism of furfural formation from xylose.

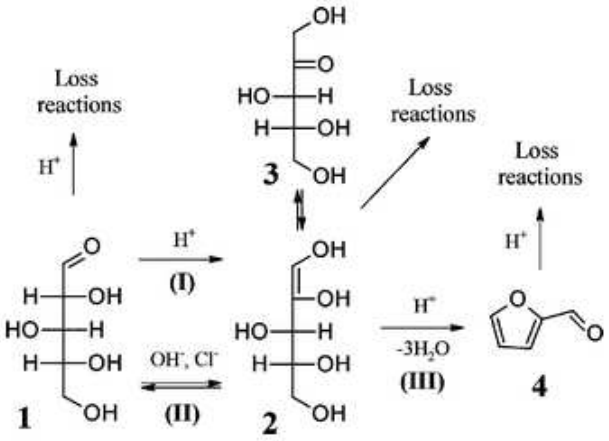

Source: Marcotullio and De Jong (2010).

Junior and Donate (2015) investigated rapidly microwave heating to the reaction temperature. The quick decrease to room temperature could avoid species degradation since reactant and product are not stable at high temperatures in which reaction occurs. Furfural yield achieved 64% at 200 °C after 10 min in aqueous HCl solution (4 mg/mL), with 95% of D-xylose being converted.

Yemiş and Mazza (2011) compared different acid catalysts under microwave-assisted reaction heating, including mineral (HCl, H_2SO_4, H_3PO_4, HNO_3) and organic acids (HCOOH, CH_3COOH) for the conversion of xylose, xylan and straw into furfural. It was found that HCl (Brønsted acid) had higher performance (furfural yield from xylose) compared to the other acids under similar reaction conditions.

2.4.3 Production of Furfural Using Heterogeneous Catalysts

Heterogeneous catalysis consists of at least two different phases, which usually corresponds to solid catalysts containing active centres and liquid/gas reactants and products.

Most studies concerning the mechanism of furfural production using heterogeneous catalysts are focused on the cyclodehydration that involves the release of three water molecules (MAMMAN et al., 2008; YAN et al., 2014; LI; JIA; WANG, 2016). In the presence of Lewis acid sites, the dominant pathway is xylose isomerisation to xylulose (CHOUDHARY; SANDLER; VLACHOS, 2012) (Figure 2.15).

The presence of Lewis acid sites is responsible for conducting the reaction to the xylose-xylulose-furfural pathway, which is faster than the xylose-furfural direct pathway with the use of Brønsted acid sites only. However, the first path also requires Brønsted sites to catalyse the dehydration of xylulose in furfural and increase the yield of furfural (CHOUDHARY; PINAR, et al., 2011). According to Li, Jia and Wang (2016), the optimal ratio of Lewis and Brønsted acid sites (LAS/BAS) ranges from 30 to 80%, since high LAS/BAS ratios favour the formation of carbon by-products due to high conversions and; low LAS/BAS ratios would increase undesired polymerisation reactions.

In this scenario, the heterogeneous catalysts tested for the xylose dehydration reaction are mostly composed of silica, zeolites, phosphates, ion exchange resins, and oxides (PRASENJIT; LAXMIKANT, 2016).

Bhaumik and P. L. Dhepe (2017) studied several metal oxides (WO_3, MoO_3, Ga_2O_3) catalysts supported on silica prepared by sol-gel method and isolated silica in the synthesis of furfural directly from lignocellulosic biomass (isolated xylans and crop wastes). Among the catalysts tested, the highest furfural yields ranged from 72 to 87% and were obtained from crop wastes conversion using either WO_3/SiO_2 or Ga_2O_3/SiO_2 under a biphasic system of water/toluene (60 mL; 1:2 v/v), 170 °C and 8 h. The performance of both WO_3/SiO_2 and Ga_2O_3/SiO_2 was attributed to the high acidity of these catalysts, specially high metal oxide dispersion and silicotungstic acid type species anchored on the WO_3/SiO_2 surface in the case of WO_3/SiO_2 catalyst.

Zeolites have also been studied for furfural production from xylose (MOREAU et al., 1998; O'NEILL et al., 2009). By changing the composition ratio (Si/Al) and preparation conditions, a desired acidity and structure of zeolite catalysts can be achieved. Moreover, pore size plays an important role during xylose dehydration. Pore sizes smaller than xylose (6.8 Å) and furfural (5.7 Å) molecules can inhibit their diffusion, whilst larger pore sizes facilitate rearrangement of furfural to undesired larger molecules (O'NEILL et al., 2009; LI; JIA; WANG, 2016).

Moreau et al. (1998) investigated xylose dehydration in the presence of microporous catalysts such as H-Y faujasites and H-mordenites in a solvent mixture composed of water and either toluene or methylisobutylketone as co-solvent (1:3 by volume) at 170 °C. Under similar operating conditions, H-mordenite with a Si/Al ratio of 11 was found to be more selective for the formation of furfural from xylose than H-Y faujasite with a Si/Al of 15. Furfural selectivity was 90 and 82% for mordenite and faujasite, respectively. The authors attributed the lower selectivity of H-Y faujasites to the presence of larger cavities within its structure (up to 13 Å), which allows further rearrangement of furfural or degradation into secondary products. On the other hand, selective mordenites had pore sizes no larger than 6.5 x 7.0 Å.

O'Neill et al. (2009) studied the kinetics of aqueous phase dehydration of xylose into furfural catalysed by ZSM-5 zeolite at 413, 433, 453, 473, and 493 K (helium atmosphere at 30-50 bar). The reaction scheme is represented by a series of elementary steps which involve xylose isomerisation, and xylose/lyxose dehydration to form furfural and two main side reactions that lead to organic acids and solid species. The average pore size of about 1.2 nm (12 Å) allowed oligomerisation of furfural by aldolic condensation, which cannot easily escape pore network and thus remain as solid deposits on the catalyst. Moreover, organic acids (mostly formic acid) also dehydrate to form carbonaceous deposits. The reaction network proposed by these authors is shown in Figure 2.17.

Figure 2.17: Reaction network for xylose dehydration to furfural (O'NEILL et al., 2009).

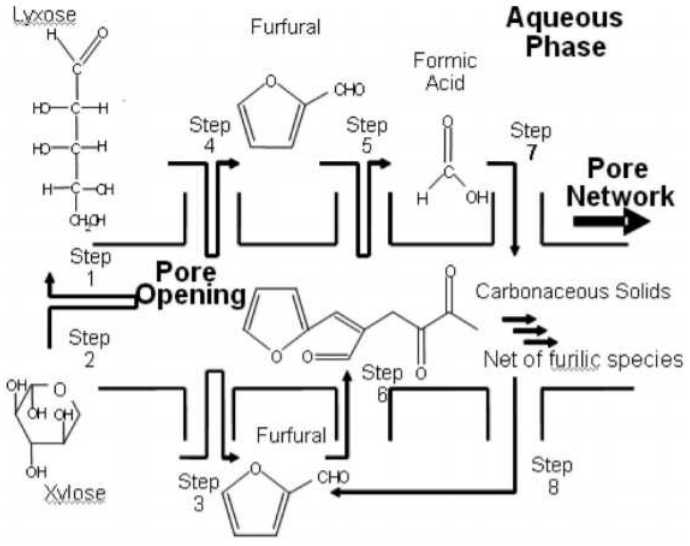

Source: O'Neill et al. (2009)

The reaction network proposed by O'Neill et al. (2009) include: xylose isomerisation to lyxose (apparent rate constant k_{f1}); lyxose conversion to xylose (k_{f2}); xylose conversion to furfural (k_{f3}); lyxose conversion to furfural (k_{f4}); formation of acids from furfural (k_{f5}); formation of two- and tridimensional furilic oligomers (T-T-DF) from furfural (k_{f6}); formation of T-T-DF from acids (k_{f7}) and; furfural formation from T-T-DF (k_{f8}). The reaction rates of xylose, furfural, lyxose, acids and T-T-DF are listed from Equation 2.1 to 2.5, respectively. Furfural yield of 46% was achieved at 473 K and a first-order kinetic model with an apparent activation energy of 32.1 kcal/mol (134.2 kJ/mol) was observed for the direct conversion of xylose (initial concentration of 10% in water and mass ratio of catalyst to xylose of 0.3) to furfural.

$$r_{xylose} = -k_{f1}[XYL] - k_{f3}[XYL] + k_{f2}[LYX] \tag{2.1}$$

$$r_{furfural} = +k_{f3}[XYL] + k_{f8}[T-T-DF] + k_{f4}[LYX] - k_{f6}[FUR] - k_{f5}[FUR] \tag{2.2}$$

$$r_{lyxose} = +k_{f1}[XYL] - k_{f2}[LYX] - k_{f4}[LYX] \tag{2.3}$$

$$r_{acids} = +k_{f5}[FUR] - k_{f7}[acids] \tag{2.4}$$

$$r_{T-T-DF} = +k_{f7}[acids] + k_{f6}[FUR] - k_{f8}[T-T-DF] \tag{2.5}$$

Agirrezabal-Telleria, Larreategui, et al. (2011) investigated the furfural production in aqueous and biphasic (toluene as co-solvent) system from xylose using commercial Amberlyst 70 catalyst, which possesses Brønsted acid sites and low surface area (1 m^2/g). The kinetic model proposed includes xylose cyclodehydration (k_1), condensation (k_2) and furfural resinification (k_3) (Equations 2.6 and 2.7). In the presence of 60wt.% catalyst in the aqueous system at 175 °C, furfural yield achieved a maximum of 38% while xylose initial concentration and conversion was 1wt.% and 83%, respectively.

$$\frac{d[XYL]}{dt} = -k_1[XYL] - k_2[XYL][FUR] \tag{2.6}$$

$$\frac{d[FUR]}{dt} = +k_1[XYL] - k_2[XYL][FUR] - k_3[FUR] \tag{2.7}$$

Among the oxide catalysts tested for the production of furfural, the ones based on Zr, Ti and Nb have been vastly investigated (DELBECQ et al., 2018). In particular, the

interest in using niobium relies on its great abundance on Earth, where the main reserves are located in Brazil. Brazil accounts for approximately 78% of the world reserves, and most reserves outside Brazil are located in Canada, Nigeria and Zaire (ALBRECHT; CYMOREK; ECKERT, 2011).

Niobium presence in catalysts and supports has been investigated in several chemical reactions (ALBRECHT; CYMOREK; ECKERT, 2011; GARCÍA-SANCHO et al., 2014a; LEUNG et al., 2017). Moreover, niobium oxide has been studied in reactions such as dehydration, hydration, esterification, hydrolysis, condensation, oxidation, polymerisation and alkylation reactions (OLIVEIRA et al., 2012).

Leung et al. (2017) studied two supports for copper oxide catalyst, including niobium oxide (Nb_2O_5) and alumina (Al_2O_3), for the CO oxidation. It was found that CuO_x/Nb_2O_5 had higher activity than CuO_x/Al_2O_3 and comparable activity to 1%Pt supported on Al_2O_3 under 500 °C.

Datka et al. (1992) investigated the acidic properties of Nb_2O_5 supported on SiO_2, Al_2O_3, MgO, TiO_2 and ZrO_2. According to their results of chemisorption of pyridine, Lewis acid sites were found in all catalysts, whilst Brønsted acid sites were only found in Nb_2O_5/Al_2O_3 and Nb_2O_5/SiO_2 when niobium oxide contents were higher than 8% and 6%, respectively.

The authors also studied the effect of calcination temperature on Nb_2O_5 and found that at 200 °C both Lewis and Brønsted acid sites are present, however at 500 °C both sites were not detected. Moreover, the increase in Nb_2O_5 content supported on Al_2O_3 allowed the formation and detection of Brønsted acid sites, whereas Lewis acid sites density decreased from 263 $\mu mol \cdot g^{-1}$ for 5% Nb_2O_5 to 154 $\mu mol \cdot g^{-1}$ for 19% Nb_2O_5. For instance, some of acidic properties of niobium oxide are present in Table 2.3.

Table 2.3: Acidic properties of Nb_2O_5/Al_2O_3.

Catalyst	Lewis acid sites ($\mu mol\ g^{-1}$)	Brønsted acid sites ($\mu mol\ g^{-1}$)
12% Nb_2O_5/Al_2O_3	130	38
19% Nb_2O_5/Al_2O_3	154	54

Source: Datka et al. (1992).

Kitano et al. (2012) also investigated the acidic properties of different Nb_2O_5 loadings (5-30%) supported on alumina and calcined at high temperatures for acid-catalysed reactions. It was found that Brønsted acid sites were stable even after

calcination at 1123 K and 16% Nb_2O_5 had the highest Brønsted acidity among all loadings tested.

García-Sancho et al. (2014a) prepared different Nb_2O_5 loadings (4, 12 and 20%) on Al_2O_3 for xylose dehydration to furfural. After catalyst preparation by impregnation, samples were calcined at 550 °C and tested for the acid-catalysed reaction at 160 °C in aqueous and biphasic (water/toluene) systems. Although the use of toluene as co-solvent had increased furfural selectivity (20-30% more than aqueous system), the xylose dehydration activity had little change, indicating that the major explanation for the higher selectivity was the furfural extraction and the decrease in the secondary reaction extent in the aqueous phase. The authors also investigated a kinetic model including xylose dehydration, condensation and furfural resinification reactions. It was indeed found that kinetic differences with and without toluene were minimal for xylose dehydration, whereas for condensation and resinification a significant change was found.

2.4.4 Solvents for Xylose Dehydration Reaction

The proper choice of solvent for xylose conversion to furfural is of prime importance because of its direct impact on separation cost after furfural production (AGIRREZABAL-TELLERIA; LARREATEGUI, et al., 2011). Moreover, studies suggest that the presence of organic solvents reduces secondary reactions and increases furfural selectivity (AGIRREZABAL-TELLERIA; LARREATEGUI, et al., 2011; PHOLJAROEN et al., 2013). According to Zeitsch (2000c), the main cause of furfural loss in its production is the secondary reactions that furfural undergoes in aqueous phase, hence showing the importance of moving furfural to vapour phase, where no secondary reactions occur.

Although water is the most appropriate solvent due to its presence in biomass itself, abundance and non-toxicity, several solvents have been studied for the xylose dehydration reaction, such as organic compounds, ionic liquids and supercritical CO_2 (GAIROLA; SMIRNOVA, 2012; HU et al., 2014; LIMA et al., 2009).

Studies have shown that the use of aqueous mixtures containing aprotic polar co-solvents is essential since a minimal amount of water is commonly required to facilitate solvation of biomass derivatives, while co-solvent increases reaction performance. An example is the furfural xylose dehydration reaction itself: in an aqueous system with γ-

valerolactone as co-solvent, the dehydration rate increased about 30-fold compared to the pure water system, while the formation of undesirable humins by reactant and product degradation was inhibited (WALKER et al., 2018).

Moreau et al. (1998) applied toluene and methyl isobutyl ketone (MIBK) as a co-solvent in xylose dehydration reaction and found similar catalyst performance for both tested: H-mordenite and H-Y faujasite. In about 30 minutes the MIBK system achieved 44% xylose conversion and 60% furfural yield, while in the toluene system at the same time achieved 30% and 92% for conversion and yield, respectively.

The study conducted by Molina et al. (2015) tested isopropanol, cyclopentyl methyl ether (CPME) and γ-valeractone (GVL) as co-solvents for xylose dehydration. The xylose conversion values obtained were all above 90%, and the furfural yield was always above 50%.

This review aimed to give a simple overview of studies using different organic compounds and also their importance for increasing furfural selectivity.

2.5 Conclusion

According to Nhien et al. (2016), industrial production of furfural has received few improvements since its creation in the 1920s. Current processes have a relatively low yield (about 50%) and use inefficient technology. The use of heterogeneous catalysts in the dehydration reaction of xylose to furfural has a recent history compared to other processes. Nevertheless, there is a great potential to be explored in this topic, especially to improve processes by the development of active, selective and stable catalysts, as well as in the study and design of systems that optimise industrial operation.

Although some authors have been investigating the textural properties of the catalyst Nb_2O_5/Al_2O_3 (KITANO et al., 2012) in the dehydration reaction of xylose (GARCÍA-SANCHO et al., 2014a), we observe the lack of work involving the experimental study of this reaction and its kinetic modelling. In this scenario, supporting Nb_2O_5 on Al_2O_3, a commonly used support for catalysts, is a topic demanding further investigation. Thus, the present project aims to investigate the kinetics of the xylose dehydration reaction in the presence of Nb_2O_5/Al_2O_3 pristine catalyst and modified by acid treatment.

The results from kinetic modelling will be important for the simulation of the integrated process, combining the use of heterogeneous catalysts for the chemical reaction and the separation of furfural in a single unit. Only a few studies have shown that such integration is possible.

Consequently, the contribution of this work will be vital in the kinetic modelling of the xylose dehydration reaction in the presence of Nb_2O_5/Al_2O_3 as a catalyst, as well as in the simulation of the reactive stripping column. The simulation will allow to obtain insights in the optimum parameters of operation of the reactive column. Hence, this study can guide future works involving the experimental design of this column. It is important to emphasise that this work may serve as a long term basis for the development of an industrially viable process for the production of this building-block molecule as an alternative to petroleum-derived compounds with minimal environmental impact.

Chapter 3

Objectives

The main objective of this work is to simulate a reactive stripping for both producing and separating furfural. The kinetic parameters necessary for describing xylose dehydration reaction are obtained experimentally prior to simulation using 16% Nb_2O_5/γ-Al_2O_3 catalysts. A graphical abstract of the project is presented in Figure 3.1.

Figure 3.1: Graphical abstract of the project.

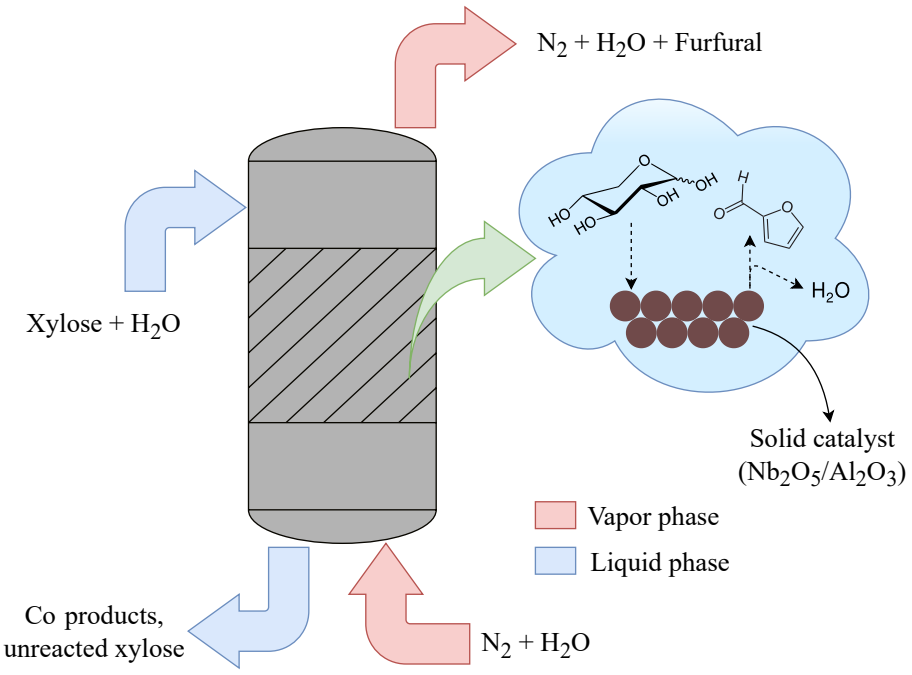

The specific objectives of this work are:

- To conduct xylose dehydration reaction using Nb_2O_5/γ-Al_2O_3 based catalysts previously prepared by wet impregnation, treated with acid HNO_3 or H_3PO_4 and

characterised by N_2 physisorption (B.E.T. and B.J.H. method), XRF, laser diffraction, TPD-NH_3, and FTIR;

- To obtain kinetic parameters of xylose dehydration reaction to furfural;
- To model a reactive stripping of furfural production using Aspen Plus® and kinetic parameters from modelling results;
- To conduct design of experiments for different process parameters to estimate the optimal operating condition.

Chapter 4

Methodology

The methodology of this work can be described in the following steps: catalyst preparation and characterisation; xylose dehydration reaction (catalyst testings); kinetic modelling; reactive stripping simulation of both furfural production and separation, and optimisation of reactor operating condition.

4.1 Catalyst Preparation

The xylose dehydration reaction is known to occur on acid sites (CHOUDHARY; SANDLER; VLACHOS, 2012), where both Brønsted and Lewis acid sites play a specific role in the reaction. In this scenario, niobium oxide (Nb_2O_5) supported on alumina (Al_2O_3) was chosen for this study due to its acidic properties (DATKA et al., 1992). Besides, in order to investigate the effect of acid treatment on catalyst performance and texture, the Nb_2O_5/Al_2O_3 catalyst was treated with HNO_3 and H_3PO_4. Accordingly, three different catalyst samples were prepared: 16% Nb_2O_5/Al_2O_3, 16% Nb_2O_5/Al_2O_3 treated with HNO_3 and 16% Nb_2O_5/Al_2O_3 treated with H_3PO_4. These catalysts were labelled as NBAL, NBAL-N and NBAL-P, respectively (Table 4.1).

Table 4.1: Nomenclature of catalyst samples.

Catalyst	Nomenclature
Nb_2O_5/Al_2O_3	NBAL
$Nb_2O_5/Al_2O_3/HNO_3$	NBAL-N
$Nb_2O_5/Al_2O_3/H_3PO_4$	NBAL-P

The catalytic preparation steps were conducted at Laboratory of Catalytic Processes Engineering and Bio-refineries (LEPCatBior) at Unicamp. The precursor of the active phase, ammonium niobium oxalate ($NH_4NbO(C_2O_4)_2$ – CBMM), was supported on alumina (γ-Al_2O_3 - Alfa Aesar 99.99%, 40 μm powder and 200 m^2/g) by wet impregnation method (KITANO et al., 2014).

4.1.1 Support Preparation

The support was pre-treated prior to impregnation in order to achieve mechanic resistance and stability (FIGUEIREDO; RIBEIRO, 1989). Alumina was calcined at 550 °C (10 °C/min) during 6 hours under a synthetic air flow of 32 mL/min. It is expected that the temperature of calcination was not high enough to induce phase transition on the sample. According to Augustine (1995), γ-Al_2O_3 possess a phase transition to δ-Al_2O_3 only at the temperature of 850 °C.

4.1.2 Wet Impregnation

The objective of catalyst preparation was to obtain 53 g of 16% Nb_2O_5 supported on Al_2O_3. The catalyst preparation method was wet impregnation based on the procedure described by Kitano et al. (2014). In a round-bottom flask of 1000 mL, 44.52 g of γ-Al_2O_3 previously calcined, 22.31 g of $NH_4NbO(C_2O_4)_2$ (catalyst precursor) and 535 mL of deionised water were added. The mass/volume ratio of solid to water was 1:8, similar to the ratio reported by Braga et al. (2005).

The suspension was then heated to 80 °C and kept at this temperature for 2 hours under stirring (100 rpm) and ambient pressure in a rotary evaporator (Figure 4.1). After this, the pressure was reduced to 420 mbar and the solvent was continuously evaporated. The remaining slurry was dried overnight in the oven at 80 °C.

Solid particles were ground gently and then sieved (mesh number 60) to a maximum size of 250 μm.

Figure 4.1: Scheme of catalyst preparation apparatus.

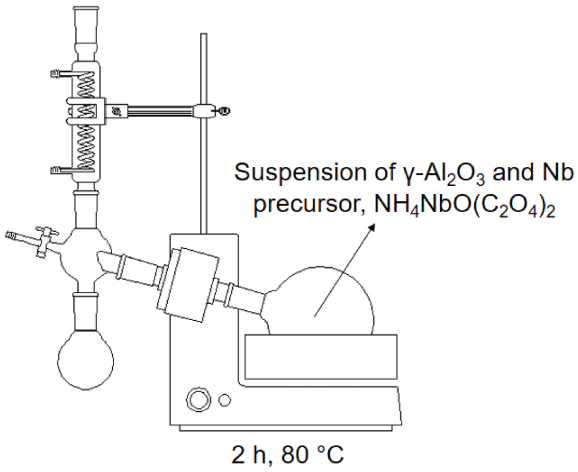

Source: Faidherbe Lille[2].

4.1.3 Calcination

The niobium precursor supported on Al_2O_3 was calcined at 300 °C for 4 hours using a temperature rate of 10 °C/min (FONTANA, 2016). A synthetic air flow of 32 mL/min was used. Catalysts modified by acid treatment were recalcined under similar conditions of gas flow, duration, and temperature.

4.1.4 Acid Treatment

The prepared catalyst (16% Nb_2O_5/Al_2O_3) was subsequently treated with either H_3PO_4 or HNO_3 according to the method reported in the literature (BRANDÃO et al., 2009). Acid solution of 1 mol/L was mixed with unmodified Nb_2O_5/Al_2O_3 catalyst respecting the ratio of 10 mL to 3 g, respectively. The suspension was kept under stirring at room temperature for 48 hours. The sample was heated to eliminate the excess of water and then led to the oven at 110 °C for 48 hours. After the drying step, catalyst samples were calcined as previously reported. The same procedure was applied to both H_3PO_4 and HNO_3 treatments.

[2]https://www.faidherbe.org/site/cours/dupuis/ethe2.htm.

4.2 Catalyst Characterisation

The main techniques for catalyst characterisation, and the information provided by them are given in Table 4.2. These analyses were conducted to understand and to elucidate the relation among catalyst physico-chemical properties and their performance for dehydration of xylose to furfural.

Table 4.2: Catalyst characterisation techniques and their information

Characterisation technique	Information
Laser Diffraction	Particle size distribution of the catalysts
X-Ray Fluorescence (XRF)	Elementary chemical composition
N_2 Adsorption	Specific surface area, pore volume and diameter
Temperature-Programmed Desorption of NH_3	Overall catalyst acidity
Fourier-transform infrared spectroscopy (FTIR)	Identification of functional groups

4.2.1 Laser Diffraction

The Laser Diffraction analysis was performed at the Laboratório de Recursos Analíticos e Calibração (LRAC), part of School of Chemical Engineering (Unicamp). The granulometric analysis is performed in wet procedures (sample suspension unit), with a Long Bench-MAM 5005 laser diffraction granulometer manufactured by Malvern Instruments Ltd. The particle sizes detected are from 0.05 to 900 μm.

In the equipment, the laser beam is sent towards the sample, in this case, catalyst particles. When the collimated beam encounters the particles, part of the laser is diffracted. The diffracted laser is then focused through the lens of the detector. The diameter of the particles is inversely proportional to the angle of deviation suffered by the laser beam (CREMASCO, 2014).

4.2.2 X-Ray Fluorescence (XRF)

X-ray fluorescence spectroscopy (XRF) is normally applied to the quantitative and qualitative characterisation of solid and molecular catalysts. In XRF, the emission of X-ray photons characteristic of the element is obtained when the catalyst sample is irradiated with X-rays from a primary source, which leads to electron release and the formation of a positive vacancy. Electrons from upper levels then fill the positive vacancy which leads to the emission of X-ray photons. This technique allows detection of concentrations in a wide range, from 100% down to 0.001-0.01% (ALBERS, 2008).

The XRF analysis was performed at the Laboratório de Recursos Analíticos e Calibração (LRAC), part of School of Chemical Engineering (Unicamp). The equipment used was a PANalytical Axes Spectrometer (1 kW) and a Omnian software. For XRF analysis, the Nb_2O_5/Al_2O_3 calcined catalyst powder was mixed with a wax binder and pressed under 20 ton for 10 seconds.

4.2.3 Nitrogen Adsorption

The nitrogen adsorption method was used in order to estimate the specific surface area by B.E.T. method (BRUNAUER; EMMETT; TELLER, 1938), and pore volume and diameter of catalysts by B.J.H. method (BARRETT; JOYNER; HALENDA, 1951).

In this technique, the catalyst sample is weighed to a precision of 1% and placed in a tube of known volume. The system is heated under vacuum to be degassed at 200 °C. The sample is then cooled down to 77 K (temperature of liquid N_2) and a known amount of nitrogen gas is introduced into the cooled tube. After the equilibrium is achieved, the pressure is measured and the procedure is repeated with successive pulses of nitrogen (AUGUSTINE, 1995). Adsorption of N_2 was performed under relative pressures (P/P_0) ranging from 0.04 to 0.35 at 77 K, with desorption performed at 298 K on a Micrometrics Tristar Model ASAP 2010 Chem. equipment at the Laboratório de Recursos Analíticos e de Calibração (LRAC).

Among different models for adsorption isotherms, the Brunauer, Emmett, and Teller (B.E.T.) method was employed (BRUNAUER; EMMETT; TELLER, 1938), which relies on several assumptions:

- Multilayer adsorption;
- First layer: Langmuir adsorption;
- Second and further layers: condensation of gas onto liquid;
- Heat of adsorption decreases from the first to the second layer and so on.

The B.E.T. Equation (4.1) relates adsorbed volume (V_{ads} in $cm^3 \cdot g^{-1}$) measured at pressure P. Thus, gas volume V_m corresponding to the monolayer is found by means of linear regression of Equation 4.1 in the range of $0.05 < P/P_0 < 0.3$.

$$\frac{1}{V_{ads}(P_0/P - 1)} = \frac{1}{CV_m} + \frac{(C-1)}{CV_m}\frac{P}{P_0} \tag{4.1}$$

Finally, specific surface area S_{BET}, which is area per mass of catalyst, is calculated by using Equation 4.2, where N_A is Avogadro's number, S_m is the cross-sectional area of the adsorbate molecule, which for nitrogen is 0.162 nm^2.

$$S_{BET} = V_m \cdot N_A \cdot S_m \tag{4.2}$$

4.2.4 Temperature-Programmed Desorption of NH_3 (TPD-NH_3)

The TPD-NH_3 analysis was carried out in AutoChem II Chemisorption Analyzer (software: AutoChem II 2920) in the Laboratório para Estudos de Processos de Adsorção e Catálise (LEPAC) at University of Campinas. The catalyst sample was weighed to a precision of 1% and placed into a U-form glass tube where the sample was supported on a certain quantity of wool. The pre-treatment for all samples took place under helium flux until the temperature of 250 °C was reached, with a ramp temperature of 10 °C/*min*. The sample was then cooled down to about 50 °C and ammonia started flowing. The physisorbed ammonia was removed by purging the system for 30 minutes under helium flow. The sample was then placed under helium flow and heated by 10 °C/*min* to 500 °C (or 250 °C for NBAL-N).

4.2.5 Fourier-Transform Infrared Spectroscopy (FTIR)

The Fourier-transform infrared spectroscopy (FTIR) analysis was performed at the Laboratório de Recursos Analíticos e Calibração (LRAC), part of the School of

Chemical Engineering (Unicamp). The equipment used was a Nicolet 6700 (Thermo Scientific) and transmission technique was utilised. For FTIR analysis, the sample was prepared by mixing catalyst powder with KBr (ratio of catalyst to KBr was 1:100) and pressed under 7 ton for 4 minutes. The spectrum is generated by measuring the transmitted energy as the infrared beam passes through the catalyst sample, thus allowing the identification of functional groups (ARMAROLI et al., 2000).

4.3 Catalytic Tests

4.3.1 Xylose Dehydration Reaction

The catalytic tests were carried out in a 300 mL Parr reactor using the prepared catalysts, deionised water and xylose (D-(+)-Xylose – Sigma-Aldrich, $\geq$ 99.99%). The procedure for each catalytic test starts with: (*i*) xylose, deionised water, and catalyst are weighed separately to a precision of 1%; (*ii*) reactor is charged with 160 mL of water and 0.800 g of catalyst and; (*iii*) 4.00 g of xylose was dissolved in 36 mL of water and injected into the sampling vessel (kept at room temperature). The reactor was then purged three times with nitrogen, pressurised to 3 MPa using nitrogen, and then heated to the reaction temperature (150, 160 or 170 °C) under stirring. When the desired temperature was reached, the solution of xylose was charged to the reactor using nitrogen as an entrainer at 4.5 MPa pressure (beginning of reaction, that is, $t = 0$). Reaction samples were collected through a liquid phase sampling port every 10, 15, 30, 45 and 60 minutes as the reaction continued during 4 hours. The liquid samples collected were frozen and stored until analysis by high-performance liquid chromatography (HPLC), which usually took place a few days later. The reaction conditions are summarised in Table 4.3.

Table 4.3: Batch reactor operating conditions.

Parameter	Value
Solvent volume (mL)	196
D-xylose mass (g)	4.00
Catalyst mass (g)	0.800
Stirring rate (rpm)	650
Pressure (MPa)	4-4.5
Temperature (°C)	150, 160 and 170
Reaction time (h)	4

The reactor pressure was kept between 4 and 4.5 MPa during reaction time in order to avoid liquid vaporisation and allow reaction sampling based on the pressure difference.

Despite of the large quantity of studies reporting the use of organic solvents, this work chose to employ only water to compose the reaction media because of its minimal environmental impact.

4.3.2 Quantification Analysis

Quantification analysis was carried out by a high-performance liquid chromatography (HPLC) equipment, which is often chosen for biomass derivatives (VAZ JUNIOR; SOARES, 2014). The methodology consists, essentially, in the preparation of the sample (unfreezing the samples, and filtering) and its manual injection for further interpretation of the signal and analytical result.

The samples were quantified by means of a Water High Performance Liquid Chromatograph (HPLC) model Water 717 plus Autosamples (Waters 410 Differential Refractometer), present in the Laboratório de Equipamentos Cromatográfico (LEC) of the School of Chemical Engineering of Unicamp. For compounds separation, a Phenomenex Rezex Monosaccharide H^+ column at 80 °C was used along with 0.6 mL/min of water as the mobile phase. The concentration for all compounds was calculated by means of a calibration curve, providing the relationship between compound signal (area) and its concentration. The overall conditions for HPLC analysis are summarised in Table 4.4.

Table 4.4: Conditions for HPLC analysis.

Column temperature (°C)	80
Detector temperature (°C)	40
Mobile phase	H_2O
Mobile phase flow (mL/min)	0.6
Run time (minutes)	60

4.3.3 Catalytic Performance

The overall catalytic performance was investigated by reactant conversion (xylose), selectivity to the desired product (furfural) and its yield. The conversion (χ), selectivity (S) and yield (Y) are presented in Equations 4.3, 4.4, and 4.5, respectively.

$$\chi = \frac{[XYL]_0 - [XYL]_f}{[XYL]_0} \tag{4.3}$$

$$S = \frac{[FUR]_f}{[XYL]_0 - [XYL]_f} \tag{4.4}$$

$$Y = \frac{[FUR]_f}{[XYL]_0} \tag{4.5}$$

The dehydration of xylose can form several side products (MARCOTULLIO; DE JONG, 2010). Thus, it is necessary to estimate the degree of carbon loss in undesired products, which is represented by the ratio of carbon quantified at the end of the reaction and carbon added at the beginning (Equation 4.6). The closer the carbon balance (ψ) is to unity, the least undesired products were formed.

$$\psi = \frac{moles\ of\ carbon\ (final)}{moles\ of\ carbon\ (initial)} \tag{4.6}$$

4.4 Kinetic Model

In order to model a chemical reaction, it is important to make sure that the observed results are free of mass transfer limitations, which can hinder the real rate of reaction. For this purpose, this section will firstly present how mass transfer effect can be studied, the expected reactions taking place and their paths, and lastly the algorithm allowing the kinetic modelling.

4.4.1 Mass Transfer Considerations

As described by Augustine (1995), mass transport effects in a solid-liquid reactive system are mostly influenced by mass of catalyst, size of catalyst particles, concentration of liquid reagent and temperature.

To study external mass transfer resistance, two reactions were performed under similar conditions, differing only by mass of catalyst. Usually, the second catalyst test is performed with half of the catalyst mass. The reaction is considered free of external mass transport resistance if the specific rate of reaction (per grams of catalyst) lies within ±5% of variation (AUGUSTINE, 1995).

The effect of internal mass transfer can be analysed by Weisz-Prater criteria, which relates observed reaction rate (r_{obs} in $mol{\cdot}cm^{-3}{\cdot}s^{-1}$), catalyst particle size measured by Laser Diffraction (R_p in cm), effective diffusion coefficient (D_{eff} in $cm^2 \cdot s^{-1}$) and concentration ($[i]$ in $mol \cdot cm^{-3}$). For a first order reaction occurring in spherical catalyst particle, Equation 4.7 is applied.

$$C_{wp} = \frac{r_{obs} R_p^2}{D_{eff}[i]} \tag{4.7}$$

If $C_{wp} < 0.3$, then internal mass transport resistance is considered negligible and there is no concentration gradient inside catalyst particle (SIEVERS et al., 2016).

The effective diffusion coefficient (D_{eff}) was estimated according to the Equation 4.8, as described in the literature by Sievers et al. (2016) and Ternan (1987). In this equation, λ is the ratio between molecule and pore radius, whereas p is an experimental parameter for catalysts that can be found in the literature (TERNAN, 1987; VANNICE, 2006). For instance, this work considered a p value of 16.26 based on measured data of liquid diffusivities of organics in silica-alumina catalysts of different pore diameters (SATTERFIELD; COLTON; PITCHER J., 1973; SIEVERS et al., 2016).

$$D_{eff} = D_{bulk} \frac{(1-\lambda)^2}{1+p\lambda} \tag{4.8}$$

The bulk diffusion coefficient (D_{bulk}) was calculated using Equation 4.9, which provides acceptable results for a dilute solute (A) diffusing through a solvent (B). In this equation, R_A is the solute-molecule radius and $\mathrm{N_A}$ is Avogadro's number (SEADER; HENLEY; ROPER, 2010).

$$D_{AB} = \frac{RT}{6\pi\mu_B R_A N_A} \tag{4.9}$$

In this scenario, the presence of external or internal mass transfer resistances was studied, respectively, by decreasing catalyst mass in the reaction and Weisz-Prater criteria.

4.4.2 Reaction Modelling

Indifferently from reactor type, a rate law (Equation 4.10) describes the behaviour of a reaction in terms of temperature (through the rate constant (k) following Arrhenius Equation), and concentration of compounds involved in the reaction through a function of concentrations, $\phi([i])$ (FOGLER, 2016).

$$r_i = k_i \phi([i]) \tag{4.10}$$

For homogeneous reactions, in which there is only one phase present, a common approach is to fit experimental data to a Power Law model (4.11), based on reacting species concentrations (FOGLER, 2016). For instance, reaction order is defined by the sum of each α_i.

$$\phi([i]) = \prod_i [i]_i^{\alpha_i} \tag{4.11}$$

The process in which a heterogeneous reaction takes place can be divided into few steps. Accordingly, the kinetic modelling of this type of reaction can be quite complicated. For a liquid-solid system, these steps are: external diffusion of reactant from the bulk liquid to the catalyst (solid) surface; internal diffusion of reactant through catalyst pores; reactant adsorption onto the catalyst surface; reaction on the surface; desorption of reaction product from the surface and; both internal and external diffusion of product to bulk liquid (FOGLER, 2016). In order to simplify kinetic models, the pseudo-homogeneous approach can be used to fit experimental data by estimating fewer parameters than complex heterogeneous models such as Langmuir-Hinshelwood-Hougen-Watson (LHHW). In pseudo-homogeneous approach, it is important to conduct reaction under minimal mass transport resistance, thus reaction rate can be described as a Power Law model in which apparent rate constants bear both reaction and adsorption/desorption information. This approach of modelling heterogeneous catalytic reactions has been generally chosen for describing xylose dehydration to furfural (O'NEILL et al., 2009; AGIRREZABAL-TELLERIA; LARREATEGUI, et al., 2011; FERREIRA et al., 2013).

The material balance of a compound i inside any control volume can be universally expressed by Equation 4.12.

$$F_{i,o} - F_i + \int r_i dV = \frac{dn_i}{dt} \tag{4.12}$$

When it is assumed that reaction rate is uniform within reaction volume (perfectly stirred) and that the latter is constant, which is true for most liquid phase reactions with low specific mass change, the material balance is simplified. Thus, a batch reactor operating with perfect stirring and at constant volume is represented by Equation 4.13.

$$r_i = \frac{d[i]}{dt} \tag{4.13}$$

In the next part, the models will be described by coupling both 4.10 and 4.13 to form Equation 4.14.

$$\frac{d[i]}{dt} = k_i \prod_i [i]^{\alpha_i} \tag{4.14}$$

4.4.3 Reaction Network

The general reaction network of xylose dehydration reaction proposed by this work is based on the one presented by O'Neill et al. (2009). The network includes xylose isomerisation (k_1); furfural formation from either xylose (k_3) or its isomer (k_2); furfural loss reactions, which include condensation (k_6) and resinification (k_7); furfural degradation (k_5) and; xylose degradation and humin formation (k_4). Accordingly, the reaction network is depicted in Figure 4.2.

Figure 4.2: Reaction network for xylose dehydration.

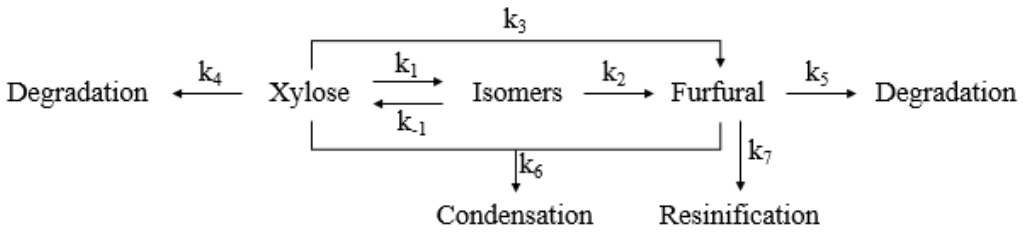

Catalytic test results were analysed using the literature review and the identification of reaction products in order to establish simplifications from the general reaction network (Figure 4.2). The differential equations representing the general reaction network, for xylose, intermediate and furfural are Equations 4.15, 4.16 and 4.17,

respectively. Thus, for each catalyst, a mathematical model was defined and the differential equations were solved numerically, as discussed in the next part.

$$\frac{d[XYL]}{dt} = -k_1[XYL] + k_{-1}[XYL] - k_3[XYL] - k_4[XYL] - k_6[XYL][FUR] \quad (4.15)$$

$$\frac{d[I]}{dt} = +k_1[XYL] - k_{-1}[I] - k_2[I] \quad (4.16)$$

$$\frac{d[FUR]}{dt} = +k_2[I] + k_3[XYL] - k_5[FUR] - k_6[XYL][FUR] - k_7[FUR] \quad (4.17)$$

4.4.4 Numerical Solver

The apparent reaction constants proposed by the reaction model were estimated by numerical modelling using a code written in Scilab. Reaction rate expressions were integrated using a 4th order Runge-Kutta method. The optimisation method chosen was the non-linear least squares (built function *leastsq* in Scilab) using the Quasi-Newton method. The minimisation of the squared difference (ξ) between experimental data (for both xylose and furfural) and the estimated values (Equation 4.18) was performed to adjust the apparent reaction rate constants. The code used for this purpose is presented in Appendix B.

$$\xi = \sum([i]_{est} - [i]_{exp})^2 \quad (4.18)$$

Once the apparent rate constants were estimated, the apparent activation energies and pre-exponential factors were obtained by linear regression of Arrhenius Equation (4.19).

$$ln(k_i) = ln(k_o) - \left(\frac{E_a}{RT}\right) \quad (4.19)$$

It is important to remark that activation energies were only estimated for reactions where the rate constant increased with temperature, following an Arrhenius behaviour. The validity of linearisation method was then analysed using coefficient of determination, denoted by R^2.

4.5 Simulation

The reactive stripping simulation was performed using the chemical process simulation program Aspen Plus V10 by AspenTech. The reactive column was represented by a RadFrac unit, which is a rigorous model for simulating all types of multistage vapor-liquid fractionation operations. The RadFrac unit can also include chemical reactions, such as Equilibrium or Rate-Controlled types.

The complexity of a reactive distillation/stripping simulation is defined by the choice of models for chemical reactions and mass transfer effects, where both can be described by applying a kinetic or an equilibrium model. For instance, representing mass transfer or reaction as a kinetic model increases complexity (SUNDMACHER; KIENLE, 2006). A qualitative analysis of their combination choices is depicted in Figure 4.3.

Figure 4.3: Model complexity in a reactive distillation/stripping simulation.

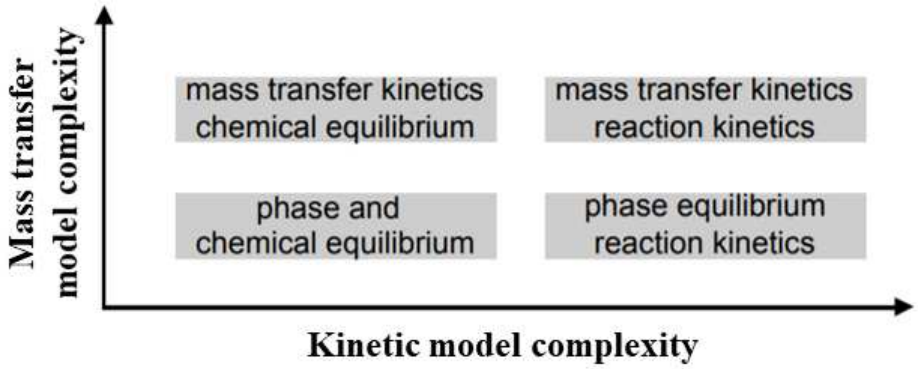

Source: Adapted from Sundmacher and Kienle (2006).

In this work, phase equilibrium and reaction kinetics were considered in the simulation. The reaction type for RadFrac was chosen to be REAC-DIST which uses either a built-in Power Law model or an user-defined subroutine to calculate reaction rates at each stage of the reaction zone. Since the dehydration of xylose to furfural was defined as Power Law when obtaining the kinetic parameters in this work, the same was used in the Aspen Plus simulation.

4.5.1 Thermodynamic Model

In to order to simulate the process, it is necessary to choose a proper thermodynamic model for describing liquid and gas phase behaviour. The gas phase was assumed to be ideal, and N_2 was declared as a Henry component.

For the liquid phase, non-ideality can be taken into account by the use of activity coefficients γ, which depend on the system's temperature and composition. Among the most popular models for calculating the activity coefficient are Wilson, NRTL (Nonrandom two liquid) and UNIQUAC (Universal quasi-chemical). One of the advantages of using the UNIQUAC model is that, in the absence of liquid-vapor equilibrium (ELV) data, the UNIFAC (Universal Quasi-chemical Functional Group Activity Coefficients) method can be used to estimate the parameters UNIQUAC from the molecular structure of the components of the mixture (SMITH, 2005).

The choice of a thermodynamic model was made based on the built-in Methods Assistant in Aspen Plus. In order to choose the model, the following hypotheses were considered:

- Pressure is below 10 bar;
- Reaction occurs in liquid phase;
- Gas phase is ideal;
- There are no carboxylic acids in the mixture;
- Two liquid phases can exist.

Accordingly, the UNIQUAC model was chosen. The UNIQUAC model can describe strongly nonideal liquid solutions, polar and non-polar compounds, and liquid-liquid equilibria. The model requires binary parameters, which can be either obtained from the literature or from the regression of experimental data. In the case of water-furfural, Aspen Plus already possesses binary parameters (Table 4.5).

Table 4.5: Parameters from UNIQUAC model.

Parameter	Value
a_{ij}	7,5657
a_{ji}	-5,4487
b_{ij}	-2926,4805
b_{ji}	1823,3735

In order to evaluate these parameters, the prediction of azeotrope formation was utilised to validate the model chosen. According to the literature, furfural and water form an azeotrope that boils at 97.85 °C (1 atm) with a water mass fraction of 65%

(ZEITSCH, 2000b). The estimated azeotrope for the water-furfural system in Aspen Plus using UNIQUAC and the one reported in the literature are presented in Table 4.6. Due to the similarity of the azeotrope prediction, water-furfural parameters were considered appropriate for this study.

Table 4.6: Azeotrope formation of water-furfural system at 1 atm.

	Temperature (°C)	Mass fraction of water
Zeitsch (2000b)	97.85	0.65
UNIQUAC	97.6	0.64

4.5.2 Process Description

The furfural production from xylose is based on the Rosenlew process described by Zeitsch (2000d). The Rosenlew process uses steam injection at 265 °C and 9.88 atm at the bottom of the reactor vessel (Figure 2.10) to convert biomass to furfural with a final yield of 59.5% without the addition of catalysts. The main operational details of Rosenlew process are listed below.

- Reactor dimensions: 2.5 m diameter by 12 m high
- Input of water: 3090 kg/h
- Input of pentosan: 809 kg/h
- Steam injection (10500 kg/h) at 265 °C and 9.88 atm
- Furfural concentration in the gas stream: 3.22%wt.
- Specific steam consumption: 30 kg of steam per kg of furfural

Experimental studies show that steam enhances the separation of furfural from reactive zone (METKAR et al., 2015), although it also increases the complexity of further water-furfural separation systems (AGIRREZABAL-TELLERIA; GANDARIAS; ARIAS, 2013). In order to decrease steam content, the simulation on this work modified Rosenlew process by injecting N_2 along with steam. In the base case, the mass fraction of water is 50% for the gas feed stream.

Moreover, the simulation proposed in this work used xylose instead of pentosan (pentose sugars) at the reactive stripping column input.

The flowsheet of furfural production simulation built in Aspen Plus is shown in Figure 4.4. In the following topics, each equipment used in the simulation will receive a description of its main operational details. The values of each variable, such as temperatures, pressures, and mass flows were not mentioned because their ranges were all studied by means of Design of Experiments (DOE) aiming for an optimal operating condition.

Figure 4.4: Flowsheet of Aspen Plus simulation for furfural production.

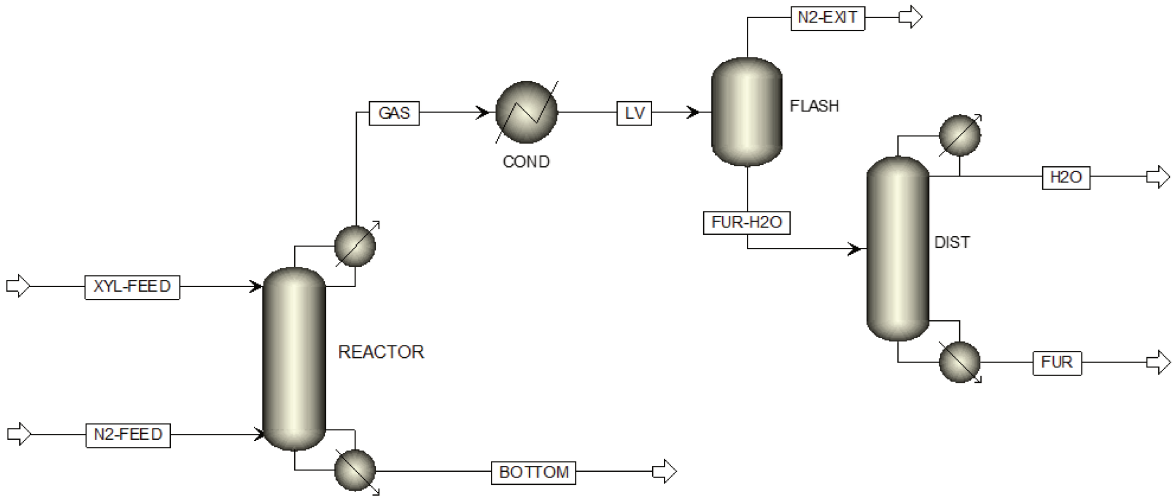

Stripping Reactor

The reactive stripping vessel is represented by the RadFrac block and it was labelled as *REACTOR*. This block has two inputs, which are (*i*) an aqueous solution of xylose (*XYL-FEED*) and (*ii*) a steam/N_2 injection (*N2-FEED*). On the other hand, there are two outputs. The top output is ideally composed of steam/N_2 and furfural (*GAS*), whilst the bottom output is mainly composed of an aqueous solution of unreacted xylose. The number of stages was fixed at 30, whilst the number of reactive stages was considered as an independent variable in the optimisation step.

The reaction type for this simulation was the Power Law, and its parameters were the ones obtained in the experimental part of this work regarding Nb_2O_5/Al_2O_3 catalysts. The parameters include the pre-exponential factor (k_o) and the apparent activation energy (E_a), as shown in Equation 4.20.

$$k = k_o \cdot exp\left(- \frac{E_a}{R \cdot T} \right) \tag{4.20}$$

Moreover, phase equilibrium was considered instead of rigorous mass transfer kinetics.

The column stages were numbered from the top to the bottom, with stage 1 as the xylose solution feed and the last stage (30) as the steam/N_2 feed. In the base case, the reactive stages had 15 kg of catalyst per stage and they were numbered from 5 to 20 (total mass of catalyst was 225 kg). The choice of catalyst mass per stage in the base case was arbitrary due to the fact that Rosenlew process do not add neither homogeneous nor heterogeneous catalysts to the reaction medium, thus catalyst mass in the base case needed to be arbitrarily chosen.

Moreover, it was assumed that there was no pressure drop across the reactive stripping column. The operating pressure of the column was chosen in a certain range to ensure the occurrence of the reaction in liquid phase.

Condenser

The condenser (*COND*) operated at the same pressure of the reactive stripping column and decreased *GAS* temperature to 25 °C in the liquid-vapour (*LV*) stream. Other condensers in the process (present in the separation unit) were also considered free of pressure drop between inlet and outlet streams.

Flash Separation

After leaving the condenser, the *LV* stream enters a flash vessel (*FLASH*) were pressure is decreased to 1 bar, thus separating a non-condensable gas (*N2-EXIT*) from the liquid phase composed of water and furfural (*FUR-H2O*).

Separation Unit

Lastly, the liquid phase containing both water and furfural enters a separation unit, herein depicted as a distillation column (*DIST*) in Aspen Plus. However, the separation unit for obtaining furfural at high purity described in this work is more complex, including several other equipments, such as decanter, two distillation columns, splitter and condensers. The full description of separation process for furfural production will be discussed in Results and Discussion section after reactive stripping column optimisation. When using distillation columns, the model used was a DSTWU,

which performs a Winn-Underwood-Gilliland shortcut design calculation for the specified recovery of the light and heavy key components. According to Aspen Plus built-in Guide, DSTWU can also estimate optimum feed stage location and condenser/reboiler duties.

Base Case

A base case was defined prior to design of experiments. The main operating parameters are listed in Appendix D, including temperature, pressure, enthalpy, mass/mole fractions and mass/molar flows of each stream. Moreover, the equipment's specifications were chosen according to the description presented above.

4.6 Design of Experiments

The Design of Experiments was chosen to study variables effects on certain response variables, such as furfural yield and furfural recovery, then estimate the optimum range of operation. At first, this work proposes to use the experimental matrixes from Plackett & Burman (PB) method (PLACKETT; BURMAN, 1946). This choice allows finding key factors (X's) affecting response variables (Y's) with the least amount of experiments when the number of factors is superior to four (RODRIGUES; IEMMA, 2014). Once the number of factors has been narrowed, the Central Composite Rotatable Design (CCRD) was used to perform analysis of variance (ANOVA), to build a mathematical model for response variables and to find an optimum condition. The data were analysed by the Protimiza Experiment Design Software[3]. A summary of process variables (factors) and responses studied in this design of experiment are shown in Table 4.7. The range of these factors is carefully chosen and detailed in the following sections.

[3]http://experimental-design.protimiza.com.br

Table 4.7: Factors and responses studied in the design of experiments.

#	Factors (X)	Responses (Y)
1	*XYL-FEED* mass flow	Furfural yield
2	Mass fraction of xylose in *XYL-FEED*	Fraction of furfural
3	Temperature of xylose feed ($T_{XYL-FEED}$)	
4	Mass fraction of H_2O in *N2-FEED*	
5	Temperature of gas feed ($T_{N2-FEED}$)	
6	Feed and column pressure	
7	Number of reactive stages	
8	Catalyst mass per reactive stage	

4.6.1 Study of Process Variables

Each factor presented in Table 4.7 is investigated to find its range of operation, based on process constraints, literature or assumptions. Lastly, the response variables are detailed.

Mass Flow of Xylose Solution (X_1)

In Rosenlew process, the mass flow of pentosan solution is 3899 kg/h, composed of two fractions: 3090 kg/h for water and 809 kg/h for pentosan. As previously presented, xylose solution was chosen in lieu of pentosan under the same ratio (809:3090). Due to the absence of constraints for feed mass flow ($\dot{m}_{XYL-FEED}$), the range of X_1 was arbitrarily defined from 2000 to 4000 kg/h.

$$2000 \leq \dot{m}_{XYL-FEED} \leq 4000 \quad (kg/h) \tag{4.21}$$

Mass Fraction of Xylose in the Feed (X_2)

According to Zeitsch (2000a), xylose is highly soluble in water (approximately 117 g of xylose per 100 mL at 20 °C). As a consequence, feed solution can have a maximum xylose mass fraction of around 54%. Knowing that the xylose mass fraction in the feed is 20.75% in the base case, the range of xylose mass fraction (x_{XYL}) is chosen between 20.75% and 50%. A mass fraction lower than 20.75% was not considered due to the interest in maximising furfural production.

$$0.2075 \leq x_{XYL} \leq 0.50 \tag{4.22}$$

Temperature of Xylose Feed (X_3)

The minimal temperature of xylose feed was 20 °C, based on the xylose solubility constraint discussed above. As for the ceiling temperature, it was arbitrarily chosen at 60 °C.

$$20 \leq T_{XYL-FEED} \leq 60 \quad (^{\circ}\mathrm{C}) \tag{4.23}$$

Mass Fraction of Water in N2-FEED (X_4)

The base case included nitrogen gas to reduce steam consumption and costs in the process. According to Agirrezabal-Telleria, Gandarias and Arias (2013), furfural stripping using N_2 can reduce process costs and efficiently strip furfural from liquid phase. Thus, the gas feed is composed of N_2/steam. The chosen range of steam fraction y_w in the feed was from 0.3 to 0.7.

$$0.3 \leq y_w \leq 0.7 \tag{4.24}$$

Temperature of N2-FEED (X_5)

The gas temperature in the feed ranged from 265 °C, similar to Rosenlew process, to 365 °C. A range of 100 °C was considered ideal to study the process while maintaining column temperature from 150-170 °C, where kinetic parameters are valid.

$$265 \leq T_{N2-FEED} \leq 365 \quad (^{\circ}\mathrm{C}) \tag{4.25}$$

Column and Feed Pressure (X_6)

An azeotrope search (built-in tool in Aspen Plus) was conducted to identify water-furfural conditions which have a constant boiling point at a particular composition in a homogeneous or heterogeneous mixture. From UNIQUAC range of validity and Rosenlew operating parameters, the highest column pressure was 10.05 bar. It was found that between 7.5 and 10.05 bar there is no azeotrope formation in the water-furfural system. Thus, the same pressure range was considered in the design of experiments.

$$7.5 \leq P \leq 10.05 \quad (bar) \tag{4.26}$$

Number of Reactive Stages (X_7)

The reactive stripping column had fixed 30 stages in the base case, however, the number of reactive stages (N_r) was arbitrarily chosen from 5 to 20. Each reactive stage possess a certain quantity of catalyst.

$$5 \leq N_r \leq 20 \tag{4.27}$$

Mass of Catalyst per Stage (X_8)

Bîldea et al. (2017) investigated the production of dimethyl ether (DME) by means of reactive distillation. For a column with 2.1 m of diameter by 28 m high, the optimum mass of catalyst per reactive stage was 193.2 kg. Further design information about catalytic packing can be found elsewhere (GÖTZE et al., 2001). Bearing this example in mind, where a similar column diameter was used, the range of catalyst mass per stage varied from 5 to 65 kg in this work. The choice of 65 kg for the maximum amount of catalyst is due to the higher cost of Nb_2O_5 based catalyst compared to alumina and ion exchange resin used in the work of Bîldea et al. (2017).

$$5 \leq m_{cat} \leq 65 \quad (kg) \tag{4.28}$$

Furfural Yield (Y_1)

The first response variable studied in this work is the furfural yield, which is represented by Equation 4.29. The desired value is the one that approaches 100%.

$$Y_1 = \frac{Total\ furfural\ produced\ (kmol/h)}{Xylose\ feed\ (kmol/h)} \cdot 100\% \tag{4.29}$$

4.6.2 Plackett-Burman

Once the eight factors are known and their range defined, the 12-run Plackett-Burman design was conducted (Table E.1) for factor screening. These results provide information about each factor and its relevance regarding the response variable Y_1.

4.6.3 Central Composite Rotatable Design (CCRD)

After factor screening, the remaining factors are used to build a Central Composite Rotatable Design, thus allowing the analysis of variance and optimising process conditions. Along with Y_1, another response variable (Y_2) and reactor temperature are studied in the CCRD.

Fraction of Furfural (Y_2)

The second response variable is the molar fraction of furfural that is recovered at the top of the reactive stripping column. The fraction of furfural is calculated according to Equation 4.30. The objective is to recover furfural at the top of the column, thus the desired value for this response value should be the highest possible.

$$Y_2 = \frac{Furfural\ in\ GAS\ (kmol/h)}{Total\ furfural\ produced\ (kmol/h)} \cdot 100\% \tag{4.30}$$

Reactor Temperature

The stripping reactor temperature is of prime importance to validade the simulation results. Since kinetic data from experimental part was obtained under 150-170 °C, the same range of operating temperature must be considered inside the column. Thus, the results from both Plackett-Burman and CCRD were neglected when they had not satisfied the temperature constraint.

Chapter 5

Results and Discussion

5.1 Catalyst Characterisation

5.1.1 Textural Properties

The textural properties of a catalyst can provide relevant information and insights on catalyst performance. Some of the textural properties investigated in this work include: specific surface area, pore volume, pore diameter and particle size distribution.

The particle size distribution of unmodified NBAL catalyst was studied after calcination (Figure 5.1) using laser diffraction. The mean particle diameter was approximately 69 μm, which is close to the nominal γ-Al_2O_3 diameter given by the manufacturer (40 μm). The increase in diameter after impregnation and calcination can be explained by the addition of the catalyst precursor over the support and the effect of thermal treatment (calcination), which could possibly rearrange catalyst structure, thus resulting in larger particle sizes.

Moreover, certain values of cumulative volumes provide additional information about particle size distribution. The Table 5.1 shows three cumulative volumes: 10, 50 and 90% (D10, D50 and D90, respectively). For instance, D90 indicates that 90% of the sample volume have a maximum particle size of 112 μm.

Figure 5.1: Distribution of particle size for NBAL catalyst.

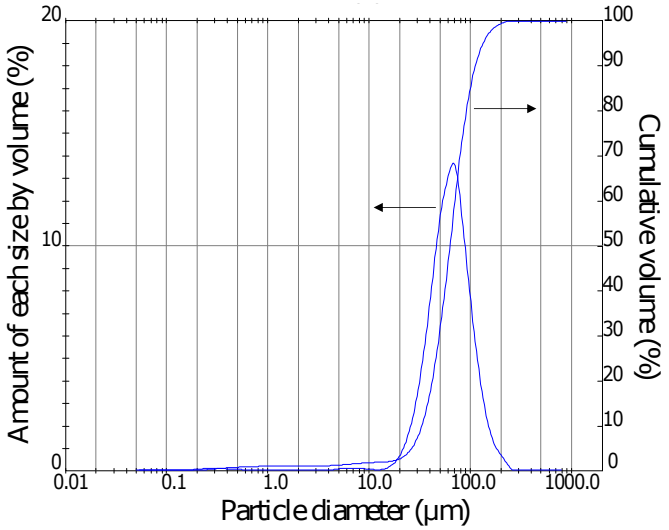

Table 5.1: Particle size information for 10, 50 and 90% of sample volume (NBAL).

	Particle size (μm)
D10	33
D50	63
D90	112

The catalyst sample was also qualitatively analysed by optical microscopy to ensure that the same range of particle size was found. The image shown in Figure 5.2 validates laser diffraction results by showing a similar range of particle distribution, since most particles have a particle size near 60 μm.

These results of particle size mean value and distribution are relevant for further investigation of internal mass transport effects.

Figure 5.2: Optical microscope image of NBAL catalyst.

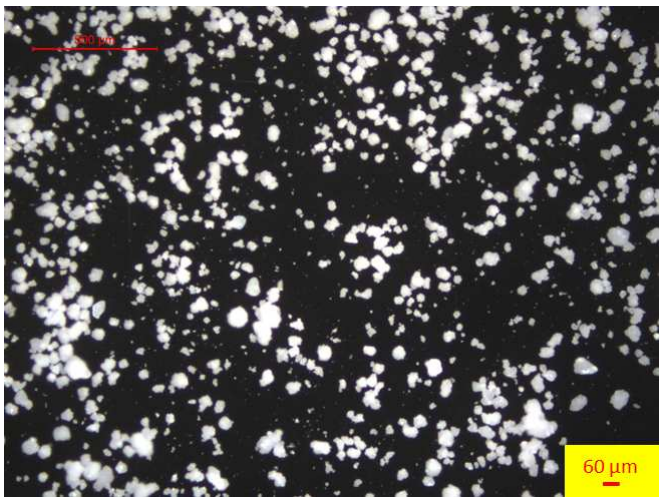

The surface area was determined by N_2 physisorption and calculated by the B.E.T. method and pore distribution by B.J.H. method. These properties are summarised in Table 5.2.

Table 5.2: Textural properties of calcined niobium oxide based catalysts.

Catalyst	S_{BET} $(m^2 \cdot g^{-1})$	V_{pore} $(cm^3 \cdot g^{-1})$	D_{pore} (Å)
NBAL	133	0.20	59
NBAL-N	114	0.19	62
NBAL-P	33	0.08	87

It is noticed from nitrogen adsorption results that both unmodified and HNO_3 treated catalysts showed quite similar pore diameter and pore volume, whilst surface area was about 17% higher for the unmodified one. Consequently, it is reasonable to consider that nitric acid treatment had minimal impact on the textural properties of the catalyst. Additionally, the impact on catalytic performance may not be similar, thus both catalysts will be further investigated in the following sections.

On the other hand, phosphoric acid treatment on Nb_2O_5/Al_2O_3 catalyst had a significant effect on textural properties, reducing surface area to 33 $m^2 \cdot g^{-1}$ and pore volume to 0.08 $cm^3 \cdot g^{-1}$, whilst pore diameter slightly increased to 87 Å comparing to 59 and 62 Å from the first two catalysts analysed. These results suggest that pore depth is being reduced for NBAL-P, thus decreasing its pore volume.

In terms of surface area, Table 5.3 presents a few results found in the literature for comparison. It is noticeable that for 16% Nb_2O_5 catalysts the calcination temperature had no significant impact on the surface area, although other minimal differences in catalyst preparation could exist and therefore impact surface area.

Table 5.3: Reported values of surface area of Nb_2O_5 supported on Al_2O_3.

Nb_2O_5 content (%)	Calcination temperature (°C)	S_{BET} $(m^2 \cdot g^{-1})$	Reference
12	550	252	García-Sancho et al. (2014a)
16	850	106	Kitano et al. (2012)
16	500	155	Kitano et al. (2013)
16	300	133	This work

All catalyst samples showed nitrogen adsorption-desorption isotherm of type IV (Appendix A.1), which is typical of mesoporous materials according to the IUPAC classification.

5.1.2 Chemical Composition

For XRF analysis, calcined Nb_2O_5/Al_2O_3 catalyst powder (1.018 g) was mixed with wax binder and pressed under 20 ton for 10 seconds. Results are presented in Table 5.4.

Table 5.4: Chemical composition of the catalyst.

Species	Concentration (%wt.)
Nb_2O_5	15.9
Al_2O_3	82.6
Impurities	1.5

Both Nb_2O_5 and Al_2O_3 presented concentrations similar to the ones desired after wet impregnation, which were 16 and 84%, respectively. Impurities detected include silica, iron, manganese and other metal oxides in small quantities. Overall, XRF analysis showed that wet impregnation was efficient to support Nb_2O_5 on Al_2O_3 in the desired quantities.

5.1.3 Catalyst Surface Acidity

Xylose dehydration is an acid-catalysed reaction as previously described. Accordingly, the investigation of catalyst surface acidity is of prime importance. For this reason, TPD-NH_3 was conducted for all catalyst samples. The catalyst with HNO_3 treatment was also investigated but maximum temperature was lower than the one used for NBAL and NBAL-P. The NBAL-N sample was heated up to 250 °C instead of 500 °C to avoid release of nitric acid that could possibly damage the equipment.

The acid treatment can modify catalyst surface acidity by (*i*) changing surface structure and/or; (*ii*) functionalising catalyst surface due to the bonding of new species, thus changing overall acidity and strength of acid sites. The HNO_3 treatment is expected to impact on the catalyst structure, whilst H_3PO_4 treatment could impact on both overall structure and acid sites formed by the anchorage of phosphate groups (GUPTA; FUKUOKA; NAKAJIMA, 2017). From textural properties analysis, it was seen that H_3PO_4 acid treatment had a significant impact on catalyst structure, thus reducing its specific surface area. In the following discussion, the impact on the overall acidity will be presented.

NBAL

The profile of NH_3 desorption over time (and temperature) indicates the presence of acid sites with a wide range of strength (Figure 5.3). The total amount of NH_3 desorbed was 9.1 $\mu mol \cdot m^{-2}$, which is quite higher than usually reported in the literature for catalysts used in xylose dehydration to furfural. García-Sancho et al. (2014a) found 1.7 $\mu mol \cdot m^{-2}$ of NH_3 desorbed for the 12% Nb_2O_5/Al_2O_3 calcined at 550 °C. Many variables can influence the final performance of the catalyst, such as calcination temperature, Nb_2O_5 loading and preparation method, distribution of Lewis and Brønsted acid sites on the surface, etc. In this scenario, it is imprecise to justify a certain behaviour based only on TPD-NH_3. A greater understanding could be achieved by conducting FTIR-pyridine analysis to identify Lewis and Brønsted acid sites (KITANO et al., 2013).

Figure 5.3: TPD-NH_3 profile for NBAL catalyst.

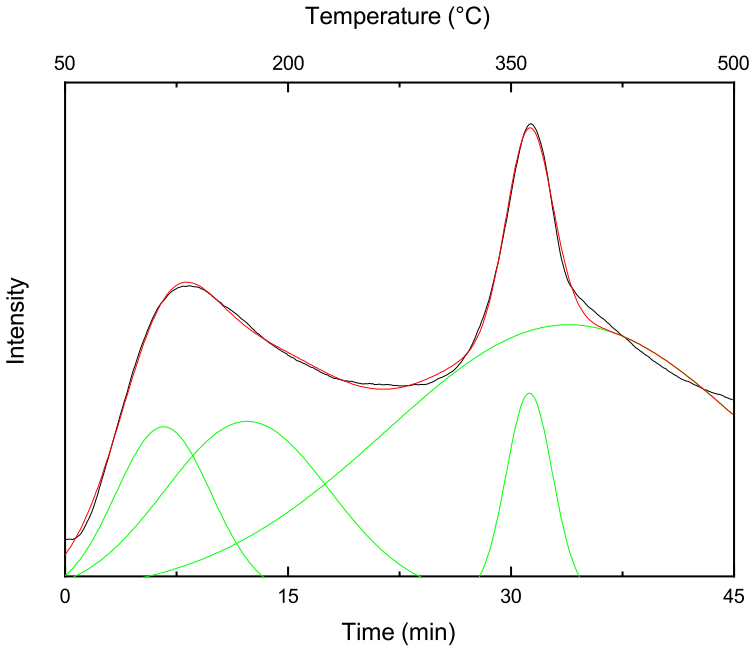

The integration results for NBAL catalyst and the main peak information, such as temperature, amount of NH_3 desorbed, peak contribution and strength are shown in Table 5.5.

Table 5.5: Peak description of TPD-NH_3 analysis for NBAL catalyst.

Peak	Temperature (°C)	$\mu mol\ NH_3 \cdot m^{-2}$	Contribution (%)	Strength[a]
1	115.7	0.95	10.5	Weak
2	170.8	1.70	18.7	Weak
3	362.4	0.55	6.1	Intermediate
4	389.7	5.88	64.7	Intermediate
Total		9.1	100	

[a]Acidity strength (BERTEAU; DELMON, 1989).

The peak number 4 (389.7 °C) had the larger contribution (64.7%) to total catalyst acidity. The results possibly indicate that strength of acid sites vary from weak (peaks 1 and 2) to intermediate (peaks 3 and 4), in which intermediate strength account for about 71% of total acidity.

NBAL-N

The TPD-NH_3 analysis for NBAL-N was conducted at a lower temperature compared to NBAL and NBAL-P as previously discussed. The profile of NH_3 desorption over time (and maximum temperature of 250 °C) for NBAL-N catalyst is presented in Figure 5.4.

Figure 5.4: TPD-NH_3 profile for NBAL-N catalyst.

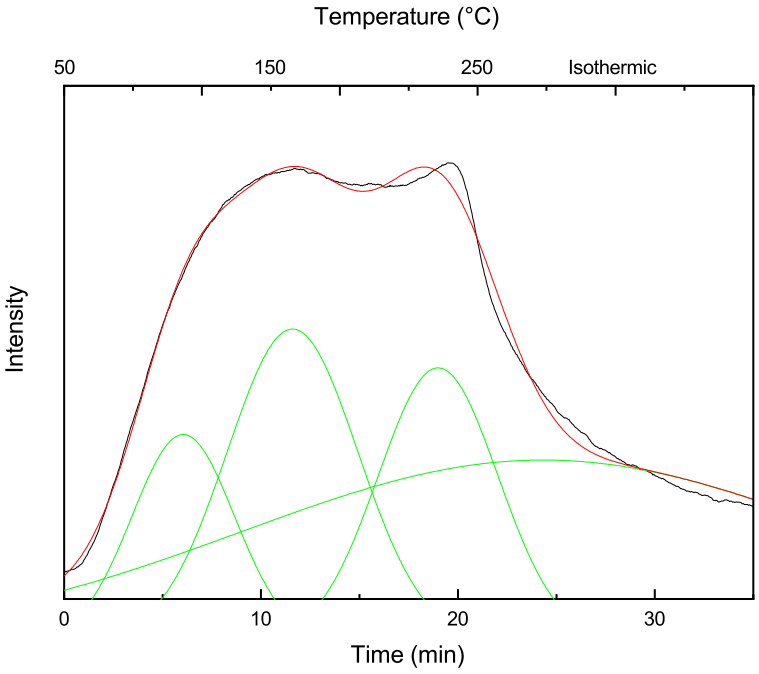

The main peak information, such as temperature, amount of NH_3 desorbed, peak contribution and strength are shown in Table 5.6.

Table 5.6: Peak description of TPD-NH_3 analysis for NBAL-N catalyst.

Peak	Temperature (°C)	$\mu mol\ NH_3 \cdot m^{-2}$	Contribution (%)	Strength[a]
1	110.1	0.51	10.4	Weak
2	164.7	0.98	20.1	Weak
3	237.2	0.79	16.1	Intermediate
4	249.7	2.62	53.5	Intermediate
Total		4.9	100	

[a]Acidity strength (BERTEAU; DELMON, 1989).

Similarly to NBAL catalyst, the highest peak contribution for NBAL-N is associated with acid sites of intermediate strength. However, the comparison between the amount of desorbed NH_3 would be more appropriate under similar range of temperature, that is, under 250 °C. For instance, NBAL catalyst had a total acidity of 2.7 μmol $NH_3 \cdot m^{-2}$ under 250 °C, whilst NBAL-N acidity was 4.9 μmol $NH_3 \cdot m^{-2}$. Since these values are similar and both contributions are related to weak acid sites, it is suggested that these catalysts have similar overall acidity.

NBAL-P

In the integration of TPD-NH_3 curve shown in Figure 5.5 a different number of peaks and distribution were obtained. The integration results for NBAL-P catalyst and the main peak information, such as temperature, NH_3 consumption, peak contribution and strength are shown in Table 5.7.

The larger contribution to the catalyst acidity was detected at a high temperature (411.8 °C), which is slightly superior compared to the unmodified catalyst (389.7 °C) under similar overall contribution (62.7 and 64.7%, respectively). This result indicates that stronger acid sites are found in NBAL-P catalyst. Overall, the total acidity of NBAL-P was 46.9 $\mu mol \cdot m^{-2}$ of NH_3, which is significantly close to the total acidity of Nb_2O_5 treated with H_3PO_4 (40.2 $\mu mol \cdot m^{-2}$) investigated by Fontana (2016). Similarly to the NBAL catalyst, the profile of NH_3 desorption over temperature indicates the presence of acid sites with a wide range of strength in NBAL-P catalyst (Figure 5.5).

Further discussion is presented in Catalytic Performance and Reaction Modelling sections.

Figure 5.5: TPD-NH_3 profile for NBAL-P catalyst.

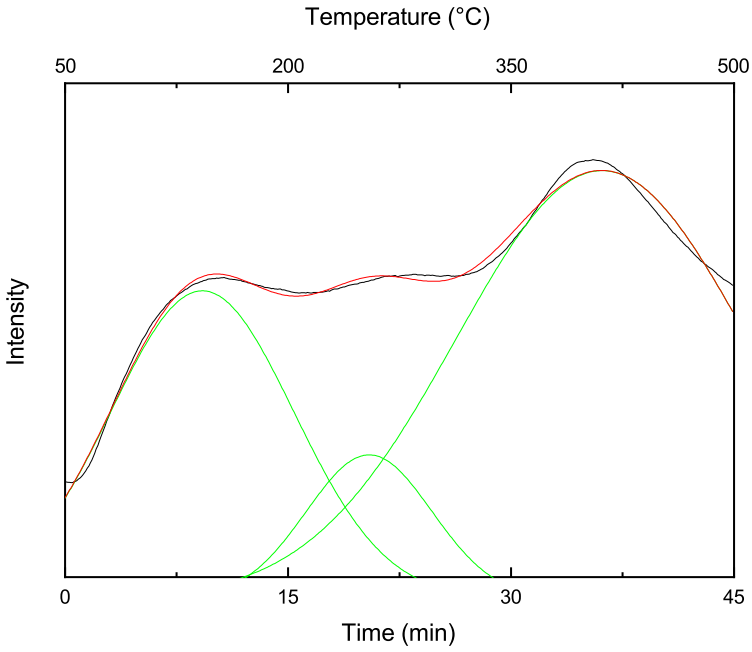

Table 5.7: Peak description of TPD-NH_3 analysis for NBAL-P catalyst.

Peak	Temperature (°C)	$\mu mol\ NH_3 \cdot m^{-2}$	Contribution (%)	Strength[a]
1	141.3	13.3	28.3	Weak
2	252.0	4.2	9.0	Intermediate
3	411.8	29.4	62.7	Strong
Total		46.9	100	

[a]Acidity strength (BERTEAU; DELMON, 1989).

5.2 Reactor Modification

Prior to catalytic tests, the reactor was submitted to a structural modification in order to operate with approximately 2/3 of its volume. In sequence, tests were carried out to evaluate the validity of few hypotheses, such as perfect mixing (residence time distribution, RTD), and absence of mass transfer resistances (both internal and external).

The Parr reactor (300 mL) used for catalyst testings was modified in order to uniformly distribute reaction components, and thus operate with approximately 200 mL reaction volume. For this purpose, the shaft was equipped with two 4-blade impellers as depicted in Figure 5.6.

Figure 5.6: Scheme of two 4-blade impeller used in the reaction.

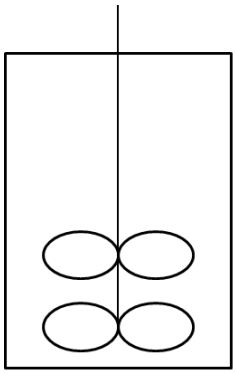

The ideality of reaction stirring was verified by experiments of residence time distribution (RTD). A theoretical 20%wt. xylose concentration (grams of xylose per kg of solution) inside the reactor was obtained by adding xylose solution (4.00 g of xylose dissolved in 36 mL of water) into the reactor containing 160 mL of water under room temperature to avoid xylose conversion or degradation. At the time of xylose injection ($t = 0$) samples were collected every few minutes for 35 minutes. Stirring was kept at 650 rpm during the RTD test while xylose concentration reaches between 19 and 20%wt. within less than five minutes, as shown in Figure 5.7. This result indicates that conditions of stirring rate, the volume of water inside the reactor and the injected solution volume are sufficient to validate the hypotheses of perfect mixing. Consequently, similar conditions of xylose injection, water volume, and stirring rate were used in each catalyst testing.

Figure 5.7: Distribution of residence time of xylose inside the Parr reactor (300 mL) using two 4-blade impellers.

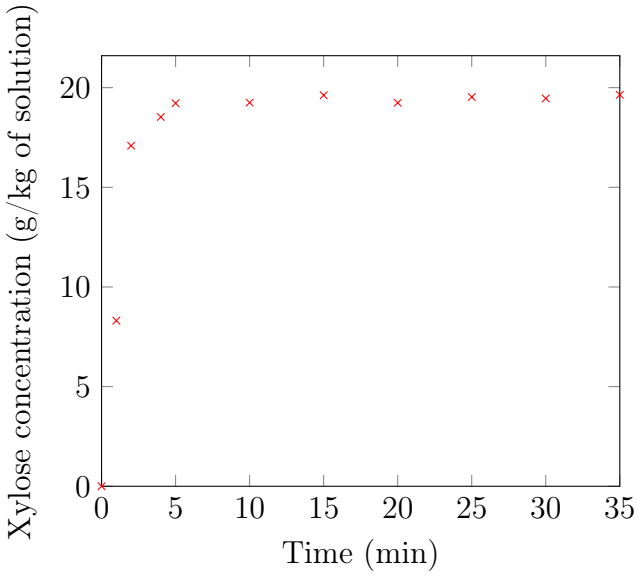

5.3 Effect of External Mass Transport

Two catalyst testings were conducted at 150 °C using different mass of catalyst (Nb_2O_5/γ-Al_2O_3): 0.800 and 0.400 g. Table 5.8 shows specific rate of reaction 2 hours after its beginning.

Table 5.8: Specific rate of reaction varying mass of catalyst.

Mass of catalyst (g)	0.800	0.400	Relative Error (%)
Rate of reaction (10^{-5} mol ${g_{cat}}^{-1}$min^{-1})	1.79	1.63	8.9

The relative error between the two tests was 8.9%, which lies slightly above the expected value (maximum of 5%) for a condition where external mass transfer resistance is negligible (AUGUSTINE, 1995). Tests with increased stirring rate were also performed, however increasing stirring rate above 650 rpm led to undesired mixture patterns, and thus were not chosen. As a consequence of the relative error found, the reaction system can be considered under minimal external mass transfer resistance. Accordingly, all reaction constants and activation energies calculated were referred to as apparent.

5.4 Effect of Internal Mass Transport

Results from laser diffraction suggest that resistance to internal diffusion can be neglected due to the small particle size obtained, however, Weisz-Prater criteria was calculated to validate this assumption.

In order to use Equation 4.8, parameter λ was calculated using xylose radius (LI; JIA; WANG, 2016) and pore radius from adsorption analysis results, whereas p was assumed to be 16.26 based on measured data of liquid diffusivities of organics in a silica-alumina catalyst (SATTERFIELD; COLTON; PITCHER J., 1973). This approach was used due to the absence of data for the species studied in this work. Similar approximation was made elsewhere (VANNICE, 2006).

The Weisz-Prater numbers (C_{WP}) for NBAL catalyst in all temperatures were estimated using the aforementioned method. The C_{WP} value was calculated for all reaction points (Figure 5.8), and the highest C_{WP} value for each reaction temperature is presented in Table 5.9. It is noticeable that all values lie in the range $C_{WP} < 0.3$, which confirms that resistance to internal diffusion is minimal (SIEVERS et al., 2016).

Figure 5.8: Weisz-Prater number (C_{WP}) during the reaction.

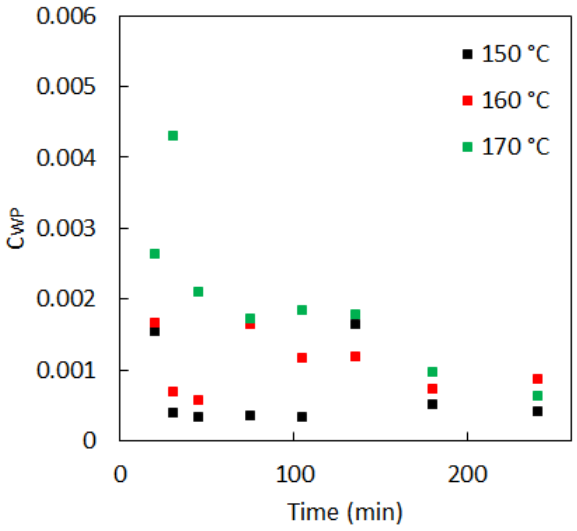

Table 5.9: Estimated values of Weisz-Prater criteria for all reaction temperatures using NBAL catalyst.

Reaction Temperature (°C)	C_{WP}
150	0.0016
160	0.0017
170	0.0043

5.5 Catalytic Performance

The overall performance for each catalytic test is presented in Table 5.10. It is noticeable that NBAL and NBAL-N, solids with surface areas of 133 and 114 m^2/g, respectively, had higher xylose conversions compared to NBAL-P in all range of temperatures after 4 hours of reaction. Another remark from NBAL and NBAL-N performance is that, even though xylose conversion increases with temperature, the selectivity to furfural remains at similar values at 160 and 170 °C, indicating that secondary reactions occur in a larger extent at higher temperatures. This is confirmed by analysing the carbon balance, which shows a decrease when reaction temperature is higher. The carbon balance also decreases over time (as the reaction occurs), indicating that secondary and degradation reactions occur in the entire reaction time, as seen is Figures 5.9 and 5.10 for NBAL and NBAL-N, respectively.

Table 5.10: Overall performance for all catalysts (conversion of xylose, furfural yield and selectivity to furfural).

Catalyst	Temperature (°C)	Conversion (%)	Yield (%)	Selectivity (%)	Carbon Balance (%)
NBAL	150	71	17	24	65
	160	85	28	33	57
	170	93	30	32	48
NBAL-N	150	83	19	22	44
	160	91	32	35	46
	170	98	34	35	37
NBAL-P	150	19	16	88	98
	160	40	30	75	90
	170	62	49	79	87

Reaction conditions: water as solvent at 150, 160 and 170 °C during 4 hours. Initial xylose loading: 20 $g \cdot kg^{-1}_{solution}$; catalyst mass: 0.800 g.

Figure 5.9: Carbon balance profile during the reaction for NBAL catalyst.

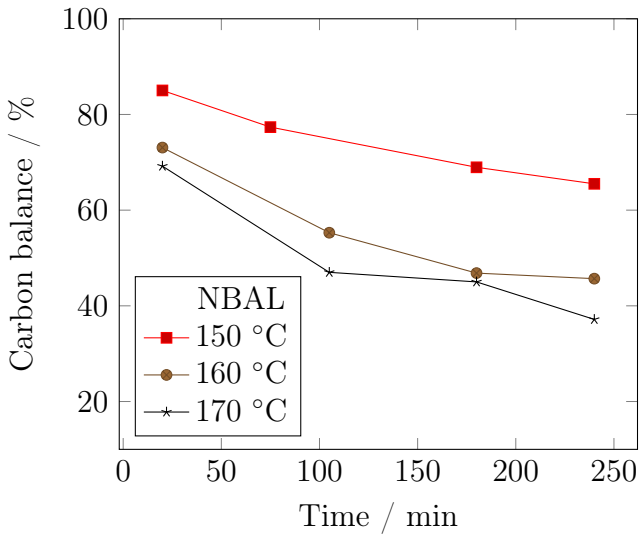

In order to compare catalytic performance, the xylose conversion and furfural yield was plotted (Figures C.1, C.2 and C.3). When analysing points at the same temperature and conversion (isoconversion), it is observed that both NBAL and NBAL-N had similar furfural yield, with most points overlapping one another. However, NBAL-P catalyst showed a higher furfural yield compared to both NBAL and NBAL-N when observing at the same conversion and temperature.

Figure 5.10: Carbon balance profile during the reaction for NBAL-N catalyst.

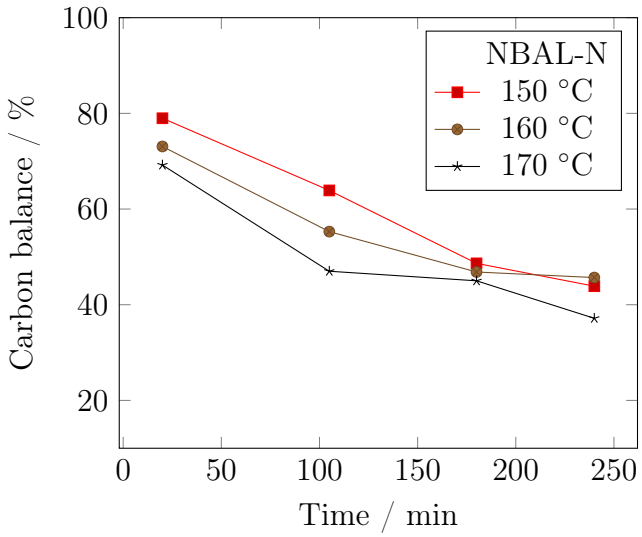

Since selectivity is of prime importance in biomass conversion, the selectivity towards furfural was investigated near isoconversion at 150 °C (Figure 5.11), 160 °C (Figure 5.12) and 170 °C (Figure 5.13). It is observed that NBAL-P catalyst had higher selectivities towards furfural at all temperatures. In addition to the lower selectivities for NBAL and NBAL-N, both catalysts had similar trend, indicating that their selectivity to furfural is quite comparable.

Figure 5.11: Furfural yield and selectivity at 150 °C at isoconversion.

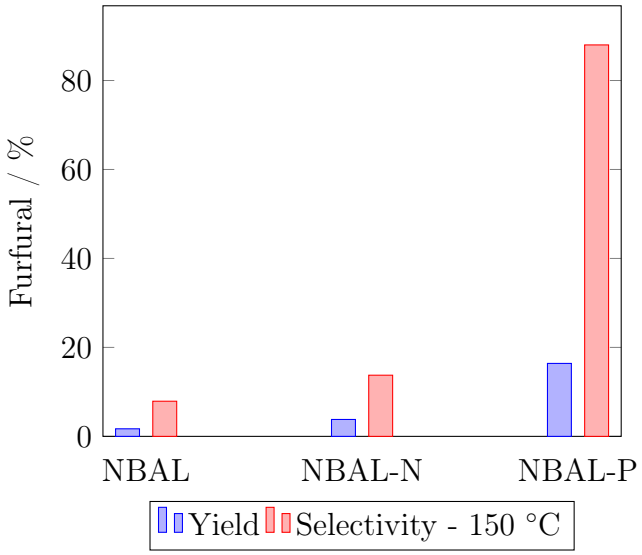

Conversions: NBAL (21.5%), NBAL-N (27.5%) and NBAL-P (18.6%).

Moreover, due to the similar textural properties and catalytic performance of both NBAL and NBAL-N, it is reasonable to infer that the treatment using HNO_3 had

minimal effect on the catalytic performance. To further investigate this inference, it would be necessary to perform characterisation techniques, such as FTIR-pyridine to estimate Lewis and Brønsted acid sites on both catalysts and understand whether acid treatment had an impact on catalytic acidity.

Figure 5.12: Furfural yield and selectivity at 160 °C at isoconversion.

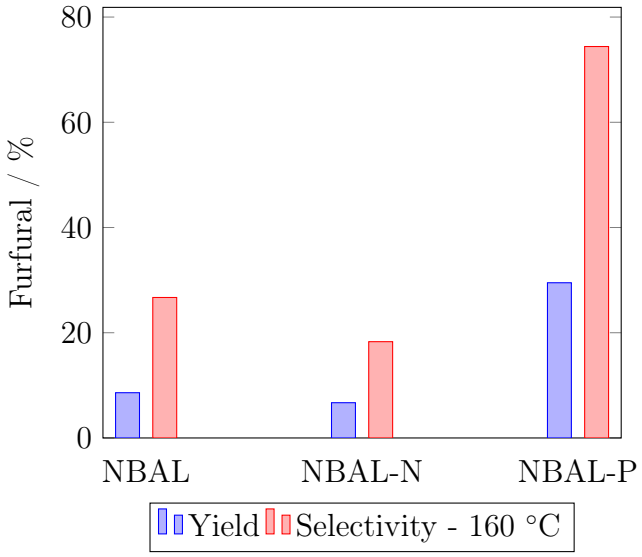

Conversions: NBAL (32.1%), NBAL-N (36.4%) and NBAL-P (39.7%).

Figure 5.13: Furfural yield and selectivity at 170 °C at isoconversion.

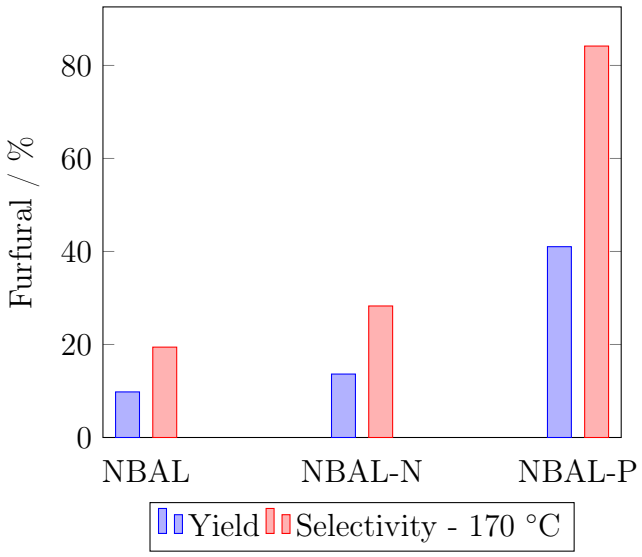

Conversions: NBAL (50.2%), NBAL-N (48.2%) and NBAL-P (48.8%).

Despite of the lower surface area obtained for NBAL-P, which is an indication of lower conversions in heterogeneously catalysed reactions, the surface acidity can also play an important role. The effect of H_3PO_4 acid treatment seems to have affected

not only superficial area (a sharp decrease to 33 m^2/g) but also the selectivity towards furfural, which reached about 75-88% after 4 hours of reaction and higher values compared to NBAL and NBAL-N as discussed above. It is also observed that NBAL-P catalyst presented the highest carbon balances, which indicate that secondary reactions occur in a lower extent compared to NBAL and NBAL-N catalysts. The carbon balance evolution using NBAL-P catalyst during the reaction is presented in Figure 5.14. Similarly to NBAL and NBAL-N, NBAL-P has also a decrease in carbon balance for higher temperatures and exhibit formation of undesired products all along the reaction.

Another interesting remark from the catalyst modified by phosphoric acid treatment is the absence of intermediates in reaction media during the entire reaction time. This observation indicates that the increase in selectivity towards furfural can be explained by both (i) decrease in surface area, thus hampering oligomerisation and side-reactions inside catalysts pores and; (ii) inhibition of isomerisation reaction occurring on Lewis acid sites. In addition to the higher selectivity and carbon balance found for NBAL-P catalyst, it is also interesting to compare qualitatively the colour of catalyst samples after 4 hours of reaction (Figure 5.15). It is noticeable that the increase in temperature darkens catalysts samples (indicating solid depositions), whilst NBAL-P catalyst presents a lighter colour for all temperatures.

Figure 5.14: Carbon balance profile during the reaction for NBAL-P catalyst.

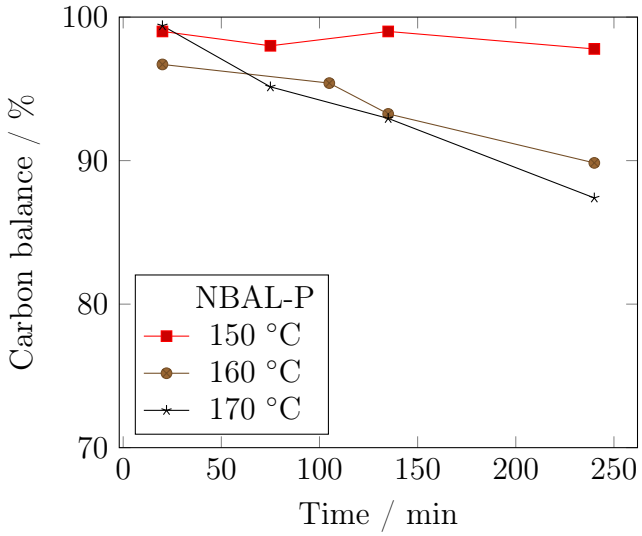

Although the amount of desorbed NH_3 was significantly higher for the catalyst treated with phosphoric acid, about five times higher compared to NBAL, the overall conversion during xylose dehydration was not enhanced for NBAL-P. On the contrary,

the NBAL-P catalyst had lower conversions, but yield and selectivity to furfural was enhanced.

Figure 5.15: Catalysts samples after 4 hours of reaction.

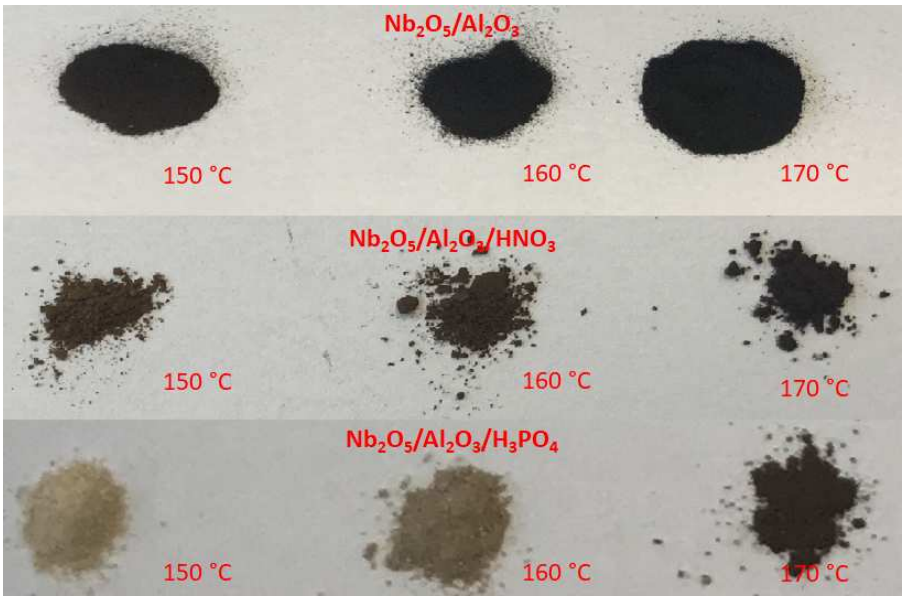

The impact of phosphoric acid modification has also been observed by Gupta, Fukuoka and Nakajima (2017) in their work, where they investigated the modification of non-supported Nb_2O_5 by H_3PO_4 acid treatment for furfural production. They remarked that the acid modification increased furfural selectivity from 48 to 67%, and this was due to a high density of phosphate groups on Nb_2O_5, which prevents the access of xylose molecules to Lewis acid sites. Their conclusion was based on the results of Nakajima et al. (2011), who compared the density of phosphate group (1 mmol/g) to Lewis acid site (0.03 mmol/g) on Nb_2O_5, and thus concluded that the acid treatment is probably causing a steric hindrance. However, special care must be taken to validate this explanation. Although the authors had justified the density of phosphate group to be larger than Lewis acid sites based on mmol per grams, it would be more appropriate to present these data in a more reliable way, that is, in mmol per area (mmol/m^2 for example).

In order to understand carbon balances found for each catalyst, a series of compounds were injected in HPLC, such as lyxose, formic acid, glucoaldehyde, glyceraldehyde, dihydroxyacetone, hydroxyacetone and lactic acid. These compounds are soluble in water and mainly formed in side-reactions involving xylose under hydrothermal conditions, except for lyxose, which is a xylose isomer and formic acid, which is a furfural degradation product (AIDA et al., 2010; MÖLLER; SCHRÖDER,

2013). The formation of humins as unidentified products in liquid phase and solid depositions, which are mainly responsible for catalyst darkening (Figure 5.15), are also present. The reaction network involving these compounds and the ones that were found in this work are presented in Figure 5.16 and Table 5.11, respectively.

Figure 5.16: Xylose and furfural reactions network (LBET: Lobry de Bruyn–Alberda van Ekenstein-transformation).

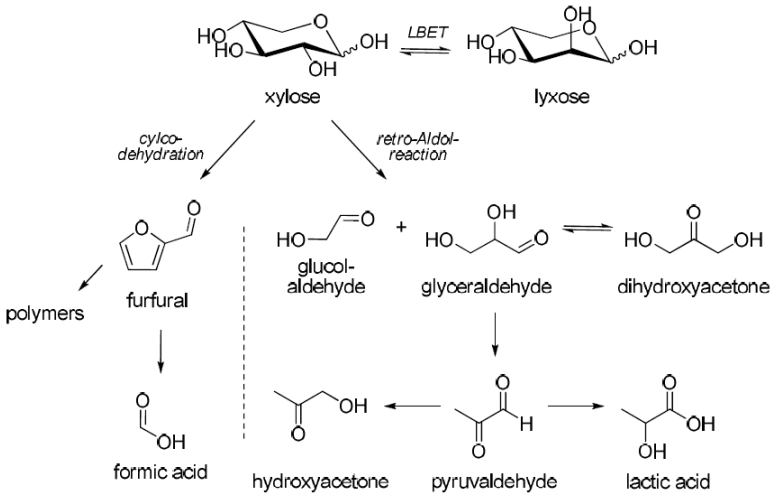

Source: Adapted from Möller and Schröder (2013).

Table 5.11: Possible soluble compounds formed during the reaction for each catalyst.

Catalyst\Compound	LYX	FAC	GLU	GLY	DHA	HA	LAC
NBAL	Yes	Yes	Yes	No	Yes	Yes	Yes
NBAL-N	Yes	Yes	Yes	No	Yes	Yes	Yes
NBAL-P	No	Yes	Yes	No	No	No	No

LYX: lyxose, FAC: formic acid, GLU: glucoaldehyde, GLY: glyceraldehyde, DHA: dihydroxyacetone, HA: hydroxyacetone, LAC: lactic acid.

From Table 5.11 results, it is observed that reactions using NBAL and NBAL-N formed more undesired products than the one using NBAL-P. In particular, the only compound that was not detected at all reactions was glyceraldehyde, although its role as an intermediate in the formation of dihydroxyacetone and pyruvaldehyde. This observation indicates that glyceraldehyde could be consumed instantly during the reaction by both (*i*) dehydration to pyruvaldehyde or (*ii*) isomerisation to dihydroxyacetone (MÖLLER; SCHRÖDER, 2013). Since traces of dihydroxyacetone and lactic acid were found for NBAL and NBAL-N catalysts, it is possible to infer that both reaction paths are occurring. Another interesting remark is the absence of lyxose for reactions conducted using NBAL-P catalyst, indicating that Lewis acid sites are

either not present or in minimal amount on this catalyst at the reaction conditions. According to Santos et al. (2018), the formation of lactic acid from pyruvaldehyde is heterogeneously catalysed by Lewis acid sites in the Cannizzaro reaction, in which Brønsted acid sites play no role. In this scenario, the absence of lactic acid formation when using NBAL-P provide more evidence that Lewis acid sites are not present in this catalyst. The presence of lyxose and lactic acid when using NBAL and NBAL-N catalysts is an indication that Lewis acid sites have a higher density on these catalysts compared to NBAL-P.

Most results found in the literature for xylose dehydration using niobium based catalysts show that high selectivities towards furfural are hardly achieved without the use of an organic solvent (Table 5.12). Since Nb-based catalysts hardly achieve 50% of selectivity towards furfural, the results from NBAL-P catalyst herein presented can be seen as a promising approach towards selective production of furfural from xylose. For instance, Pholjaroen et al. (2013) obtained a selectivity of 39.5% to furfural (xylose conversion of 44.1%) at 160 °C when using a NbP catalyst and water as solvent. In this work, the reaction using NBAL-P at 160 °C reached 74% of selectivity (xylose conversion of 40%), indicating a more interesting performance despite the longer duration of the reaction.

Furthermore, the results from NBAL and NBAL-N catalysts suggest that the low carbon balance and the lower selectivity towards furfural are mostly caused by high reaction temperature, high surface areas, and the higher concentration of Lewis acid sites on the catalyst surface (thus, increasing degradation reactions) compared to NBAL-P, as suggested by the side-products obtained in each reaction. Moreover, it is also possible to infer that Al_2O_3 as support (present in all catalysts) had not significantly contributed as Lewis acid (DATKA et al., 1992), based on the aforementioned evidence and also on the work of Abdel-Rehim et al. (2006), who showed that strong alumina-associated Lewis acid sites are covered by niobia addition and niobium-associated weak Lewis acidic sites are formed. As a consequence, the results suggest that acid treatment with H_3PO_4 not only decreased specific surface area, but also increased catalyst acidity and favoured the direct conversion of xylose to furfural on Brønsted acid sites.

Table 5.12: Overall performance of heterogeneous catalysts for xylose conversion.

Catalyst	Reaction Condition	χ_{xyl} (%)	S_{fur} (%)	Reference
γ-Al_2O_3	Water (4 h, 140 °C)	84.2	24.5	A
NbP	Water (1 h, 160 °C)	44.1	39.5	B
NbP	Water+Toluene (1 h, 160 °C)	51.8	43.4	B
Nb_2O_5	Water (2 h, 130 °C)	96.8	42.1	C
Nb_2O_5	Water (3 h, 120 °C)	93	48	D
(12%)Nb_2O_5/Al_2O_3	Water+Toluene (4 h, 160 °C)	62	59	E

A: S. B. Kim et al. (2011); B: Pholjaroen et al. (2013); C: Vieira et al. (2018); D: Gupta, Fukuoka and Nakajima (2017); E: García-Sancho et al. (2014a).

Further discussion involving reaction network for each catalyst will be presented in each model proposed below.

5.6 Kinetic Model

Knowing that the reaction system is under minimal influence of mass transfer resistances (both internal and external), the mathematical model herein presented is considered pseudo-homogeneous of first-order for xylose dehydration and rate constants and activation energies are apparent. The mathematical model developed for each catalyst derived from the general reaction network (Figure 4.2) is presented thereafter.

5.6.1 NBAL

The mathematical model proposed for NBAL catalyst is based on the one described by Agirrezabal-Telleria, Larreategui, et al. (2011) (Equation 2.6 and 2.7) and experimental evidence found in this work. In the work of Agirrezabal-Telleria, Larreategui, et al. (2011), three rate constants were investigated: xylose cyclodehydration, condensation, and furfural resinification. However, a reaction of furfural with itself, commonly called "furfural resinification", is known to occur in a significant lower extent compared to condensation, which is the reaction between furfural and an intermediate (xylose, xylulose or lyxose) of xylose-to-furfural conversion (ZEITSCH, 2000c). Moreover, Zeitsch (2000c) also indicates that both furfural resinification and condensation reactions decrease their extent at higher temperatures due to the entropy effect.

Zeitsch (2000c) described that furfural loss reactions, condensation, and resinification, exhibit a behaviour similar to polimerisation. Accordingly, the formation of larger molecules leads to a decrease in entropy, making the change of entropy in the reaction (ΔS_R) a negative quantity. As it was reported, knowing that the enthalpy change in the reaction (ΔH_R) is also negative, the furfural loss reactions reach an inhibition at certain temperatures, where these reactions path become thermodynamically unfavourable. This observation is represented by Equation 5.1.

$$\Delta G_R = \Delta H_R - T \cdot \Delta S_R \tag{5.1}$$

In this scenario, the model proposed by Agirrezabal-Telleria, Larreategui, et al. (2011) was modified in this work by eliminating furfural resinification and condensation reactions, whilst adding xylose secondary reactions and isomerisation. Thus, the reactions proposed for NBAL catalyst are xylose isomerisation (k_1), furfural formation from isomers (k_2), direct xylose dehydration to furfural (k_3) and xylose degradation reactions (k_4), as shown in Figure 5.17. Due to the impossibility of individual quantification of xylulose and lyxose, they were considered as a single intermediate in the reaction model and labelled as isomers. A similar approach was used by Gallo et al. (2013) when studying xylose conversion in the presence of beta-zeolites.

Figure 5.17: Reaction network proposed for NBAL catalyst.

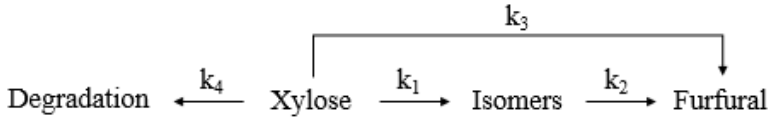

The reactions proposed for this catalyst generate one differential equation for each compound: xylose, furfural and intermediates represented by 5.2, 5.3 and 5.4, respectively. Although its simplicity, the proposed model can fit well experimental data at 150, 160 and 170 °C for xylose and furfural concentrations, as seen in Figures 5.18, 5.19 and 5.20. The Scilab code used to estimate rate constants is shown in Appendix B.

$$\frac{d[XYL]}{dt} = -k_1[XYL] - k_3[XYL] - k_4[XYL] \tag{5.2}$$

$$\frac{d[FUR]}{dt} = +k_2[I] + k_3[XYL] \tag{5.3}$$

$$\frac{d[I]}{dt} = +k_1[XYL] - k_2[I] \tag{5.4}$$

Figure 5.18: Concentration profile at 150 °C for NBAL catalyst.

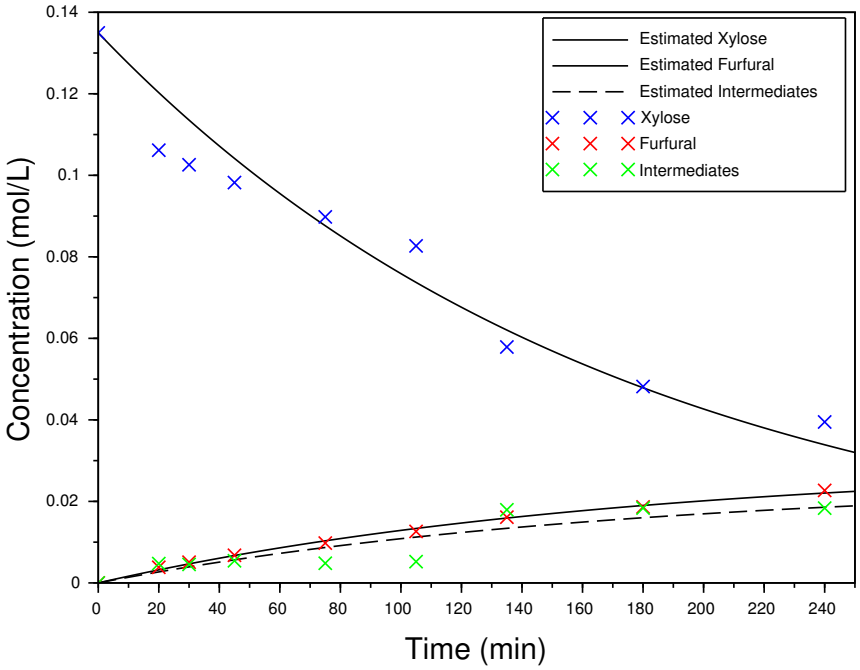

Figure 5.19: Concentration profile at 160 °C for NBAL catalyst.

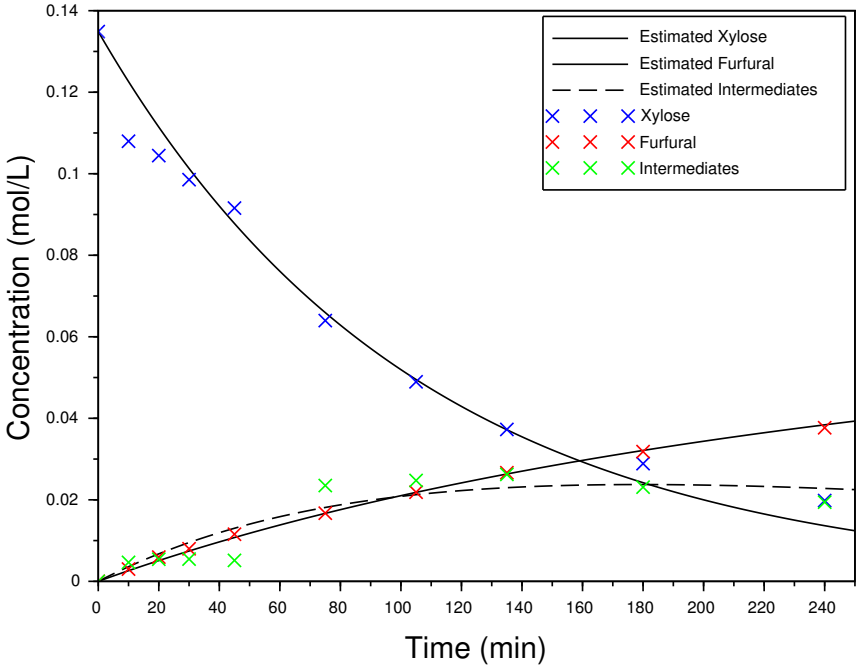

Figure 5.20: Concentration profile at 170 °C for NBAL catalyst.

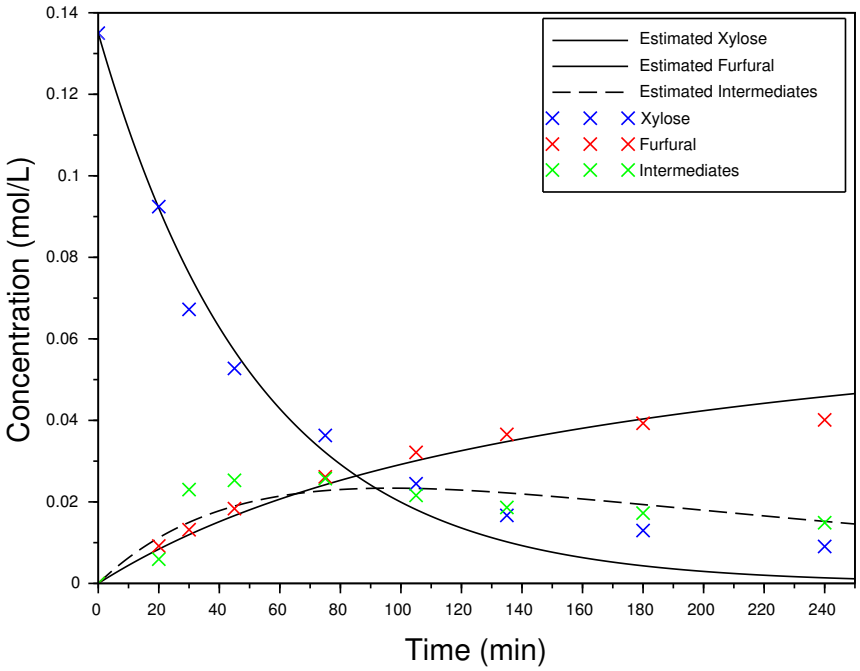

It is noticeable from concentration profiles obtained by the mathematical modelling that both xylose and furfural estimated concentrations fit with minimal divergence during the entire reaction at 150 °C, which is due to the better result for carbon balance at 150 °C compared to it at 160 and 170 °C. At higher temperatures, the carbon balance has a sharp decrease during reaction time (Figure 5.9), thus leading to a more significant deviation between estimated and experimental values. However, intermediates concentration at 150 °C did not show a similar profile compared to higher temperatures. To further investigate this observation, a duplicate reaction was conducted and similar behaviour was found: late formation of intermediates during reaction time. As a consequence, the fit of intermediates concentration was not satisfactory at 150 °C and led to a poor estimation of apparent reaction constant k_2, as seen in Table 5.13.

Furfural concentration profiles show modelling results with significant concordance with experimental data during the entire reaction time. Although traces of furfural degradation product (formic acid) was detected in reaction samples (concentrations around 10^{-5} and 10^{-6} $mol \cdot L^{-1}$), the low extent of secondary reactions involving only furfural is also suggested by the satisfactory fit compared to the estimated concentration profile of xylose.

The Table 5.13 shows apparent rate constants for all reactions in the network, and also the result of least squares difference (Equation 4.18) minimisation. From these results, it is observed that apparent rate constant for xylose degradation reactions (k_4) is about twice to three times higher than xylose isomerisation constant (k_1) and direct conversion to furfural (k_3). This observation agrees with the aforementioned discussion, where catalytic performance results showed that selectivity to furfural is considerably low (24-32%) and several products from undesired xylose reactions were identified.

Table 5.13: Apparent reaction constants and objective function for NBAL catalyst.

Temperature (°C)	10^3 k_1 (min^{-1})	10^3 k_2 (min^{-1})	10^3 k_3 (min^{-1})	10^3 k_4 (min^{-1})	Objective Function
150	1.1	0.0	1.3	3.4	$5.7 \cdot 10^{-3}$
160	2.8	2.9	2.0	4.7	$5.0 \cdot 10^{-3}$
170	5.3	4.8	3.5	10.4	$5.4 \cdot 10^{-3}$

As presented in literature review, García-Sancho et al. (2014a) studied 12% Nb_2O_5 supported on Al_2O_3 and found that rate constant of xylose dehydration reaction had little change when using toluene as co-solvent. Moreover, the specific rate constant at 160 °C for xylose dehydration found in their study ($7.3 \cdot 10^{-3}$ $min^{-1} \cdot g_{cat}^{-1}$) was quite higher compared to the one found for 16% Nb_2O_5 (NBAL) in this work ($2.0 \cdot 10^{-3}$ min^{-1} or $2.5 \cdot 10^{-3}$ $min^{-1} \cdot g_{cat}^{-1}$). The difference could be due to the different niobium oxide loading, and thus the acidic properties of the catalysts and difference in surface area. However, the primary influence on reaction rate may be due to the higher surface area in the catalyst used by García-Sancho et al. (2014a), since their catalyst acidity measured by TPD-NH_3 was lower than the one measured for NBAL (1.7 against 9.1 $\mu mol \cdot m^{-2}$ of NH_3, respectively). They obtained a specific surface area of 252 $m^2 \cdot g^{-1}$, which is almost twice higher than the one obtained for 16% Nb_2O_5 in this work (133 $m^2 \cdot g^{-1}$).

For all reactions involved in this model, the apparent rate constants increased with temperature, and thus Arrhenius Equation could be used to estimate apparent activation energies. However, due to the fit of intermediates at 150 °C, the apparent activation energies for k_1 and k_2 were not estimated. The apparent activation energies are presented in Table 5.14, as well as the coefficient of determination (R^2).

Table 5.14: Apparent activation energies for the NBAL reaction network.

	Apparent activation energy ($kJ \cdot mol^{-1}$)	R^2
Xylose $\rightarrow$ Furfural (k_3)	79.5	0.995
Xylose degradation (k_4)	85.8	0.936

Pre-exponential factors: $k_{3,o} = 7.0 \cdot 10^4\ min^{-1}$ and $k_{4,o} = 2.1 \cdot 10^6\ min^{-1}$

Both reactions studied followed Arrhenius Equation behaviour and resulted in high correlation coefficients. The apparent activation energy found for direct xylose dehydration to furfural was 79.5 $kJ \cdot mol^{-1}$, which lies below the range usually reported in the literature. O'Neill et al. (2009) found respectively 134 and 98 $kJ \cdot mol^{-1}$ for both xylose and lyxose dehydration to furfural using ZSM-5 zeolite in H^+ form. A similar range of activation energies was also found in the work of Choudhary, Sandler and Vlachos (2012) using homogeneous catalysts. It was reported that activation energies of xylose direct conversion and intermediate conversion to furfural were 133.7 and 96.5 $kJ \cdot mol^{-1}$. Although these works investigated different catalysts and mechanisms, the estimated value in this work (79.5 $kJ \cdot mol^{-1}$) is probably affected by the poor fit of intermediates profile at 150 °C. Further discussion will be done when presenting NBAL-N model results, since NBAL and NBAL-N had similar catalytic performance and textural properties.

The coefficient of determination (R^2) for xylose degradation reaction was, as expected, not close to the unity. The reason for a R^2 equals to 0.936 is mainly due to the several reactions represented by xylose degradation in the reaction network and also the formation of humins. These unknown reactions have a variety of activation energies, which impact directly on the fitting (R^2).

In terms of mass transport limitations, it is interesting to remark that the high apparent activation energies estimated in this work could be a strong evidence that rate is controlled by chemical reaction steps. According to Augustine (1995), when apparent activation energies are greater than 40 $kJ \cdot mol^{-1}$ it is generally an indication of rate being controlled by chemical reaction steps, whereas apparent activation energies lower than 10-15 $kJ \cdot mol^{-1}$ indicate that mass transport resistance is not negligible.

5.6.2 NBAL-N

The reaction network proposed for NBAL-N catalyst was based on the same observations of the unmodified catalyst (NBAL), that is, both resinification and

condensation were not considered, whereas xylose isomerisation reaction was taken into account (Figure 5.17).

According to the reaction network proposed for this catalyst, the mathematical equations to be solved simultaneously are 5.2, 5.3 and 5.4. The solution obtained using the Scilab code is summarised in Table 5.15.

The apparent rate constant of direct xylose conversion to furfural (k_3) had similar results to the ones found for the unmodified NBAL catalyst. For NBAL-N, the estimated values were $1.8{\cdot}10^{-3}$, $3.3{\cdot}10^{-3}$ and $8.2{\cdot}10^{-3}$ whereas for the unmodified catalyst values were $1.3{\cdot}10^{-3}$, $2.0{\cdot}10^{-3}$ and $3.5{\cdot}10^{-3}$ min^{-1}, respectively. The larger difference occurred at 170 °C, the same temperature in which degradation reactions become more significant and carbon balance is lower than 50%. The apparent rate constant for reaction 4 (degradation) was significantly superior than reactions 1, 2 and 3. The same behaviour was observed in NBAL results, where degradation rates were superior to xylose dehydration at all temperatures. An idea of the extent and rate in which degradation reactions occur in comparison with xylose isomerisation and direct conversion to furfural can be analysed by the ratio of k_4 to k_1 and k_3 ($\frac{k_4}{k_1+k_3}$). At all temperatures the ratio is above 1.0, indicating that secondary reactions are kinetically favoured.

Table 5.15: Apparent reaction constants and objective function for NBAL-N catalyst.

Temperature (°C)	10^3 k_1 (min^{-1})	10^3 k_2 (min^{-1})	10^3 k_3 (min^{-1})	10^3 k_4 (min^{-1})	Objective Function
150	1.5	2.0	1.8	7.4	$6.8 \cdot 10^{-3}$
160	3.1	5.4	3.3	10.3	$6.9 \cdot 10^{-3}$
170	5.5	9.6	8.2	20.9	$4.6 \cdot 10^{-3}$

Moreover, xylose direct conversion to furfural (k_3) and isomerisation (k_1) show similar apparent rate constants, although lower value was found for isomerisation reaction. Similar trend was found between xylose isomerisation (k_1) and isomer conversion to furfural (k_2), in which isomer conversion has an apparent rate constant slightly higher. Overall, NBAL-N catalyst presented higher rates and conversion of xylose compared to NBAL, despite its lower surface area (133 against 114 $m^2 \cdot g^{-1}$, respectively). Another interesting remark is the lower carbon balance obtained for NBAL-N catalyst, which is expected since degradation reactions rate is higher. For

instance, at 170 °C the carbon balance was 37%, which is about 10% lower than the one obtained for NBAL (Table 5.10).

The concentration profiles and the estimated curves for xylose, intermediate, and furfural at all reaction temperatures are shown in Figures 5.21, 5.22 and 5.23. Similarly to the NBAL catalyst, furfural fit was satisfactory, whilst for the xylose concentration the estimated and experimental values disagree considerably after 80-100 minutes of reaction. Moreover, the concentration profile of isomer becomes prominently similar to an intermediate behaviour at higher temperatures, especially at 170 °C, which suggests that xylose-isomer-furfural path is related to reaction temperature. In comparison with NBAL catalyst, it is observed that temperature might have a significant influence on reaction path.

Figure 5.21: Concentration profile at 150 °C for NBAL-N catalyst.

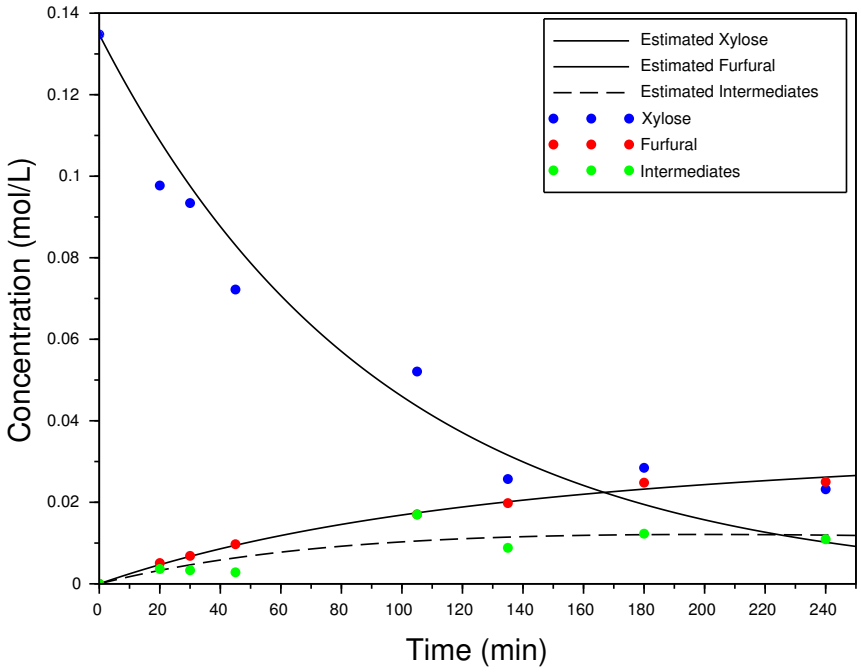

From modelling results, it is suggested that higher temperatures initially favour the xylose-isomer-furfural route, since intermediate concentration reaches its maximum sooner (around 30 min at 170 °C) compared to lower temperatures.

Figure 5.22: Concentration profile at 160 °C for NBAL-N catalyst.

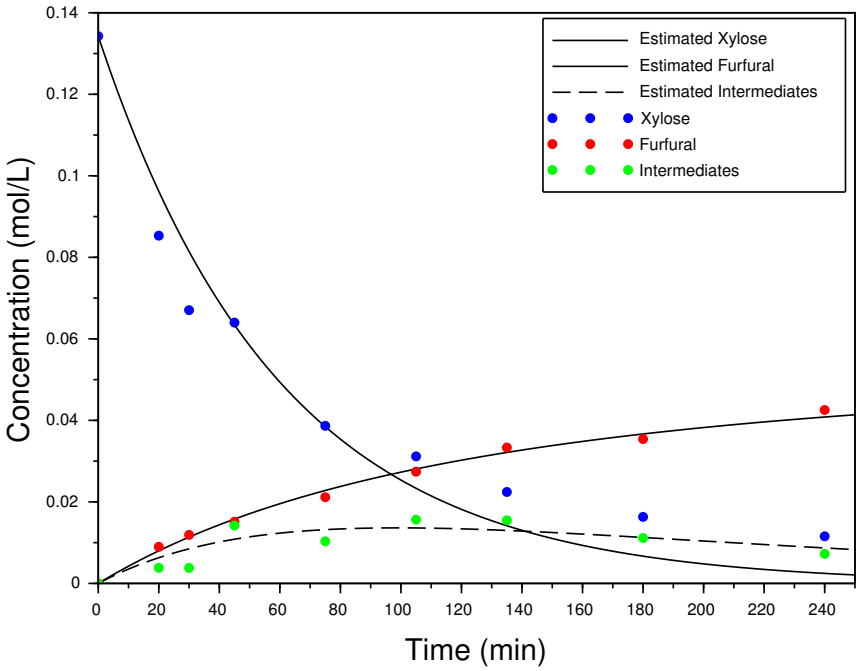

Figure 5.23: Concentration profile at 170 °C for NBAL-N catalyst.

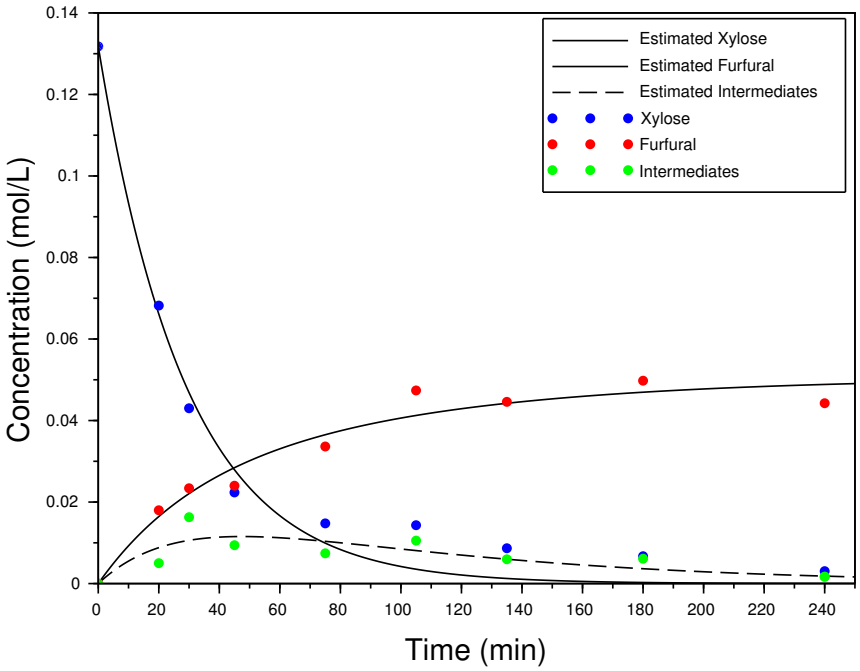

It is also observed that all four reactions involved in the network had an increase in the apparent rate constants with temperature, thus allowing the estimation of apparent activation energies by means of Arrhenius Equation. The estimated values are presented in Table 5.16.

Table 5.16: Apparent activation energies for the NBAL-N reaction network.

Reaction	Apparent activation energy ($kJ \cdot mol^{-1}$)	R^2
1	98.8	0.99
2	123.5	0.98
3	115.4	0.98
4	80.9	0.95

Pre-exponential factors: $k_{1,o} = 8.3 \cdot 10^7\ min^{-1}$, $k_{2,o} = 4.7 \cdot 10^{10}\ min^{-1}$, $k_{3,o} = 1.0 \cdot 10^{10}\ min^{-1}$ and $k_{4,o} = 1.1 \cdot 10^6\ min^{-1}$

Comparing results of xylose degradation reaction, it is noticed that both NBAL and NBAL-N had similar apparent activation energies. This observation agrees with catalytic performance and textural properties of these catalysts, which suggests that HNO_3 modification had minimal impact on catalyst activity and properties. Differently from the phosphoric acid treatment, the catalyst treated with HNO_3 possibly shows no presence of nitrogen species attached to the catalyst structure, as they probably evaporate in the form of NO_x during drying and calcination steps (JIAO et al., 2018).

Another remark is that isomer conversion to furfural (k_2) had higher apparent activation energy compared to xylose isomerisation (k_1). A similar trend was observed by Choudhary, Sandler and Vlachos (2012) using Lewis and Brønsted acid catalysts in aqueous media. Moreover, all reactions had a satisfactory fit using Arrhenius Equation as observed by the R^2 close to 1.0, except for reaction 4 (xylose degradation) that exhibited an R^2 equals to 0.95, which indicates that xylose degradation is composed of several reactions with different activation energies. The direct conversion of xylose to furfural using NBAL-N had an apparent activation energy closer to the values reported in the literature (O'NEILL et al., 2009; CHOUDHARY; SANDLER; VLACHOS, 2012), whilst NBAL catalyst fit for the same reaction had not behaved similarly due to the poor fit of intermediates at 150 °C.

5.6.3 NBAL-P

Among strategies that have been tested to improve the catalytic activity of heterogeneous catalysts to produce furan derivatives, it is important to remark (*i*) the immobilisation of phosphate groups on the catalyst surface by post-synthetic treatment and (*ii*) *in situ* extraction of furfural from aqueous solution to avoid secondary reactions

(GUPTA; FUKUOKA; NAKAJIMA, 2017). Although several groups have been investigating these strategies, there are few reported studies concerning the acid treatment of Nb_2O_5 supported catalysts to this date. Accordingly, this section will discuss the effect of H_3PO_4 acid treatment on Nb_2O_5/Al_2O_3 along with the mathematical modelling of the reactions involved.

The NBAL-P catalyst showed the highest carbon balance for all three temperatures compared to the other catalysts tested. Moreover, xylose isomer was not detected in any reaction temperature during 4 hours of reaction and side products formation was minimal. Thus, it is suggested that a different secondary reaction path could be favoured (condensation), since most undesired products found in NBAL and NBAL-N tests were not identified when using NBAL-P (Table 5.11). In consequence, the reaction system is simplified to take into account the furfural formation from xylose, condensation reaction and xylose degradation (Figure 5.24). As previously discussed in NBAL modelling assumptions, the condensation reaction decreases its extent at higher temperatures (ZEITSCH, 2000c). Thus, the choice of condensation as a secondary reaction could justify the higher carbon balance and selectivity found for NBAL-P catalyst.

Figure 5.24: Reaction network proposed for NBAL-P catalyst.

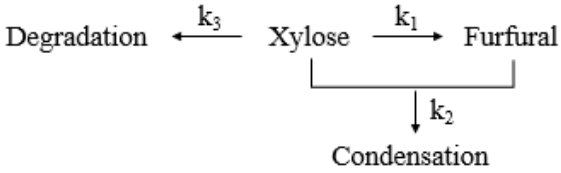

The mathematical model (Equations 5.5 and 5.6 for xylose and furfural, respectively) for the proposed reaction network was solved using Scilab similarly to the other catalysts aforementioned.

$$\frac{d[XYL]}{dt} = -k_1[XYL] - k_2[XYL][FUR] - k_3[XYL] \tag{5.5}$$

$$\frac{d[FUR]}{dt} = +k_1[XYL] - k_2[XYL][FUR] \tag{5.6}$$

Even though reaction rate has decreased for NBAL-P catalyst (along with xylose conversion), its selectivity towards furfural achieved values about twice as high as the other two catalysts studied (NBAL and NBAL-N). The higher selectivity can be an

interesting aspect to be further investigated because xylose normally undergoes several side-reactions that form undesired products. As discussed in the Catalyst Performance section, the possible higher density of phosphate groups compared to Lewis acid sites on the catalyst surface might hinder the xylose isomerisation route, which takes place on Lewis acid sites. As a consequence, the main route for furfural formation is the direct conversion of xylose, which occurs on Brønsted acid sites with lower reaction rates and higher activation energies (CHOUDHARY; SANDLER; VLACHOS, 2012).

Among all reaction networks, the one proposed for NBAL-P catalyst had the lowest values of objective function, as presented in Table 5.17. The more significant fit between experimental and estimated values can also be seen in the concentration profiles (Figures 5.25, 5.26 and 5.27).

Table 5.17: Apparent reaction constants and objective function for NBAL-P catalyst.

Temperature (°C)	$10^4\ k_1$ (min^{-1})	$10^3\ k_2$ (L mol^{-1} s^{-1})	$10^4\ k_3$ (min^{-1})	Objective Function
150	8.6	0.20	0.9	$2.5{\cdot}10^{-4}$
160	17.6	10.4	1.3	$1.2{\cdot}10^{-4}$
170	34.5	11.3	0.25	$0.97{\cdot}10^{-4}$

Figure 5.25: Concentration profile at 150 °C for NBAL-P catalyst.

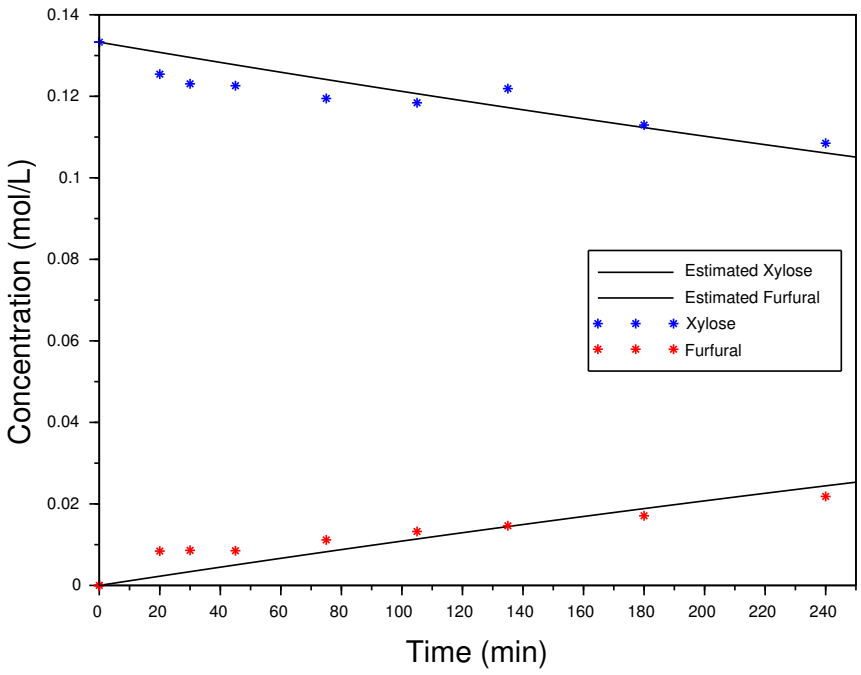

Figure 5.26: Concentration profile at 160 °C for NBAL-P catalyst.

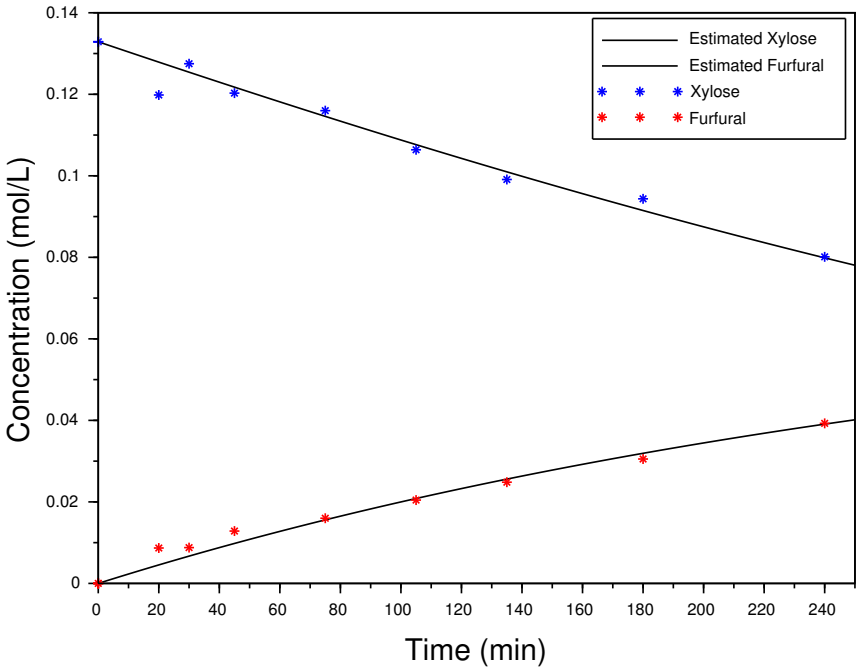

Figure 5.27: Concentration profile at 170 °C for NBAL-P catalyst.

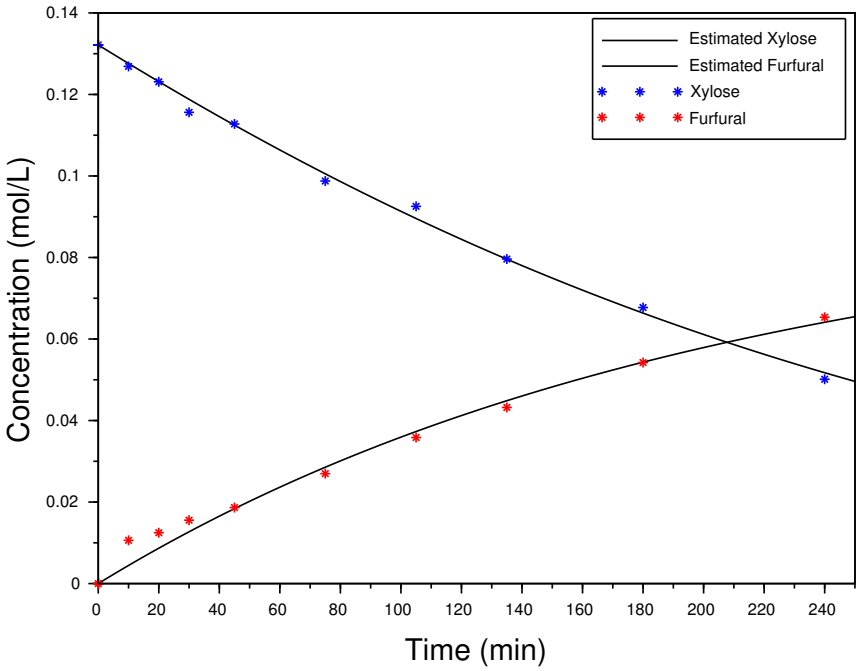

The higher carbon balance at 150, 160 and 170 °C indicates that NBAL-P catalyst promotes a selective furfural formation. This observation was validated by the fact that fewer side-products were detected in reaction samples (Table 5.11). Accordingly, it leads to a significant fit of estimated and experimental values. Differently from the last

two catalyst models presented, there was a satisfactory agreement between estimated and experimental values of xylose concentration during all reaction time and temperatures.

Moreover, the estimation of apparent activation energy was conducted for reaction 1, that is, xylose conversion to furfural. The Arrhenius Equation was not appropriate for reaction 3 and presented a low value of R^2 for reaction 2 due to similarity of apparent rate constants k_2 at 160 and 170 °C. The apparent activation energy of reaction 1 and its R^2 are presented in Table 5.18.

Table 5.18: Apparent activation energy for the NBAL-P reaction network.

Reaction	Apparent activation energy ($kJ \cdot mol^{-1}$)	R^2
1	108.6	0.99

Pre-exponential factor: $k_{1,o} = 3.6 \cdot 10^8\ min^{-1}$

In order to deepen the study of apparent activation energies for xylose degradation and condensation reactions, it would be necessary to identify the predominant route(s) of secondary reaction in NBAL-P catalyst, that is, xylose degradation, condensation or a different reaction not considered in this work. From these reactions information, a more appropriate reaction network could be tested. The impact of these changes in the reaction network would not significantly change the apparent rate constant for xylose dehydration to furfural compared to the value found in this work due to the high selectivity and carbon balance using NBAL-P catalyst.

Another interesting aspect is the comparison between apparent activation energies of direct conversion of xylose to furfural for NBAL-N and NBAL-P presented in Figure 5.28, in which xylose isomerisation was considered an endothermic reaction, similarly to glucose isomerisation to fructose (CHOUDHARY; BURNETT, et al., 2012). It is noticeable that both catalysts had very similar apparent activation energies for the same reaction (xylose conversion to furfural) despite of the acidic treatment. However, the similarity of these activation energies had not clearly affected the rate of reaction. Although the catalyst treated with phosphoric acid had the lowest activation energy, the rate of reaction did not exceed the other catalysts rate, as it would be expected due to the lower energy barrier to be overcome. Instead, the influence of active sites and their acidity are probably having a more significant impact on the rate of reaction.

Even though catalyst total acidity was about five times higher to the one modified by phosphoric acid compared to NBAL (46.9 against 9.1 $\mu mol \cdot m^2$, respectively),

the lower conversion, yield, and apparent rate constants may indicate that the reaction path where activation energy is higher was favoured. According to Choudhary, Sandler and Vlachos (2012), the path with higher activation energy is the one where xylose is dehydrated to furfural on Brønsted acid sites. Knowing that the reactions using NBAL-P did not form xylose isomers (xylulose and lyxose), it is likely that reaction path using this catalyst occurred only on Brønsted acid sites. Moreover, high selectivity towards furfural and carbon balances were obtained for NBAL-P. As it was previously discussed, xylose isomers were not detected, indicating that Lewis acid sites were either not present or in a small density on the catalyst surface. This result also shows that secondary reactions might be favoured in the presence of Lewis acid sites or xylose isomers, since NBAL and NBAL-N had low carbon balances and xylose isomers were detected in the reaction samples.

Figure 5.28: Diagram of apparent activation energies for NBAL-N and NBAL-P.

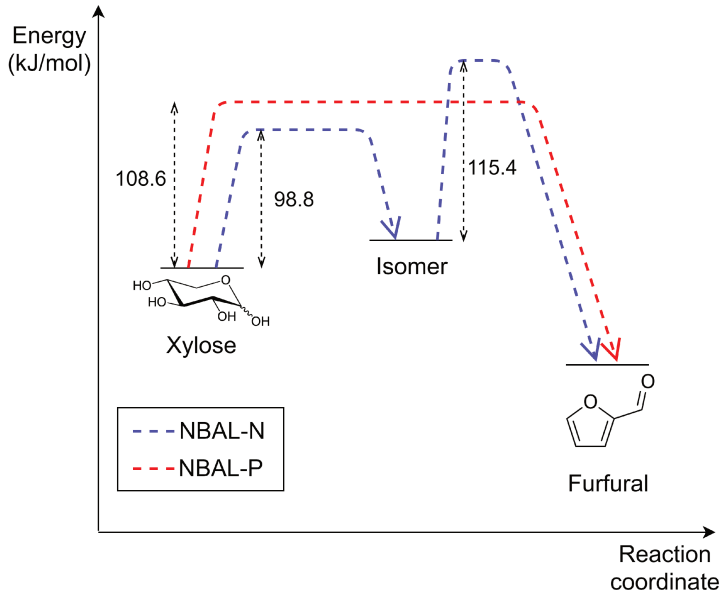

Study of NBAL-P Stability

The FTIR analysis was conducted to study the stability of phosphate groups present in NBAL-P. In order to compare the signal of phosphate groups, FTIR was conducted for both NBAL and NBAL-P before and after the reaction at 170 °C. The choice of 170 °C is due to the larger extent of secondary reactions at this temperature compared to 150 and 160 °C. Furthermore, the comparative study of NBAL and

NBAL-P allows the qualitative identification of groups related to phosphoric acid treatment. The FTIR spectra for NBAL and NBAL-P is presented in Figure 5.29.

The identification of phosphate group is of prime importance before and after the reaction in order to study the stability of this functional group on the catalyst structure, thus providing an insight about long-term stability of NBAL-P. In Figure 5.29, it is observed that NBAL-P catalyst presents a signal at 1130 cm^{-1} corresponding to O=P=O asymmetric stretching modes of phosphate or polyphosphate species (1000-1100 cm^{-1}) (ARMAROLI et al., 2000). In addition to that, the comparison between NBAL and NBAL-P spectra shows that NBAL do not present the signal at 1130 cm^{-1}, thus validating that this band is associated with phosphate groups from H_3PO_4 acid treatment.

Figure 5.29: FTIR spectra of NBAL and NBAL-P catalyst before and after reaction at 170 °C.

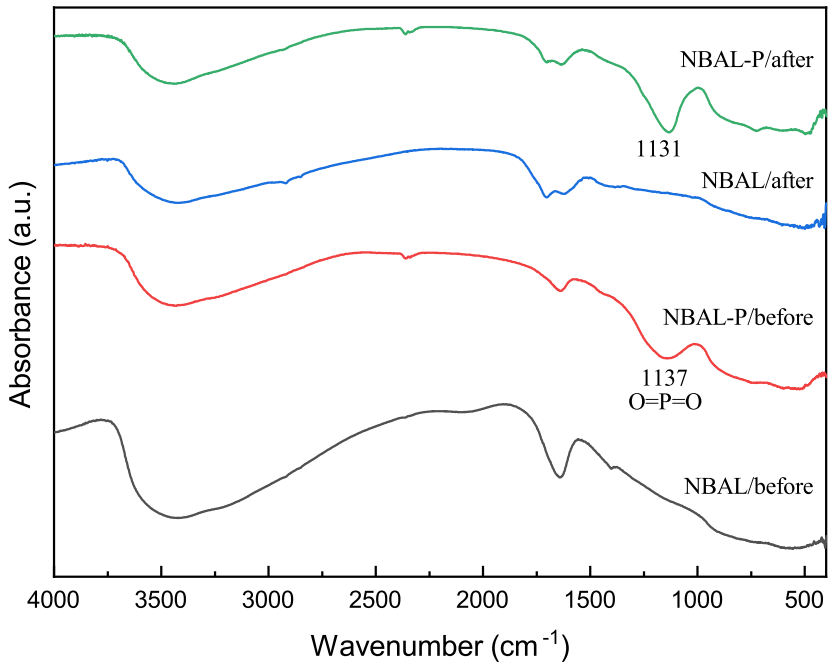

Moreover, the analysis of NBAL-P spectra shows that 1130 cm^{-1} band is present in both catalyst samples: before and after the reaction. Thus, it is suggested that phosphate group remains on the catalyst structure, whereas the extent of a possible H_3PO_4 leaching cannot be estimated by FTIR analysis. In order to further improve the investigation of a possible H_3PO_4 leaching, catalytic tests using NBAL-P recycled

from previous reactions could be conducted to provide information about the long-term stability of the H_3PO_4 acid treatment.

Due to the significant concordance between estimated model and experimental data, along with the high carbon balance obtained for NBAL-P catalyst, its kinetic parameters were chosen to be used in Aspen Plus simulation.

5.7 Simulation

In this work, a reactive stripping column in which furfural is both produced and stripped from the liquid phase to avoid secondary reactions was simulated. The furfural production flowsheet was built considering Rosenlew process (ZEITSCH, 2000d) conditions as a base case (Figure 4.4).

The kinetic parameters obtained for NBAL-P catalyst were used due to its high selectivity towards furfural, which is an interesting aspect knowing that xylose can undergo several undesired reactions. Based on the NBAL-P modelling results, the apparent pre-exponential factor and activation energy were estimated by Arrhenius Equation and used as input in the simulation.

The following sections are divided into (*i*) the optimisation of the reactive stripping column (REACTOR); (*ii*) the description of a separation unit for furfural purification and; (*iii*) the overall performance of the entire process.

5.8 Optimisation

The design of experiments was performed to estimate the optimum parameters of a reactive stripping column for furfural production. A few process variables were chosen from a base case, then the range of operation for each factor was presented in the Methodology section. In this section, the results of factor screening and optimisation by CCRD are presented.

5.8.1 Plackett–Burman

The 12-run Plackett-Burman (PB-12) was utilised in the preliminary factor screening, and results are shown in Table 5.19.

Table 5.19: Results from 12-Run Plackett-Burman design.

	Factors								Response
Run	X_1 (kg/h)	X_2	X_3 (°C)	X_4	X_5 (°C)	X_6 (bar)	X_7	X_8 (kg)	Y_1 (%)
1	4000	0.2075	60	0.3	265	7.5	20	65	73.71
2	4000	0.54	20	0.7	265	7.5	5	65	70.94
3	2000	0.54	60	0.3	365	7.5	5	5	0.01
4	4000	0.2075	60	0.7	265	10.05	5	5	36.26
5	4000	0.54	20	0.7	365	7.5	20	5	37.75
6	4000	0.54	60	0.3	365	10.05	5	65	60.38
7	2000	0.54	60	0.7	265	10.05	20	5	81.15
8	2000	0.2075	60	0.7	365	7.5	20	65	99.95
9	2000	0.2075	20	0.7	365	10.05	5	65	90.18
10	4000	0.2075	20	0.3	365	10.05	20	5	33.91
11	2000	0.54	20	0.3	265	10.05	20	65	98.29
12	2000	0.2075	20	0.3	265	7.5	5	5	10.2

X_1: mass flow of xylose solution; X_2: mass fraction of xylose in the feed; X_3: temperature of xylose feed; X_4: mass fraction of water in N2-FEED; X_5: temperature of N2-FEED; X_6: column and feed pressure; X_7: number of reactive stages; X_8: mass of catalyst per stage and; Y_1: furfural yield.

The choice of 12-run method is based on the fact that at least $k + 4$ runs are necessary when the number of factors is k (RODRIGUES; IEMMA, 2014). Bearing in mind that eight factors are being considered (X_1 to X_8), the 12-run Plackett-Burman was the appropriate choice.

Since kinetics parameters were obtained from 150 to 170 °C, the range of column temperature must be the same. Accordingly, the runs in which the column temperature was not within this range were not taken into account (runs 1, 3, 4, 9 and 12). Conversely, the runs 2, 5, 6, 7, 8, 10 and 11 presented both high furfural yield (Y_1 between 33.9% and 99.95%) and a column temperature within its range of validity.

For the PB-12 analysis, the results are discussed based on Pareto chart for the response variable with a statistical significance of 5%. The Pareto chart for Y_1 is shown in Figure 5.30. In the chart, the vertical bar represents the statistical significance of 5%, which is about 3.26 in terms of standardised effect. Thus, the factors that possess a standardised effect (t-calc) lower than 3.26 have no influence on the response variable. Conversely, the factors with an effect higher than 3.26 are considered relevant and have an impact on the response variable (furfural yield).

The Pareto chart in the Figure 5.30 shows that the mass fraction of xylose in the feed (X_2) and temperature of xylose solution in the feed (X_3) were not relevant for the

global furfural yield (Y_1) among all factors investigated and their respective range. Even though the furfural yield depends on the xylose content in the feed, this dependency is expressed by the overall xylose content, which is the xylose solution mass flow (X_1). The temperature is another important variable affecting xylose conversion to furfural, however, gas feed temperature and xylose mass flow seem to be the main factors responsible for high furfural yields (Table 5.19) among all eight factors. Although the gas feed temperature (X_5) had an effect close to the limit value, its influence was not neglected.

It is also noticeable from Table 5.19 results that when xylose mass flow (X_1) is lower, the furfural yield can reach values above 90%. In this scenario, the xylose mass flow was fixed at 2000 kg/h in order to decrease the number of factors under investigation. Furthermore, the variables X_2 and X_3 were fixed at 0.2075 (similar to Rosenlew process) and room temperature (30 °C), respectively.

Figure 5.30: Pareto chart for Y_1 using 12-run Plackett-Burman.

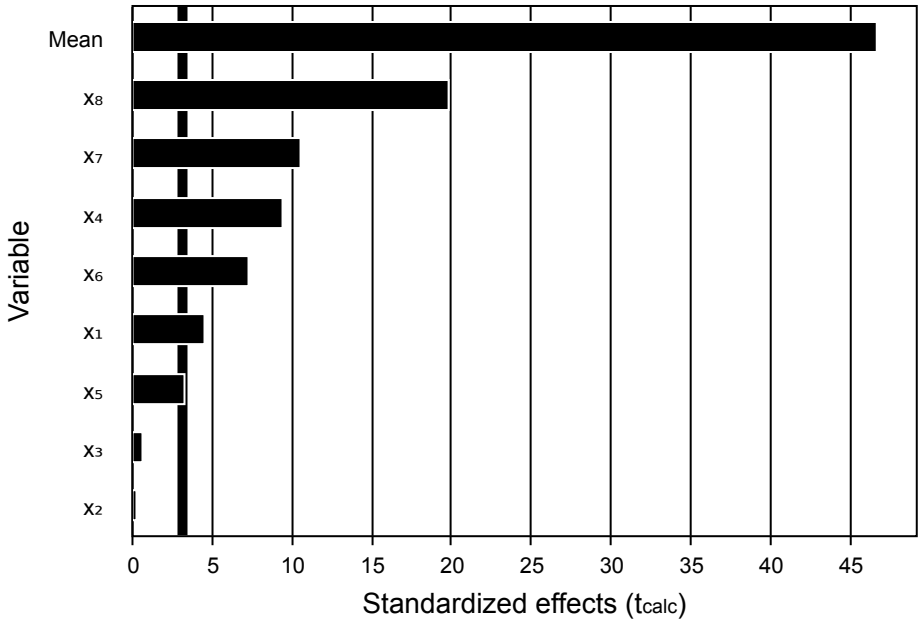

5.8.2 Central Composite Rotatable Design (CCRD)

From Plackett-Burman preliminary study only five factors (from X_4 to X_8) remained relevant to be further investigated by means of CCRD. The number of runs for CCRD is calculated according to Equation 5.7, where k is the number of factors and n the number of central points. For the factors under investigation (X_4 to X_8) with zero central points, the number of runs is 42.

$$Number\ of\ experiments = 2^k + 2 \cdot k + n \tag{5.7}$$

In order to deepen the study of gas stream temperature in the feed (X_5) and maintain the column temperature within 150-170 °C, X_5 range was modified. The new range of gas feed temperature was from 200 to 340 °C.

The regression coefficients were calculated and mathematical models were built for both responses: furfural yield (Y_1) and recovery of furfural at the top of the column (Y_2). A summary of CCRD results is presented in Table E.2. For each CCRD run, the temperature range of the reactive zone (reactive stages) is presented. It is observed that for most runs the temperature is within the kinetic range of validity (150-170 °C). The only exceptions are runs 6, 8, 14, 16, 24, 32, and 34, which were neglected for this study.

Since the calculated F-value for each response variable was superior to its respective tabulated F-value, the mathematical model for each response variable was built by neglecting the coefficients that were not statistically significant in order to reparameterise the model. The model in terms of coded factors (x_i) for furfural yield (Y_1) and furfural recovery (Y_2) are shown in Equations 5.8 and 5.9, respectively.

$$\begin{aligned} Y_1(\%) &= 118.43 + 5.05 \cdot x_4 - 5.73 \cdot x_4^2 - 4.38 \cdot x_5^2 + 2.72 \cdot x_6 - 4.75 \cdot x_6^2 + 3.52 \cdot x_7 \\ &\quad -5.50 \cdot x_7^2 + 6.91 \cdot x_8 - 8.07 \cdot x_8^2 - 1.95 \cdot x_4 \cdot x_8 \end{aligned} \tag{5.8}$$

$$\begin{aligned} Y_2(\%) &= 43.17 + 10.87 \cdot x_4 + 4.69 \cdot x_5 - 6.98 \cdot x_6 + 1.56 \cdot x_7 - 3.50 \cdot x_8 \\ &\quad +2.25 \cdot x_8^2 \end{aligned} \tag{5.9}$$

In general, all predicted values were close to the experimental values (simulation results). The distribution of predicted versus experimental values is presented in Figures 5.31a and 5.31b, whilst R^2 and F-values in Table 5.20. Both R^2 values were acceptable and relative errors did not exceed 20.4% and 25.2% for Y_1 and Y_2, respectively. Since simulation results show no variation at the central points, the F-value for lack of fit and pure error was not considered.

Table 5.20: Percentage of variance (R^2), calculated and tabulated F-values for each response variable at 5% significance level.

Response	R^2 (%)	Calculated F	Tabulated F
Furfural yield (Y_1)	91.64	34.0	2.15
Furfural recovery (Y_2)	93.54	84.4	2.37

Figure 5.31: Experimental versus predicted values for each response variable.

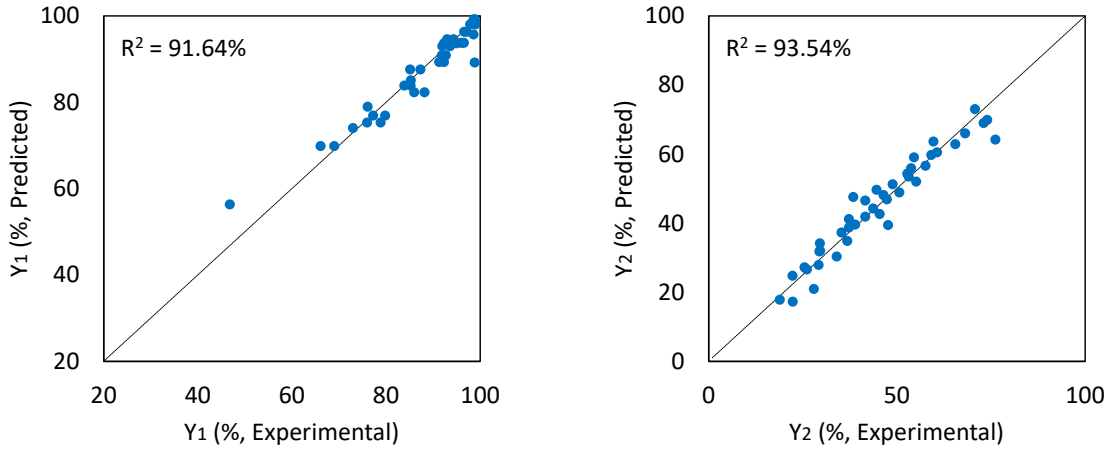

(a) Furfural yield (Y_1). (b) Furfural recovery (Y_2).

Among all 42 runs in the CCRD, the run number 4 presented the highest furfural yield (Y_1) and furfural recovery at the top of the column (Y_2), 85.2 and 74.0%, respectively (Table 5.21). It is observed from the comparison between simulation and model results presented in Table 5.21 that these values possess a significant similarity, thus validating the use of the model to predict reactor performance. Moreover, the temperature in the reactive stages varied from 162 to 167 °C, which is within the desired kinetic range. Thus, this optimised condition can be described in terms of the factors, which are presented in Table 5.22 along with its coded values.

Table 5.21: Optimum responses in both simulation and model prediction.

	Simulation	Model
Furfural yield (Y_1)	85.2	83.9
Furfural recovery (Y_2)	74.0	69.9

Some groups also report the use of organic solvents to enhance the amount of furfural recovered at the top of the column. Metkar et al. (2015) investigated the use of sulfolane as solvent in the reactive distillation for the production of furfural. In their experiments, they observed that a high-boiling solvent such as sulfolane could be

collected at the bottom of the column along with undesired products and unreacted reagent, whereas furfural was stripped from liquid phase to gas phase by nitrogen and steam with ∼75% yield. In light of these findings, it is suggested that the use of an appropriate amount of nitrogen and steam can perform similarly to reactors containing organic solvents. These observations indicate that maximising furfural recovery could be approached by (*i*) recycling BOTTOM stream to the reactor; (*ii*) investigating different organic solvents, in particular the ones that are biomass-derived or; (*iii*) testing post-treatment strategies to separate furfural from undesired products and unreacted reagent, based on the lower solubility of furfural in water compared to xylose.

Table 5.22: Factor values (coded and model) for the optimised condition.

Factor	Coded value (x_i)	Model value (X_i)
Vapour mass fraction in N2-FEED	1	0.584
Temperature of N2-FEED (°C)	1	299.4
Pressure (bar)	-1	8.24
Number of reactive stages	-1	10
Catalyst mass per stage (kg)	-1	22.4

In terms of total mass of catalyst utilised in the reactive column, it is interesting to remark that, even though furfural yield increases when the amount of catalyst per stage is higher, other factors can play a significant role to maximise furfural yield with minimal catalyst content. For instance, the optimum condition herein presented and the run 17 from CCRD had similar furfural yield, however, the total amount of catalyst was 224 kg (22.4 kg in each reactive stage, numbered from 10 to 20) and 476.05 kg, respectively.

5.9 Furfural Separation

Similarly to the current furfural production processes, further separation steps are necessary to obtain furfural in a high purity. These steps are composed of an azeotropic distillation, followed by a combination of distillation columns and decanters, which require an excessive amount of energy (ZEITSCH, 2000b; NHIEN et al., 2016). Since furfural has a higher solubility in organic solvents, many groups have been investigating biphasic systems/reactors to avoid secondary reactions occurring in aqueous phase or to reduce energy consumption in distillation steps. However, these studies are mainly focused on toxic and/or petroleum-derived organic solvents, such as toluene and MIBK (SAHU; P. L. DHEPE, 2012; LI; JIA; WANG, 2016).

In order to overcome this drawback, Jiwon et al. (2019) proposed the use of a biomass-derived solvent to extract furfural in a less energy-consuming process. In their work, they demonstrated that 2-pentanone (2PT), a compound produced from the hydrogenation of 2-methylfuran (MF) at higher temperatures compared to the ones used in the production of furfuryl alcohol (FA) (SITTHISA; WEI; RESASCO, 2011; BISWAS et al., 2014), had higher partition coefficient, allowing the recovery of more than 95% of furfural in the extraction step and smaller number of trays in the distillation column compared to usual solvents, such as toluene and MIBK. In this work, the 2-pentanone was also chosen as solvent for furfural extraction from aqueous phase. The choice is based on the low boiling point compared to furfural (approximately 60 °C lower), high partition coefficient and its biomass-derived aspect, which can enhance process performance in biorefineries.

Figure 5.32: Reaction pathway for the formation of 2-pentanone from xylose/furfural.

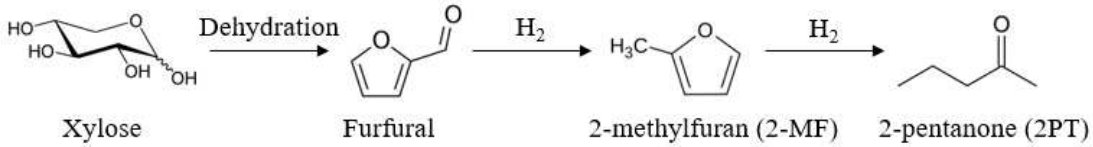

Source: Adapted from Jiwon et al. (2019).

The proposed furfural production process, including the furfural purification steps are presented in Figure 5.33. The mixture of furfural, water and non-condensed nitrogen gas (LV) is fed into a flash separator, which provides immediate separation of gas (N2-EXIT) and liquid phase (FUR-H2O). The liquid phase is then fed to a decanter (phase split is determined by equating component fugacities of the two liquid phases considered: organic and pure water), where furfural is mainly recovered in the organic phase by using 2-pentanone as solvent in the liquid-liquid extraction process (JIWON et al., 2019). According to Jiwon et al. (2019), about 95% of furfural could be recovered in organic phase when using a 0.5 molar ratio of solvent (2PT) to furfural and water. To assure complete recovery of furfural in the decanter, a ratio higher than 1.0 was considered in this work.

Figure 5.33: Flowsheet of Aspen Plus simulation for furfural production.

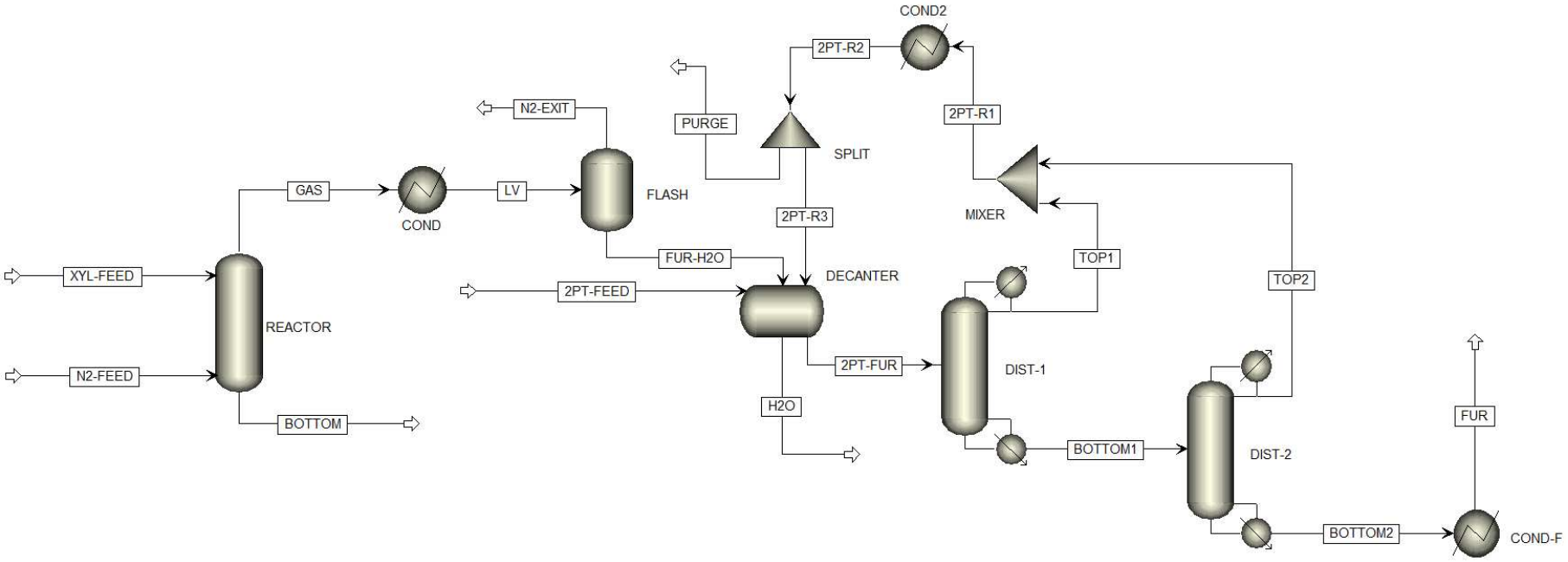

There are also recycle and make-up streams entering the decanter: (*i*) recycle stream mainly composed of 2PT coming from two distillation columns (2PT-R3) and; (*ii*) make-up stream to balance solvent loss. In order to enable Aspen Plus convergence, a PURGE stream was added to the solvent recycle stream, thus allowing the estimation of a make-up stream (2PT-make-up) by the difference between 2PT mass flow in 2PT-FEED and PURGE. A summary of stream information for both flash and decanter are shown in Table 5.23.

Table 5.23: Stream information for flash vessel and decanter.

Stream	LV	N2-EXIT	FUR-H2O	2PT-make-up	2PT-R3	H2O	2PT-FUR
Temperature (°C)	25	25	25	25	25	25	25
Pressure (bar)	8.24	1.00	1.00	1.00	1.00	1.00	1.00
Mass flow (kg/h)	10672.5	4043.8	6628.7	14.8	30780.0	5994.5	32706.2
Mass fraction (%)							
Furfural	6.0	0.3	9.5	0.0	0.1	0.0	2.0
H_2O	57.0	2.0	90.5	0.0	0.3	100.0	0.3
N_2	37.0	97.7	0.0	0.0	0.0	0.0	0.0
2PT	0.0	0.0	0.0	100.0	99.6	0.0	97.7

The organic stream exiting the decanter (2PT-FUR) is composed of 2PT (higher fraction) and furfural. This stream enters a 10-stage distillation column (DIST-1, DSTWU type) on stage number 5, which recovers 98% (mass) of 2PT at the top (TOP1) and 95% of furfural at the bottom (BOTTOM1). The equimolar mixture of 2PT and furfural in BOTTOM1 is then fed to second distillation column (DIST-2, DSTWU type), in which feed stage and number of stages are similar to DIST-1. In the second distillation column, both recoveries are 99.9% and furfural is obtained in high purity in FUR stream at room temperature (629.5 kg/h and 99.8% mass fraction). Both TOP1 and TOP2 are mixed, condensed to 25 °C and recycled to the decanter. A summary of DSTWU and stream results are presented in Table 5.24 and 5.25, respectively.

With DSTWU results, it is observed that both condensers have similar cooling requirement, with a lower value for DIST-2 condenser due to significant higher mass flow in TOP1 compared to TOP2.

Table 5.24: Summary of DSTWU results for DIST-1 and DIST-2.

Column	DIST-1	DIST-2
Minimum reflux ratio	0.0062	0.366
Actual reflux ratio	0.069	1.88
Minimum number of stages	4	8
Number of actual stages	10	10
Feed stage	5	7
Reboiler heating required (MW)	5.31	0.21
Condenser cooling required (MW)	0.56	0.204
Distillate to feed fraction	0.964	0.531

The required heat in DIST-1 reboiler is considerably superior DIST-2 reboiler because 2PT-FUR enters DIST-1 at 25 °C and DIST-1 operating temperature is between 101 and 115.8 °C. The BOTTOM1 temperature does not differ significantly from the DIST-2 operating temperature, thus heat required in DIST-2 reboiler is lower.

Table 5.25: Stream information for both distillation columns.

Stream	TOP1	BOTTOM1	TOP2	BOTTOM2	FUR
Temperature (°C)	101.2	115.8	101.6	160.6	25
Pressure (bar)	1.00	1.00	1.00	1.00	1.00
Mass flow (kg/h)	31437.8	1268.4	638.9	629.5	629.5
Mass fraction (%)					
Furfural	0.1	49.6	0.1	99.8	99.8
H_2O	0.3	0.0	0.0	0.0	0.3
N_2	0.0	0.0	0.0	0.0	0.0
2PT	99.6	50.4	99.9	0.2	0.2

The results from separation unit aforementioned indicate the possibility of producing 628.4 kg/h (15.08 ton per day) of furfural in a high purity (99.8%) using a biomass-derived solvent (2-pentanone) with a solvent to furfural ratio of 48.1:1 in the decanter. Moreover, the amount of 2PT in the make-up stream shows that liquid-liquid extraction requires 0.0235 kg of solvent per kg of furfural, and a 2PT daily consumption of 355.2 kg.

5.10 Overall Performance

A few process parameters were also analysed once the optimum process conditions and separation unit were defined. The amount of steam consumed is a key parameter regarding process feasibility and overall costs. In the optimised condition, the consumption of steam in the reactor reached about 8.7 kg per kg of produced furfural,

which is significantly lower than the original steam consumption in Rosenlew process and Huaxei plant (ZEITSCH, 2000d; KRZELJ et al., 2019), even though the temperature of steam was 35 °C higher in the optimum condition compared to Rosenlew process. The reduction in steam consumption is due to the addition of nitrogen in the gas feed, which is known to be a cost-effective alternative to current steam-stripping processes (AGIRREZABAL-TELLERIA; GANDARIAS; ARIAS, 2013).

Moreover, the furfural yield inside the reactive stripping column was also higher than the one described for Rosenlew process, that is, 85.2% against 59.5%, respectively. This result shows that further investigation of Nb_2O_5 based catalyst modified by phosphoric acid is of prime importance and can lead to a significant advantage in terms of corrosion and separation of furfural. A summary of the aforementioned process parameters is presented in Table 5.26.

Table 5.26: Summary of steam consumption and yield in the reactor.

	Steam consumption per produced furfural (kg/kg)	Carrier gas input	Furfural yield (%)
Rosenlew process[a]	30	Pure steam (10500 kg/h)	59.5
Huaxei plant[b]	25-35	Steam	50
This work	8.7	58.4% steam (5548 kg/h)	85.2

[a]Zeitsch (2000d), [b]Krzelj et al. (2019).

The required duty in the condenser (COND) after the reactive stripping column is another example of enhancement in operating conditions compared to current furfural production process. Agirrezabal-Telleria, Gandarias and Arias (2013) also investigated a furfural production based on Rosenlew process. Their investigation showed that N $_2$-stripping process can reduce condenser duty from 8655 kW to 1904 kW in comparison with steam-stripping. In this work, where N_2-steam stripping was used, the required duty achieved a value within this range, 4901 kW, as seen in Table 5.27. Although energy consumption decreases by using N_2-stripping, the efficiency of furfural recovery is lower compared to steam-stripping process.

Table 5.27: Results for condenser (COND) duty in different process types.

Process type	Duty (kW)	Reference
Steam-stripping	8655	Agirrezabal-Telleria, Gandarias and Arias (2013)
N_2-stripping	1904	Agirrezabal-Telleria, Gandarias and Arias (2013)
Steam-N_2-stripping	4901	This work

In both distillation columns, the required heat for reboilers amounted to 5.52 MW (or 31.6 GJ per ton of furfural), which can be partially decreased by integrating available heat in the process. For instance, BOTTOM stream leaving the stripping reactor is a high-pressure liquid at 161 °C (mainly water), which could be used to provide a certain amount of heat to distillation reboilers or to be recycled to the reactor. Moreover, a high amount of heat is also required to produce nitrogen and steam in order to feed the reactor (N2-FEED), thus increasing the amount of heat required. The Figure 5.34 depicts a suggested process for obtaining N2-FEED to a desired temperature, pressure and composition for entering the stripping reactor (N2-FEED stream). In this case, both N2 and H2O-FEED mass flows could be partly composed of recycle streams, such as N2-EXIT and BOTTOM, respectively. To study the amount of energy required, the limiting case would be the one when no recycling is made, thus energy consumption for N2-FEED production is maximum at 4.9 MW (28.1 GJ per ton of furfural). A summary of these energy requirements are shown in Table 5.28.

Figure 5.34: Process flowsheet for N2-FEED formation.

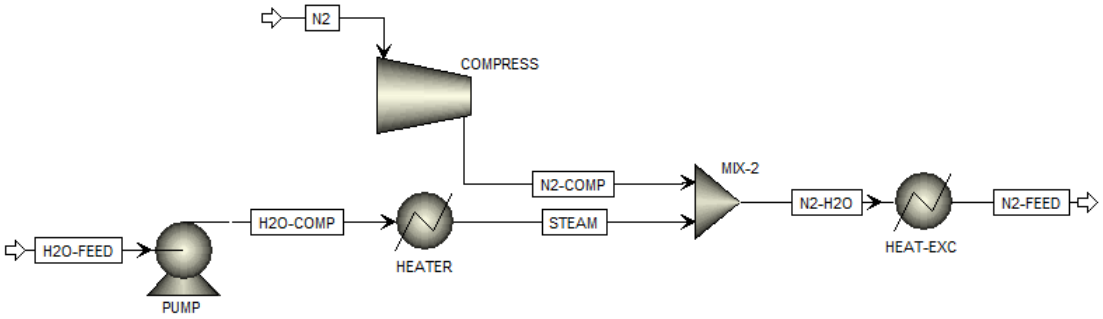

Feed conditions: N2 (3952 kg/h) and H2O-FEED (5548 kg/h) at 25 °C and 1 bar.

Table 5.28: Energy requirements for obtaining N2-FEED.

Equipment	Specification (MW)
Compressor (COMPRESS)	0.4
Pump (PUMP)	$3.4 \cdot 10^{-3}$
Heaters (HEATER and HEAT-EXC)	4.5
Sum	4.9

Considering the entire heat requirement in the furfural production, these findings suggest that an optimal separation unit, in which less amount of required energy is desired, is still a major challenge for further research and developments. A comparison with an industrial process (Huaxei plant) and literature is presented in

Table 5.29. Furthermore, it is worth mentioning that a furfural production process also includes other nonidealities, costs and energy requirements that were not considered in the simulation herein presented.

Table 5.29: Energy consumption in different processes for furfural production.

Energy consumption ($GJ \cdot t_{furfural}^{-1}$)	Reference
108.1 - 136.8	Krzelj et al. (2019)
123.6 - 156.7	Huaxei plant (KRZELJ et al., 2019)
∼59.7	This work

The results of furfural production process herein presented are based on several assumptions. For instance, the simulation did not take mass transfer resistances into account, which is an inevitable drawback when scaling up bench-scale processes. Another aspect is the long-term stability of the NBAL-P catalyst. In a reactive operation using heterogeneous catalysts, long catalyst stability is desired to reduce costs related to replacement or regeneration. A summary of process parameters obtained in this work is presented in Table 5.30.

Table 5.30: Summary of furfural production process simulated in this work

Furfural yield (%)	85.2
Furfural purity (%)	99.8
Furfural production ($ton_{furfural}$/day)	15.08
Mass of catalyst (kg)	224
Mass of catalyst per stage (kg)	22.4
Solvent consumption (ton_{2PT}/day)	0.355
Solvent to furfural mass ratio (make-up)	0.0235
Steam consumption ($kg_{steam}/kg_{furfural}$)	8.7
Energy consumption (GJ/$ton_{furfural}$)	∼59.7

Moreover, the use of xylose for furfural production in lieu of biomass (such as corncob, bagasse) is a model simplification also adopted by other groups (KRZELJ et al., 2019). Krzelj et al. (2019) suggests that this approach is valid when compared to more complex feedstocks in terms of energy savings/consumption. Agirrezabal-Telleria, Gandarias and Arias (2013) investigated nitrogen stripping in furfural production from either xylose or corncobs. Their findings show that in both scenarios the furfural yield is quite similar, although higher catalyst loading increased resinification reactions in water and a decay in furfural yield was observed at increasing corncob loadings. Metkar et al. (2015) also studied xylose and pre-hydrolysate liquor (PHL) as feed to a continuous reactive distillation. It was noticed that salts present in the PHL resulted in significant

catalyst deactivation compared to xylose, however, the addition of a pre-treatment with ion exchange resin was quite effective to remove most cations from PHL prior to the reactive distillation. In view of these observations, the development of selective and stable catalysts, along with less energy-consuming separation steps in the purification of furfural, is of prime importance for the production of furfural in biorefineries.

Chapter 6

Conclusion

According to the literature, the current processes for furfural production need to overcome certain obstacles, such as high steam and energy consumption, difficulties in separation steps and corrosion in process equipments due to the use of inorganic acids. In this scenario, this work investigated a heterogeneous catalyst, niobium oxide supported on alumina, for xylose dehydration to furfural, as well as the overall feasibility of a reactive stripping column using Aspen Plus process simulation software.

The NBAL catalyst was prepared by wet impregnation. XRF results show that the Nb_2O_5 content of 15.9% approached the desired value of 16%, indicating that the preparation method was satisfactory. The catalyst testings were conducted at 150, 160, 170 °C in the presence of three different catalysts: Nb_2O_5/Al_2O_3 (NBAL), and the ones treated with HNO_3 (NBAL-N) or H_3PO_4 (NBAL-P). Results show that both NBAL and NBAL-N led to similar xylose conversion, furfural yield and selectivity towards furfural. This observation indicates that HNO_3 treatment had minimal impact on catalyst performance, as it was observed that textural properties and overall acidity under 250 °C of both catalysts were similar. Conversely, the NBAL-P catalyst presented lower xylose conversion, whilst its selectivity to furfural ranged from 75 to 84%, which was considerably high compared to NBAL and NBAL-N. Moreover, carbon balance for NBAL-P catalyst was significantly high (87-98%), indicating that secondary reactions occurred in a minimal extent. This result is of prime importance for catalyst design towards selective furfural production, since xylose dehydration can lead to several undesired reactions.

Once it was verified that reaction conditions were under minimal mass transport limitations (external and internal), a kinetic modelling was proposed for each

catalyst using power law model and pseudo-homogeneous conditions. For each catalyst, a different reaction network was considered, and xylose dehydration to furfural was defined as a first-order reaction. The estimated apparent activation energies were similar to the ones reported in the literature for NBAL-N and NBAL-P and overall fit for each reaction network was satisfactory. Due to the higher carbon balance and selectivity towards furfural, the kinetic parameters obtained for NBAL-P catalyst were chosen to be used in the process simulation.

Based on an industrial furfural process (Rosenlew), a simulation of furfural production from xylose using a reactive stripping column (RadFrac) was build in Aspen Plus. The optimisation conducted by design of experiments (Plackett-Burman and Central Composite Rotatable Design) showed that furfural yield and its recovery at the top of the reactive column could achieve values superior to current furfural production processes. Moreover, the steam consumption reduced from 30 (Rosenlew) to 8.7 kg per kg of furfural in this work by a combined nitrogen/steam injection at the bottom of the reactive column. Overall energy consumption amounted to $\sim$ 59.7 GJ $\cdot ton_{furfural}^{-1}$ when using 2-pentanone (furfural-derived) as an extraction solvent in the separation unit.

Future works regarding furfural production include the set up of an experimental reactive column, in order to deepen simulation analysis and also contribute to the understanding of mass transfer and equilibrium conditions. An interesting approach is the preparation of Nb_2O_5/Al_2O_3 pellets to be used in an experimental reactive column, thus allowing the study of mass transfer effects and overall thermo-mechanical resistance of these pellets. Another aspect to be investigated is the presence of an organic solvent in the reactor feed, which can reduce even more the extent of secondary reactions and increase furfural selectivity. Along with these experiments, testing the stability of Nb_2O_5/Al_2O_3 catalysts for longer duration is of prime importance for further large-scale furfural processes. In terms of scaling up processes, it is also recommended that complex pentosan mixtures are experimentally investigated as a feedstock for furfural production.

Bibliography

ABDEL-REHIM, M. A.; SANTOS, A. C. B. dos; CAMORIM, V. L. L.; COSTA FARO, A. da. Acid–base reactions on alumina-supported niobia. *Applied Catalysis A: General*, vol. 305, pp. 211–218, 2006.

AGIRREZABAL-TELLERIA; GANDARIAS; ARIAS. Production of furfural from pentosan-rich biomass: Analysis of process parameters during simultaneous furfural stripping. *Bioresource Technology*, vol. 143, pp. 258–264, 2013.

AGIRREZABAL-TELLERIA; LARREATEGUI, et al. Furfural production from xylose using sulfonic ion-exchange resins (Amberlyst) and simultaneous stripping with nitrogen. *Bioresource Technology*, vol. 102, pp. 7478–7485, 2011.

AIDA, T. M. et al. Reaction kinetics of D-xylose in sub- and supercritical water. *The Journal of Supercritical Fluids*, vol. 55, pp. 208–216, 2010.

ALBERS, P. W. Bulk Chemical Composition. In: ALBERS, P. W. *Handbook of Heterogeneous Catalysis*. United States: American Cancer Society, 2008. chap. 3.2.1, pp. 1000–1014. ISBN: 9783527610044.

ALBRECHT, S.; CYMOREK, C.; ECKERT, J. *Niobium and Niobium Compounds*. United States: American Cancer Society, 2011. ISBN: 9783527306732.

ALONSO, D. M.; BOND, J. Q.; DUMESIC, J. A. Catalytic conversion of biomass to biofuels. *Green Chem.*, vol. 12, pp. 1493–1513, 2010.

ARMAROLI, T. et al. Acid sites characterization of niobium phosphate catalysts and their activity in fructose dehydration to 5-hydroxymethyl-2-furaldehyde. *Journal of Molecular Catalysis A: Chemical*, vol. 151, pp. 233–243, 2000.

AUGUSTINE, R. *Heterogeneous Catalysis for the Synthetic Chemist*. New York: Taylor & Francis, 1995. (Chemical Industries). ISBN: 9780824790219.

BARRETT, E. P.; JOYNER, L. G.; HALENDA, P. P. The Determination of Pore Volume and Area Distributions in Porous Substances. I. Computations from Nitrogen Isotherms. *Journal of the American Chemical Society*, vol. 73, pp. 373–380, 1951.

BERTEAU, P.; DELMON, B. Modified Aluminas : Relationship between activity in 1-butanol dehydration and acidity measured by NH_3 TPD. *Catalysis Today*, vol. 5, no. 2, pp. 121–137, 1989.

BHAUMIK, P.; DHEPE, P. L. From Lignocellulosic Biomass to Furfural: Insight into the Active Species of a Silica-Supported Tungsten Oxide Catalyst. *ChemCatChem*, vol. 9, pp. 2709–2716, 2017.

BÎLDEA, C. S.; GYŐRGY, R.; BRUNCHI, C. C.; KISS, A. A. Optimal design of intensified processes for DME synthesis. *Computers & Chemical Engineering*, vol. 105, pp. 142–151, 2017.

BISWAS, P.; LIN, J.-H.; KANG, J.; GULIANTS, V. V. Vapor phase hydrogenation of 2-methylfuran over noble and base metal catalysts. *Applied Catalysis A: General*, vol. 475, pp. 379–385, 2014.

BRAGA, V. S.; DIAS, J. A.; DIAS, S. C. L.; MACEDO, J. L. de. Catalyst Materials Based on Nb_2O_5 Supported on SiO_2 - Al_2O_3: Preparation and Structural Characterization. *Chemistry of Materials*, vol. 17, pp. 690–695, 2005.

BRANDÃO, R. F. et al. Synthesis, characterization and use of Nb_2O_5 based catalysts in producing biofuels by transesterification, esterification and pyrolysis. *Journal of the Brazilian Chemical Society*, vol. 20, pp. 954–966, 2009.

BRUNAUER, S.; EMMETT, P. H.; TELLER, E. Adsorption of Gases in Multimolecular Layers. *Journal of the American Chemical Society*, vol. 60, pp. 309–319, 1938.

CHHEDA, J. N.; ROMÁN-LESHKOV, Y.; DUMESIC, J. A. Production of 5-hydroxymeth-ylfurfural and furfural by dehydration of biomass-derived mono- and poly-saccharides. *Green Chem.*, vol. 9, pp. 342–350, 2007.

CHOUDHARY, V.; BURNETT, R. I.; VLACHOS, D. G.; SANDLER, S. I. Dehydration of Glucose to 5-(Hydroxymethyl) furfural and Anhydroglucose: Thermodynamic Insights. *The Journal of Physical Chemistry C*, vol. 116, pp. 5116–5120, 2012.

CHOUDHARY, V.; PINAR, A. B., et al. Xylose Isomerization to Xylulose and its Dehydration to Furfural in Aqueous Media. *ACS Catalysis*, vol. 1, pp. 1724–1728, 2011.

CHOUDHARY, V.; SANDLER, S. I.; VLACHOS, D. G. Conversion of Xylose to Furfural Using Lewis and Brønsted Acid Catalysts in Aqueous Media. *ACS Catalysis*, vol. 2, pp. 2022–2028, 2012.

CHU, S.; MAJUMDAR, A. Opportunities and challenges for a sustainable energy future. *Nature*, vol. 488, pp. 294–303, 2012.

CREMASCO, M. *Operações unitárias em sistemas particulados e fluidomecânicos*. São Paulo: BLUCHER, 2014. ISBN: 9788521208563.

DATKA, J.; TUREK, A.; JEHNG, J.; WACHS, I. Acidic properties of supported niobium oxide catalysts: An infrared spectroscopy investigation. *Journal of Catalysis*, vol. 135, pp. 186–199, 1992.

DELBECQ, F. et al. Hydrolysis of Hemicellulose and Derivatives—A Review of Recent Advances in the Production of Furfural. *Frontiers in Chemistry*, vol. 6, p. 146, 2018.

DHEPE Paresh, L.; FUKUOKA, A. Cellulose Conversion under Heterogeneous Catalysis. *ChemSusChem*, vol. 1, pp. 969–975, 2008.

FERREIRA, L. R. et al. Aqueous phase reactions of pentoses in the presence of nanocrystalline zeolite beta: Identification of by-products and kinetic modelling. *Chemical Engineering Journal*, vol. 215-216, pp. 772–783, 2013.

FIGUEIREDO, J.; RIBEIRO, F. *Catálise heterogénea*. Lisboa: Fundação Calouste Gulbenkian. Serviço de Educação, 1989. ISBN: 9789723100778.

FOGLER, H. *Elements of Chemical Reaction Engineering*. New Jersey: Prentice Hall, 2016. ISBN: 9780133887518.

FONTANA, J. *Evaluations of niobium based catalysts in glycerol esterification with octanoic acid*. Dec. 2016. PhD thesis – School of Chemical Engineering, University of Campinas, Brazil.

GAIROLA, K.; SMIRNOVA, I. Hydrothermal pentose to furfural conversion and simultaneous extraction with SC-CO_2 – Kinetics and application to biomass hydrolysates. *Bioresource Technology*, vol. 123, pp. 592–598, 2012.

GALLO, J. M. R. et al. Production of Furfural from Lignocellulosic Biomass Using Beta Zeolite and Biomass-Derived Solvent. *Topics in Catalysis*, vol. 56, pp. 1775–1781, 2013.

GARCÍA-SANCHO, C.; AGIRREZABAL-TELLERIA, I.; GÜEMEZ, M.; MAIRELES-TORRES, P. Dehydration of D-xylose to furfural using different supported niobia catalysts. *Applied Catalysis B: Environmental*, vol. 152-153, pp. 1–10, 2014a.

GÖTZE, L.; BAILER, O.; MORITZ, P.; SCALA, C. von. Reactive distillation with KATAPAK®. *Catalysis Today*, vol. 69, pp. 201–208, 2001.

GUPTA, N. K.; FUKUOKA, A.; NAKAJIMA, K. Amorphous $Nb_2 2O_5$ as a Selective and Reusable Catalyst for Furfural Production from Xylose in Biphasic Water and Toluene. *ACS Catalysis*, vol. 7, pp. 2430–2436, 2017.

HASSAN, S. S.; WILLIAMS, G. A.; JAISWAL, A. K. Moving towards the second generation of lignocellulosic biorefineries in the EU: Drivers, challenges, and opportunities. *Renewable and Sustainable Energy Reviews*, vol. 101, pp. 590–599, 2019.

HONGLIANG, W.; PU, Y.; RAGAUSKAS, A.; YANG, B. From lignin to valuable products–strategies, challenges, and prospects. *Bioresource Technology*, vol. 271, pp. 449–461, 2019.

HU, X. et al. Acid-Catalyzed Conversion of Xylose in 20 Solvents: Insight into Interactions of the Solvents with Xylose, Furfural, and the Acid Catalyst. *ACS Sustainable Chemistry & Engineering*, vol. 2, pp. 2562–2575, 2014.

JIAO, Z. et al. Effect of Calcination Temperature on Catalytic Performance of CeCu Oxide in Removal of Quinoline by Wet Hydrogen Peroxide Oxidation from Water. *Journal of the Brazilian Chemical Society*, vol. 29, pp. 2233–2243, 2018.

JIWON, A.; LEE, G.; HA, J.-M.; PARK, M.-J. Process analysis for biphasic dehydration of xylose: effects of solvents on the purification of furfural. *Biofuels*, pp. 1–5, 2019.

JUNIOR, S. V.; DONATE, P. Microwave-Assisted Green Production of Furfural from D-xylose of Sugarcane Bagasse. *BioResources*, vol. 10, no. 4, 2015.

KIM, S. B. et al. Dehydration of D-xylose into furfural over H-zeolites. *Korean Journal of Chemical Engineering*, vol. 28, pp. 710–716, 2011.

KIM, S. et al. Recently developed methods to enhance stability of heterogeneous catalysts for conversion of biomass-derived feedstocks. *Korean Journal of Chemical Engineering*, vol. 36, pp. 1–11, 2019.

KITANO, T.; SHISHIDO, T.; TERAMURA, K.; TANAKA, T. Acid property of Nb_2O_5/Al_2O_3 prepared by impregnation method by using niobium oxalate solution: Effect of pH on the structure and acid property. *Catalysis Today*, vol. 226, pp. 97–102, 2014.

KITANO, T.; SHISHIDO, T.; TERAMURA, K.; TANAKA, T. Brønsted Acid Property of Alumina-Supported Niobium Oxide Calcined at High Temperatures: Characterization by Acid-Catalyzed Reactions and Spectroscopic Methods. *The Journal of Physical Chemistry C*, vol. 116, pp. 11615–11625, 2012.

KITANO, T.; SHISHIDO, T.; TERAMURA, K.; TANAKA, T. Characterization of Thermally Stable Brønsted Acid Sites on Alumina-Supported Niobium Oxide after Calcination at High Temperatures. *ChemPhysChem*, vol. 14, pp. 2560–2569, 2013.

KRZELJ, V.; KAMPEN, J. van; SCHAAF, J. van der; NEIRA D'ANGELO, M. F. Furfural Production by Reactive Stripping: Process Optimization by a Combined Modeling and Experimental Approach. *Industrial & Engineering Chemistry Research*, vol. 58, pp. 16126–16137, 2019.

KUMAR, R.; MOHAN, S.; MAHAJANI, S. M. Reactive Stripping for the Catalytic Exchange of Hydrogen Isotopes. *Industrial & Engineering Chemistry Research*, vol. 52, pp. 10935–10950, 2013.

LEUNG, E.; SHIMIZU, A.; BARMAK, K.; FARRAUTO, R. Copper oxide catalyst supported on niobium oxide for CO oxidation at low temperatures. *Catalysis Communications*, vol. 97, pp. 42–46, 2017.

LI, X.; JIA, P.; WANG. Furfural: A Promising Platform Compound for Sustainable Production of C_4 and C_5 Chemicals. *ACS Catalysis*, vol. 6, no. 11, pp. 7621–7640, 2016.

LIMA, S. et al. Conversion of mono/di/polysaccharides into furan compounds using 1-alkyl-3-methylimidazolium ionic liquids. *Applied Catalysis A: General*, vol. 363, pp. 93–99, 2009.

LIN, Y.-C.; HUBER, G. W. The critical role of heterogeneous catalysis in lignocellulosic biomass conversion. *Energy Environ. Sci.*, vol. 2, pp. 68–80, 2009.

MALONE, M. F.; DOHERTY, M. F. Reactive Distillation. *Industrial & Engineering Chemistry Research*, vol. 39, pp. 3953–3957, 2000.

MAMMAN, A. S. et al. Furfural: Hemicellulose/xylosederived biochemical. *Biofuels, Bioproducts and Biorefining*, vol. 2, no. 5, pp. 438–454, 2008.

MARCOTULLIO, G.; DE JONG, W. Chloride ions enhance furfural formation from D-xylose in dilute aqueous acidic solutions. *Green Chem.*, vol. 12, pp. 1739–1746, 2010.

MARISCAL, R. et al. Furfural: a renewable and versatile platform molecule for the synthesis of chemicals and fuels. *Energy Environ. Sci.*, vol. 9, pp. 1144–1189, 2016.

METKAR, P. S. et al. Reactive distillation process for the production of furfural using solid acid catalysts. *Green Chem.*, vol. 17, pp. 1453–1466, 2015.

MOLINA, M. J. C.; GRANADOS, M. L.; GERVASINI, A.; CARNITI, P. Exploitment of niobium oxide effective acidity for xylose dehydration to furfural. *Catalysis Today*, vol. 254, pp. 90–98, 2015.

MÖLLER, M.; SCHRÖDER, U. Hydrothermal production of furfural from xylose and xylan as model compounds for hemicelluloses. *RSC Adv.*, vol. 3, pp. 22253–22260, 2013.

MOREAU, C. et al. Selective preparation of furfural from xylose over microporous solid acid catalysts. *Industrial Crops and Products*, vol. 7, pp. 95–99, 1998.

MOSIER, N. et al. Features of promising technologies for pretreatment of lignocellulosic biomass. *Bioresource Technology*, vol. 96, pp. 673–686, 2005.

NAKAJIMA, K. et al. $Nb_2O_5{\cdot}nH_2O$ as a Heterogeneous Catalyst with Water-Tolerant Lewis Acid Sites. *Journal of the American Chemical Society*, vol. 133, pp. 4224–4227, 2011.

NHIEN, L. C.; LONG, N. V. D.; KIM, S.; LEE, M. Design and optimization of intensified biorefinery process for furfural production through a systematic procedure. *Biochemical Engineering Journal*, vol. 116, pp. 166–175, 2016.

OLIVEIRA, L. C. et al. Modified niobia as a bifunctional catalyst for simultaneous dehydration and oxidation of glycerol. *Applied Catalysis B: Environmental*, vol. 117-118, pp. 29–35, 2012.

O'NEILL, R.; AHMAD, M. N.; VANOYE, L.; AIOUACHE, F. Kinetics of Aqueous Phase Dehydration of Xylose into Furfural Catalyzed by ZSM-5 Zeolite. *Industrial & Engineering Chemistry Research*, vol. 48, pp. 4300–4306, 2009.

PHOLJAROEN, B. et al. Dehydration of xylose to furfural over niobium phosphate catalyst in biphasic solvent system. *Journal of Energy Chemistry*, vol. 22, pp. 826–832, 2013.

PLACKETT, R. L.; BURMAN, J. P. The Design of Optimum Multifactorial Experiments. *Biometrika*, vol. 33, pp. 305–325, 1946.

PRASENJIT, B.; LAXMIKANT, D. P. Solid acid catalyzed synthesis of furans from carbohydrates. *Catalysis Reviews*, vol. 58, pp. 36–112, 2016.

RODRIGUES, M.; IEMMA, A. *Experimental Design and Process Optimization*. Boca Raton: CRC Press, 2014. ISBN: 9781482299564.

SAHU, R.; DHEPE, P. L. A One-Pot Method for the Selective Conversion of Hemicellulose from Crop Waste into C5 Sugars and Furfural by Using Solid Acid Catalysts. *ChemSusChem*, vol. 5, pp. 751–761, 2012.

SANTOS, K. M. A.; ALBUQUERQUE, E. M.; BORGES, L. E.; FRAGA, M. A. Discussing Lewis and Brønsted acidity on continuous pyruvaldehyde Cannizzaro reaction to lactic acid over solid catalysts. *Molecular Catalysis*, vol. 458, pp. 198–205, 2018.

SATTERFIELD, C. N.; COLTON, C. K.; PITCHER J., W. H. Restricted diffusion in liquids within fine pores. *AIChE Journal*, vol. 19, pp. 628–635, 1973.

SCHILDHAUER, T. J. et al. Reactive Stripping in Structured Catalytic Reactors: Hydrodynamics and Reaction Performance. In: SCHILDHAUER, T. J. et al. *Integrated Chemical Processes*. Weinheim: John Wiley & Sons, Ltd, 2005. chap. 8, pp. 233–264.

SCHUTYSER, W. et al. Chemicals from lignin: an interplay of lignocellulose fractionation, depolymerisation, and upgrading. *Chem. Soc. Rev.*, vol. 47, pp. 852–908, 2018.

SEADER, J.; HENLEY, E.; ROPER, D. *Separation Process Principles, 3rd Edition*. United States: John Wiley Incorporated, 2010. ISBN: 9781118139622.

SERNA-LOAIZA, S.; GARCÍA-VELÁSQUEZ, C. A.; CARDONA, C. A. Strategy for the selection of the minimum processing scale for the economic feasibility of biorefineries. *Biofuels, Bioproducts and Biorefining*, vol. 13, pp. 107–119, 2019.

SIEVERS, C. et al. Phenomena Affecting Catalytic Reactions at Solid–Liquid Interfaces. *ACS Catalysis*, vol. 6, pp. 8286–8307, 2016.

SINDHU, R. et al. Chapter 5 - Biofuel Production From Biomass: Toward Sustainable Development. In: KUMAR, S.; KUMAR, R.; PANDEY, A. (Eds.). *Current Developments in Biotechnology and Bioengineering*. The Netherlands: Elsevier, 2019. pp. 79–92. ISBN: 978-0-444-64083-3.

SITTHISA, S.; WEI, A.; RESASCO, D. E. Selective conversion of furfural to methylfuran over silica-supported NiFe bimetallic catalysts. *Journal of Catalysis*, vol. 284, pp. 90–101, 2011.

SMITH, R. *Chemical Process: Design and Integration*. 2. ed. Chichester: Wiley, 2005. p. 712. ISBN: 9780470011911.

STANKIEWICZ, A. I.; MOULIJN, J. A. Process intensification: Transforming chemical engineering. *Chemical Engineering Progress*, vol. 96, p. 22, 2000.

SUNDMACHER, K.; KIENLE, A. *Reactive Distillation: Status and Future Directions*. Weinheim: Wiley, 2006. ISBN: 9783527606269.

SUSHEEL, K. et al. Cellulose-Based Bio- and Nanocomposites: A Review. *International Journal of Polymer Science*, vol. 2011, p. 35, 2011.

TERNAN, M. The diffusion of liquids in pores. *The Canadian Journal of Chemical Engineering*, vol. 65, pp. 244–249, 1987.

VANNICE, M. *Kinetics of Catalytic Reactions*. New York: Springer US, 2006. ISBN: 9780387259727.

VAZ JUNIOR, S.; SOARES, I. P. Análise química da biomassa - uma revisão das técnicas e aplicações. *Química Nova*, vol. 37, pp. 709–715, 2014.

VIEIRA, J. L. et al. Rationalizing the conversion of glucose and xylose catalyzed by a combination of Lewis and Brønsted acids. *Catalysis Today*, 2018.

WALKER, T. W. et al. Universal kinetic solvent effects in acid-catalyzed reactions of biomass-derived oxygenates. *Energy Environ. Sci.*, vol. 11, pp. 617–628, 2018.

WANG, C. et al. Highly Efficient Conversion of Xylose Residues to Levulinic Acid over $FeCl_3$ Catalyst in Green Salt Solutions. *ACS Sustainable Chemistry & Engineering*, vol. 6, pp. 3154–3161, 2018.

YAN, K.; WU, G.; LAFLEUR, T.; JARVIS, C. Production, properties and catalytic hydrogenation of furfural to fuel additives and value-added chemicals. *Renewable and Sustainable Energy Reviews*, vol. 38, pp. 663–676, 2014.

YANG, W. et al. Optimization of furfural production from d-xylose with formic acid as catalyst in a reactive extraction system. *Bioresource Technology*, vol. 133, pp. 361–369, 2013.

YEMIŞ, O.; MAZZA, G. Acid-catalyzed conversion of xylose, xylan and straw into furfural by microwave-assisted reaction. *Bioresource Technology*, vol. 102, pp. 7371–7378, 2011.

YU, S.; ZHOU, A.; TAN, Q. Simulation of multistage catalytic stripping with A nonequilibrium stage model. *Computers & Chemical Engineering*, vol. 21, pp. 409–415, 1997.

10. Furfural processes. In: ZEITSCH, K. J. (Ed.). *The chemistry and technology of furfural and its many by-products*. The Netherlands: Elsevier, 2000. vol. 13. (Sugar Series), pp. 36–74.

11. Distillation of furfural. In: ZEITSCH, K. J. (Ed.). *The chemistry and technology of furfural and its many by-products*. The Netherlands: Elsevier, 2000. vol. 13. (Sugar Series), pp. 75–85.

6. Furfural loss reactions. In: ZEITSCH, K. J. (Ed.). *The chemistry and technology of furfural and its many by-products*. The Netherlands: Elsevier, 2000. vol. 13. (Sugar Series), pp. 19–22.

J. Operational details of the ROSENLEW process. In: ZEITSCH, K. J. (Ed.). *The chemistry and technology of furfural and its many by-products*. The Netherlands: Elsevier, 2000. vol. 13. (Sugar Series), pp. 303–304.

Appendix A

Catalyst Characterisation

A.1 Nitrogen Adsorption

Figure A.1: Isotherm plot for NBAL catalyst.

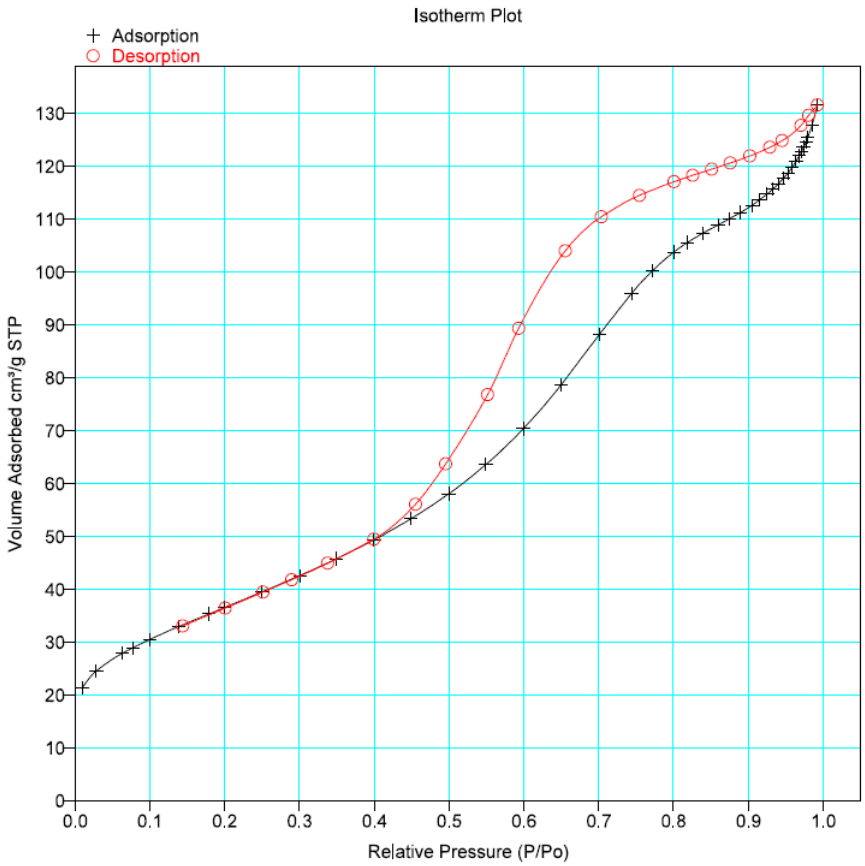

Figure A.2: Isotherm plot for NBAL-N catalyst.

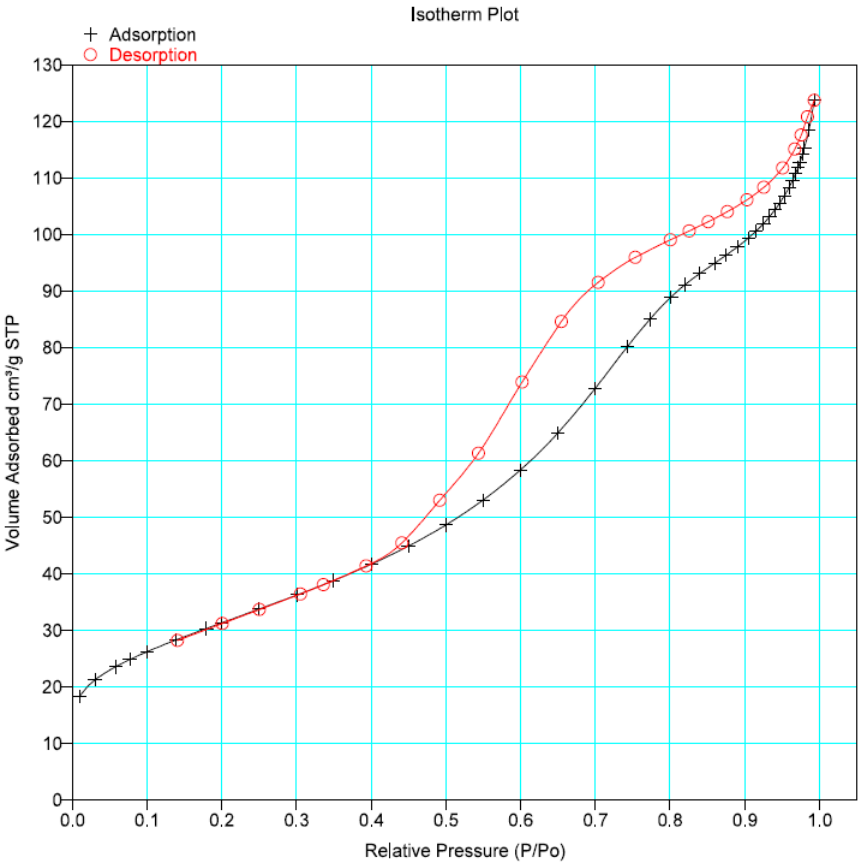

Figure A.3: Isotherm plot for NBAL-P catalyst.

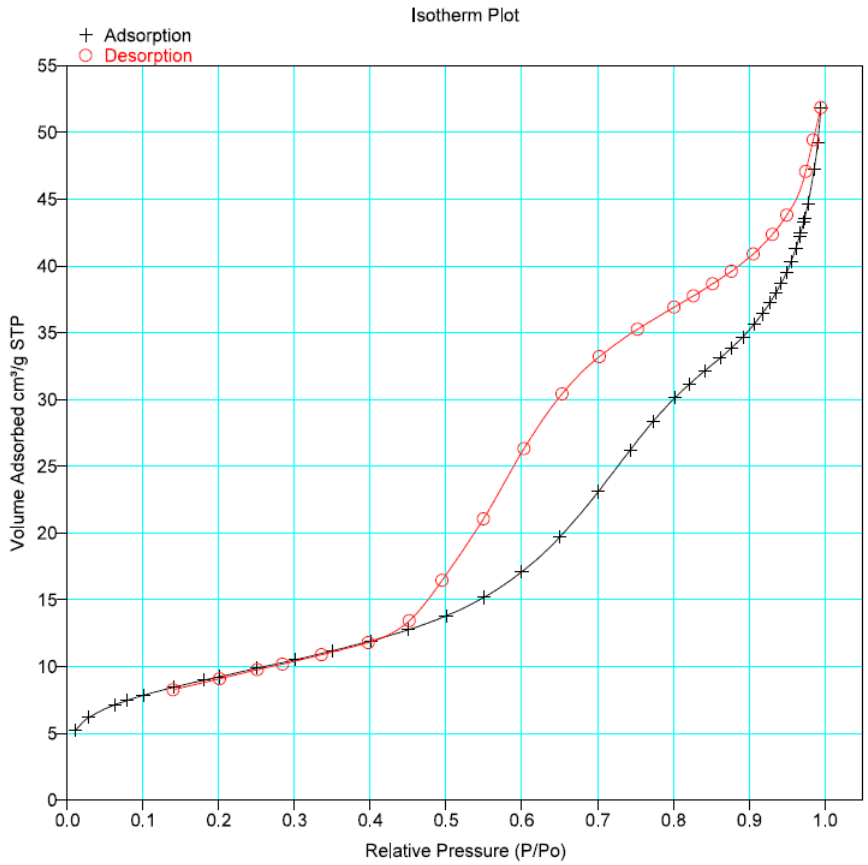

Appendix B

Scilab Code

```
clc
clear

function dy = myModel ( t , y , a, b)
   // The right-hand side of the Ordinary Differential Equation.
    dy(1) = -a*y(1) - b*y(1)
    dy(2) = a*y(1)
endfunction

function f = myDifferences ( k )
    // Returns the difference between the simulated differential
    // equation and the experimental data.
    global MYDATA
    t = MYDATA.t
    y_exp = MYDATA.y_exp
    a = k(1)
    b = k(2)
    y0 = y_exp(1,:)
    t0 = 0
    y_calc=ode("rk",y0',t0,t,list(myModel,a, b))
    diffmat = y_calc' - y_exp
    // Make a column vector
```

```
    f = diffmat(:)
    MYDATA.funeval = MYDATA.funeval+ 1
endfunction

// Experimental data

t = [0,20,30,45,75,105,135,180,240]';

y_exp = read('dataFile.txt',-1,-1);

// Store data for future use
global MYDATA;
MYDATA.t = t;
MYDATA.y_exp = y_exp;
MYDATA.funeval = 0;

function val = L_Squares ( k )
    // Computes the sum of squares of the differences.
    f = myDifferences ( k )
    val = sum(f.^2)
endfunction

// Initial guess
a = 0;
b = 0;
x0 = [a;b];

[fopt ,xopt]=leastsq(myDifferences, 'b', [0;0], [1e10;1e10],x0 )
//'b' is a constraint. a,b,c range from 0 to 1e10

y0 = y_exp(1,:);
t0 = 0;
```

```
tt=0:1:250;
yy(:,1)=0.13;
ttt=60:1:65
y_calc=ode("rk",y0',t0,tt,list(myModel,xopt(1), xopt(2)))

plot(tt, y_calc(1,:)', 'k-')
plot(tt, y_calc(2,:)', 'k-')
plot(t, y_exp(:,1), 'bx')
plot(t, y_exp(:,2), 'rx')

xlabel("Time (min)","fontsize",4);
ylabel("Concentration (mol/L)","fontsize",4);
legend(['Estimated Xylose';'Estimated Furfural';'Xylose';'Furfural']);

//Creates a .eps and .png graph
xs2eps(0,"nb1.eps")
xs2png(0,"nb1.png")
```

Appendix C

Catalytic Performance

Figure C.1: Furfural yield and xylose conversion for each catalyst at 150 °C.

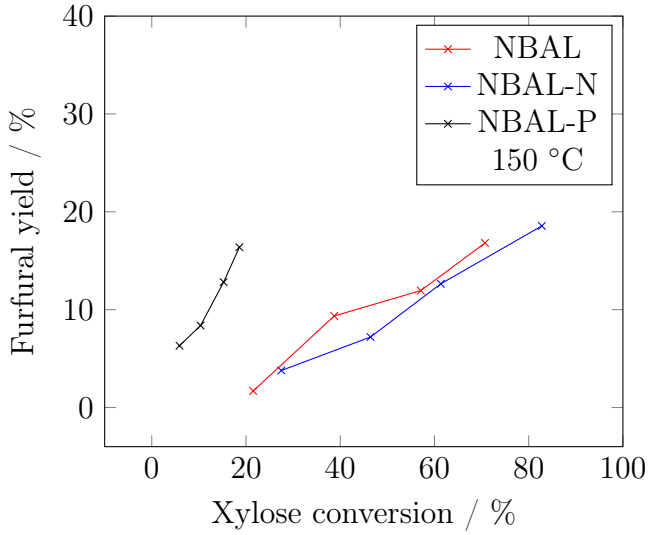

Figure C.2: Furfural yield and xylose conversion for each catalyst at 160 °C.

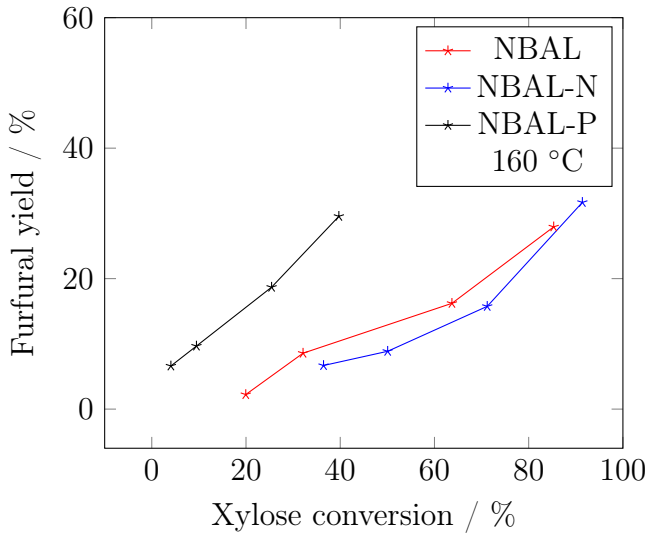

Figure C.3: Furfural yield and xylose conversion for each catalyst at 170 °C.

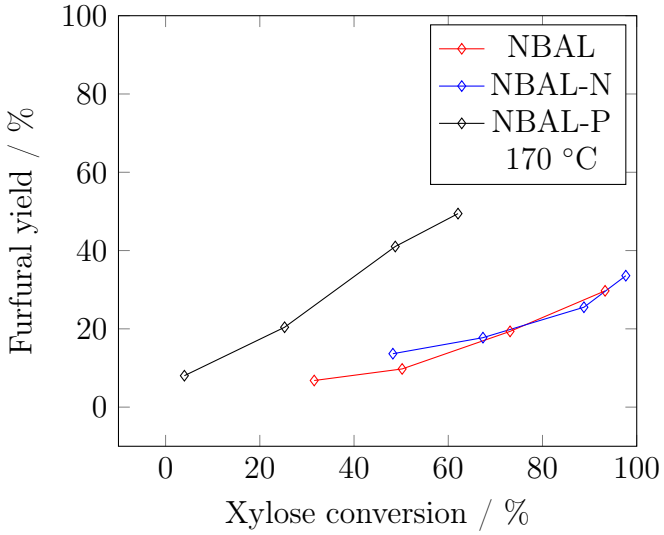

Appendix D

Base Case and Simulation Data

Figure D.1: Operating parameters for the base case simulation.

Stream ID		XYL-FEED	N2-FEED	GAS	BOTTOM	N2-EXIT	LV
Temperature	C	60,0	265,0	159,8	162,4	25,0	25,0
Pressure	bar	10,050	10,050	10,050	10,050	1,000	10,050
Vapor Frac		0,000	1,000	1,000	0,000	1,000	0,402
Mole Flow	kmol/hr	176,910	433,226	422,755	198,622	175,109	422,755
Mass Flow	kg/hr	3899,000	9500,000	9354,001	4044,999	4851,199	9354,001
Volume Flow	cum/hr	3,752	1928,765	1514,262	4,596	4340,800	424,085
Enthalpy	Gcal/hr	-12,902	-14,422	-14,174	-13,150	-0,321	-17,271
Mass Flow	kg/hr						
FUR				52,480	307,556	1,671	52,480
H2O		3090,000	4750,000	4551,624	3490,887	99,802	4551,624
N2			4750,000	4749,804	0,196	4749,725	4749,804
XYL		809,000		0,093	246,360	trace	0,093
Mass Frac							
FUR				0,006	0,076	345 PPM	0,006
H2O		0,793	0,500	0,487	0,863	0,021	0,487
N2			0,500	0,508	48 PPM	0,979	0,508
XYL		0,207		10 PPM	0,061	trace	10 PPM
Mole Flow	kmol/hr						
FUR				0,546	3,201	0,017	0,546
H2O		171,521	263,665	252,654	193,774	5,540	252,654
N2			169,561	169,554	0,007	169,551	169,554
XYL		5,389		0,001	1,641	trace	0,001
Mole Frac							
FUR				0,001	0,016	99 PPM	0,001
H2O		0,970	0,609	0,598	0,976	0,032	0,598
N2			0,391	0,401	35 PPM	0,968	0,401
XYL		0,030		1 PPM	0,008	trace	1 PPM

Appendix E

Design of Experiments

E.1 Plackett-Burman

Table E.1: Experimental matrix for Plackett-Burman-12 (PB-12).

	x_1	x_2	x_3	x_4	x_5	x_6	x_7	x_8
1	1	-1	1	-1	-1	-1	1	1
2	1	1	-1	1	-1	-1	-1	1
3	-1	1	1	-1	1	-1	-1	-1
4	1	-1	1	1	-1	1	-1	-1
5	1	1	-1	1	1	-1	1	-1
6	1	1	1	-1	1	1	-1	1
7	-1	1	1	1	-1	1	1	-1
8	-1	-1	1	1	1	-1	1	1
9	-1	-1	-1	1	1	1	-1	1
10	1	-1	-1	-1	1	1	1	-1
11	-1	1	-1	-1	-1	1	1	1
12	-1	-1	-1	-1	-1	-1	-1	-1

E.2 Central Composite Rotatable Design (CCRD)

Table E.2: CCRD matrix for five factors and results for furfural global yield (Y_1) and furfural recovery at the top (Y_2).

	Factors					Responses		Process parameter
	X_4	X_5	X_6	X_7	X_8	Y_1	Y_2	Range of temperature (°C)
1	0.416	240.6	8.24	10	22.4	66.1	37.3	156-151

Table E.2 continued from previous page

2	0.584	240.6	8.24	10	22.4	83.9	60.7	166-161
3	0.416	299.4	8.24	10	22.4	69.0	46.4	158-152
4	0.584	299.4	8.24	10	22.4	85.2	74.0	167-162
5	0.416	240.6	9.31	10	22.4	76.0	22.3	160-155
6	0.584	240.6	9.31	10	22.4	91.3	41.6	171.5-167
7	0.416	299.4	9.31	10	22.4	78.8	29.6	162.5-157.5
8	0.584	299.4	9.31	10	22.4	92.3	53.8	172.5-168
9	0.416	240.6	8.24	15	22.4	77.3	41.6	155-150
10	0.584	240.6	8.24	15	22.4	91.8	59.7	165.5-161
11	0.416	299.4	8.24	15	22.4	79.8	48.9	156.5-151.5
12	0.584	299.4	8.24	15	22.4	92.7	70.7	167-161.5
13	0.416	240.6	9.31	15	22.4	86.0	29.2	159.5-155.5
14	0.584	240.6	9.31	15	22.4	96.6	44.6	170.5-166.5
15	0.416	299.4	9.31	15	22.4	88.2	35.3	161.5-157
16	0.584	299.4	9.31	15	22.4	97.1	54.5	172-167.5
17	0.416	240.6	8.24	10	47.6	85.1	29.4	154.5-150
18	0.584	240.6	8.24	10	47.6	96.0	53.2	165-160.5
19	0.416	299.4	8.24	10	47.6	87.3	37.3	156-151.5
20	0.584	299.4	8.24	10	47.6	96.5	65.5	166-161.5
21	0.416	240.6	9.31	10	47.6	92.0	18.9	159.5-155
22	0.584	240.6	9.31	10	47.6	98.6	38.9	170-166
23	0.416	299.4	9.31	10	47.6	93.6	25.4	161.5-157
24	0.584	299.4	9.31	10	47.6	98.9	50.7	171-168
25	0.416	240.6	8.24	15	47.6	93.0	36.8	154-149.5
26	0.584	240.6	8.24	15	47.6	98.9	57.6	164-160
27	0.416	299.4	8.24	15	47.6	94.3	43.7	155.5-151
28	0.584	299.4	8.24	15	47.6	99.1	68.2	165.5-161
29	0.416	240.6	9.31	15	47.6	97.1	28.0	158.5-155
30	0.584	240.6	9.31	15	47.6	99.7	45.4	169.5-166.5
31	0.416	299.4	9.31	15	47.6	97.9	34.0	160.5-156.5
32	0.584	299.4	9.31	15	47.6	99.8	55.1	170.5-167.5

Table E.2 continued from previous page

33	0.3	270	8.775	12	35	73.0	22.3	149-144.5
34	0.7	270	8.775	12	35	99.0	73.0	174-170
35	0.5	200	8.775	12	35	92.3	29.6	162-157.5
36	0.5	340	8.775	12	35	95.0	52.7	165.5-161
37	0.5	270	7.5	12	35	85.3	59.2	157.5-152
38	0.5	270	10.05	12	35	97.9	26.1	169.5-165.5
39	0.5	270	8.775	5	35	76.1	47.7	164.5-160
40	0.5	270	8.775	20	35	98.6	47.3	163-159
41	0.5	270	8.775	12	5	46.8	76.1	167-162
42	0.5	270	8.775	12	65	98.8	38.4	162.5-159